

## ABSTRACT

Title of Dissertation: ELECTROSTATIC DISCHARGE (ESD) RISKS IN WEARABLE MEDICAL DEVICES: EVALUATING THE STANDARD TEST METHOD AND DEVELOPING A CURRENT PREDICTION MODEL

Mehdi Kohani, Doctor of Philosophy, 2018

Dissertation directed by: Professor Michael Pecht,  
Department of Mechanical Engineering

Electrostatic discharge (ESD) is a critical reliability concern for wearable medical devices. In recent years, numerous reports of device malfunction resulting in patient adverse events, and medical device recalls have been attributed to ESD. To mitigate the risk of device malfunction, sufficient ESD immunity standards and accurate ESD prediction models that represent severe discharges during usage are necessary. Thus, ESD test configurations that represent realistic discharges of wearable devices in healthcare applications need to be developed, and the severity of the ESD events need to be compared with the existing ESD immunity standards. The U.S. Food and Drug Administration (FDA) recognizes the IEC 60601-1-2 collateral standards, within which the IEC 61000-4-2 standard is the recommended ESD test method.

The severity of the discharges depends on the electrical impedance of the body and the discharging structure. To identify the realistic discharge scenarios for wearable medical

devices, the proper body posture, device location, and the realistic discharge setup need to be determined. A research gap in the literature on electrostatic charging of a human body was that only standing posture was considered. Moreover, current prediction models developed in ESD literature are not based on the physical impedance parameters of the human body and the test setup.

Through conducting surveys, electrostatic measurements in a local hospital, and conducting laboratory studies in a climate chamber, a large set of electrostatic charging activities performed routinely by patients and hospital personnel were identified. ESD measurements for these scenarios showed that the IEC 61000-4-2 is not sufficient for these devices since the peak currents and maximum current derivatives of realistic discharges were up to 1.9 and 2.4 times larger than the standard specifications, respectively.

A physics-based model for current waveform prediction was developed using the electrical impedance of the discharging structure and the human body in the identified postures of standing on the floor, sitting and lying down on a hospital bed and two device locations (hand and waist). Discharge waveforms at spark lengths between 100% to 50% of the Paschen's length were simulated with reasonable accuracy.

ELECTROSTATIC DISCHARGE (ESD) RISKS IN WEARABLE MEDICAL  
DEVICES: EVALUATING THE STANDARD TEST METHOD AND  
DEVELOPING A CURRENT PREDICTION MODEL

by

Mehdi Kohani

Dissertation submitted to the Faculty of the Graduate School of the  
University of Maryland, College Park, in partial fulfillment  
of the requirements for the degree of  
Mechanical Engineering  
2018

Advisory Committee:

Professor Michael Pecht, Chair/Advisor

Professor David Pommerenke

Professor Patrick McCluskey

Professor Jin-oh Hahn

Professor Aristos Christou

Professor Christopher Davis

© Copyright by  
Mehdi Kohani  
2018

## Acknowledgments

First and foremost, I would like to thank my mother, my father and my sisters for their endless love and continuous support for all my endeavors.

I would like to thank my adviser, Prof. Michael Pecht, for his guidance, and support and helping me always seeing the big picture of research work while at the same time looking for fine details.

Special Thanks go to my co-advisor, Prof. David Pommerenke, who was always providing me with very useful insights. Without his guidance and persistent help, this dissertation would not have been possible.

I would like to thank my dissertation committee Professors Patrick McCluskey, Christopher Davis, Jin-Oh Hahn, Peter Sandborn, and Aristos Christou. I would like to thank current and former students, faculty and staff at CALCE and the EMC lab at the Missouri University of Science and Technology. Thanks to Dr. Diganta Das and Dr. Michael Azarian for their support and guidance. Special thanks to Dr. Javad Meiguni at the EMC lab for his great assistance in my test setups and measurements. My sincere thanks to Dr. Atieh Talebzadeh, Dr. Abhishek Patnaik, Aniket Bhandare, Lane Kinslow, Li Guan, Hossein Rezaei, Jianchi Zhou, Shubhankar Marathe, and Dr. Ahmad Hosseinbeig.

I am very thankful to my collaborators at the U.S. Food and Drug Administration (FDA), especially Mr. Jeffrey Silberberg for his invaluable assistance and helpful suggestions regarding the ESD/EMC regulations of medical devices and his critique on my research articles. I would particularly like to acknowledge Mr. Hamed Ghods, who invited and me to work at the Department of Biomedical Physics at the FDA as a research fellow

and our fruitful collaboration there. I am thankful to Dr. Sandy Weininger, Mr. Michael Long, and Mrs. Nancy Pressly for their support in my analysis of the FDA's MAUDE database.

My sincere thanks also go to Mrs. Michelle Grasso, my supervisor during a summer internship at Medtronic, for her helpful guidance and her invaluable insight into the reliability issues in medical device industry. Many thanks to Dr. Paul Holdstock, chairman of the IEC TC (Technical Committee) 101: Electrostatics, and Mr. Toni Viheriakoski for sharing their ideas regarding the shortcomings of the current ESD standards for medical devices.

Finally, I would like to thank my friends and officemates at UMD, Kailyn Cage, Luis Santos, Rushit Shah, Arvind Vasan and Jose Romero who supported me through this entire process and offered me constructive advice. My heartfelt thanks to Yazdan Movahedi, Hesameddin Khosravi, Peyman Yousefian, and Ali Tivay who made my graduate life intellectually and socially enriched. I wish them all the best in their graduate lives.

# Table of Contents

Acknowledgments.....	i
List of Tables .....	vii
Table of Figures .....	viii
1. Introduction.....	1
1.1. Research Questions.....	3
1.2. Dissertation Outline .....	4
2. Basics of Electrostatic Discharge (ESD) .....	5
2.1. Charge Buildup Mechanisms .....	6
2.2. Characteristics of ESD Events .....	7
2.2.1. ESD Circuit Model .....	7
2.2.2. ESD Current Waveform.....	9
2.2.3. Contact and Air-Mode Discharges.....	11
2.3. Effect of Material Combination on Electrostatic Charging .....	13
2.4. Effects of Ambient Relative Humidity on ESD.....	14
2.5. ESD Immunity Standards for Medical Equipment .....	15
2.6. IEC 61000-4-2 Standard Test Method.....	17
2.6.1. ESD Gun Calibration .....	20
2.6.2. ESD Test Setup.....	22
3. Literature Review.....	25
3.1. Human Body Charging .....	25

3.2.	ESD Current Waveform from a Charged Human .....	32
3.3.1.	The Literature on Electrostatic Charging of a Human Body .....	42
4.	Electrostatic Charging Activities in a Hospital.....	49
4.1.	Methods .....	50
4.1.1.	Climate Chamber .....	51
4.1.2.	Voltage Measurement Setup .....	51
4.2.	Experimental Apparatus and Materials.....	53
4.3.	Measurement Results and Discussions .....	55
4.3.1.	Walking and Rolling a Medication Cart .....	55
4.3.2.	Sweater Removal .....	55
4.2.3.	Sitting on and Rising from a Bed.....	59
4.2.4.	Lying down and Rising from a Bed .....	64
4.2.5.	Patient Transfer Using a Sliding Board .....	69
4.3.	Conclusions.....	81
5.	Current Measurement and Equivalent Circuit for ESD from Wearable Medical Devices ....	85
5.1.	Discharge Configurations .....	87
5.2.	ESD Setup and Measurements.....	90
5.3.	Impedance Measurements and the Equivalent Circuit.....	94
5.3.1.	Impedance Measurement Setup .....	95
5.3.2.	Equivalent Circuit Elements of Impedance Measurement Setup.....	99
5.3.3.	Impedance Measurement Results.....	106



5.3.4.	Analysis of the Impedance Measurement Results .....	108
5.3.5.	The Validity of The Assumption of Body Capacitance .....	112
5.4.	Equivalent Circuit Model for ESD Current Prediction .....	114
5.5.	ESD Current Measurements and Estimation Results .....	117
5.6.	ESD Gun Discharge Waveform.....	123
5.7.	Current Waveform of an ESD from a Wearable Device.....	125
5.7.1.	Peak Current.....	132
5.7.2.	Peak Current Derivative.....	137
5.7.3.	Charge Transfer .....	144
5.8.	Effects of Spark Length .....	147
5.9.	Effects of the Gas Constant $K_R$ in Rompe-Weizel's Model.....	150
5.10.	Effect of Circuit Elements on the Waveform.....	151
5.11.	Effect of Removing the Short Wire on the Waveform .....	158
5.12.	Effect of RH and Speed of Approach on the Waveform .....	160
5.13.	Conclusions.....	165
6.	Contributions.....	169
	Appendix: Survey on Electrostatic Risks in Hospitals .....	173
	Bibliography .....	175

## List of Tables

Table 1. Triboelectric series table .....	14
Table 2. ESD voltage and the parameters of the current waveform for contact mode discharges of an ESD gun in the calibration setup.....	22
Table 3. The median of the voltages and the difference between the electron affinity of the material combinations for each designated letter.....	80
Table 4. Range of optimization for RLC parameters of the equivalent circuit.....	104
Table 5. List of the fitted parameters of the equivalent circuit for impedance measurement .....	110
Table 6. The accuracy of the simulation using the developed equivalent circuit for 6 test configurations at 4 voltage levels .....	121
Table 7. Spark length versus speed of approach for 1.5 kV and 9.9 kV, extracted from Pommerenke [31].....	164

## Table of Figures

Figure 2.1. Electronic structure of materials A and B before (left figure) and after triboelectric charging (right figure).....	7
Figure 2.2. ESD from wearable devices mounted on a charged subject to grounded metal objects	8
Figure 2.3. An RC circuit that describes the charging and discharging process during an ESD event.....	9
Figure 2.4. Severity parameters of an ESD current waveform .....	11
Figure 2.5. ESD testing according to the human metal model.....	18
Figure 2.6. An ESD gun (left) and it's simplified equivalent RC network representation (right) .	19
Figure 2.7. Air-mode testing on an EUT using an ESD gun .....	20
Figure 2.8. Calibration setup for an ESD gun.....	21
Figure 2.9. ESD current waveform specified in the IEC 61000-4-2 standard for direct-contact mode [34].....	21
Figure 2.10. IEC 61000-4-2 standard ESD test setup for ungrounded tabletop EUTs [34].....	24
Figure 3.1. The RH and temperature conditions for seven points tested in Talebzadeh et al.'s study [29] .....	28
Figure 3.2. Setup for impedance measurement (between the body and the grounded metal shield) .....	34
Figure 3.3. Human ESD measurement setup (top) and an equivalent circuit (bottom) .....	37
Figure 3.4. Comparison between the measurement and simulation of the discharge current at 10kV brush-by scenario in Zhou et al. s study [22] .....	41
Figure 4.1. Voltage measurement system in the climate chamber.....	53
Figure 4.2. An example of a body voltage waveform during sweater removal experiment. The polarity of static charges is shown arbitrarily. ....	56

Figure 4.3. Triboelectric charging of the sweater and the body while rubbing the sweater against underneath clothing.....	57
Figure 4.4. Histogram and the boxplot of the Peak body voltage while taking off the sweater ....	58
Figure 4.5. Histogram and the boxplot of the charge decay time constant during sweater removal .....	59
Figure 4.6. Experimental setup designed for sitting activity .....	60
Figure 4.7. A typical voltage waveform during the sitting activity; Polarity of the static charges are shown arbitrarily. ....	61
Figure 4.8. Histogram and the boxplot of the peak body voltage for sitting experiments .....	62
Figure 4.9. Histogram and the boxplot of charge decay time constant for sitting experiment .....	63
Figure 4.10. Histogram and the boxplot of decay time constant for standing posture.....	63
Figure 4.11. Boxplots of peak body voltage during sitting experiment for various types of blanket material .....	64
Figure 4.12. A typical voltage waveform while the subject is lying down on and rising from the bed; Polarity of the static charges are shown arbitrarily. ....	65
Figure 4.13. Histogram and the boxplot of the peak body voltage while lying down on the bed and rising from it.....	67
Figure 4.14. Histogram and the boxplot of the charge decay from the body to the ground while lying down on the bed.....	68
Figure 4.15. Boxplots of peak body voltage during sitting experiment for various types of blanket material .....	69
Figure 4.16. Patient transfer process using a sliding sheet and a board in two stages .....	70
Figure 4.17. Patient's body voltage profile during the transfer process .....	70
Figure 4.18. A typical voltage waveform for the nurse during patient transfer using the sliding board and the sheet.....	72

Figure 4.19. Histogram and the boxplot of the peak body voltage distribution for both subjects (stage 1 of the experiment) .....	73
Figure 4.20. Comparison between the histogram of peak body voltage during sliding experiments at 3 RH levels.....	74
Figure 4.21. Boxplots of peak body voltage at 3 RH levels .....	75
Figure 4.22. Histogram of the results with and without the antistatic coating.....	76
Figure 4.23. Comparison between the boxplots of the peak voltages with and without antistatic coating.....	77
Figure 4.24. Comparison between the distribution of the voltage levels for different types of boards at 3 RH levels .....	78
Figure 4.25. Effect of the combination of the blanket and sliding sheet on the peak body voltage. The blue dashed line represents the maximum ESD test voltage level.....	79
Figure 5.1. A square metal piece used in lieu of a wearable medical device.....	88
Figure 5.2. ESD event from a charged subject lying down on a bed, wearing a body-mounted metal piece (in lieu of a wearable device).....	89
Figure 5.3. ESD current measurement setup while the subject is lying down on the bed. A short wire is attached to the Al foil, and a longer wire connects between the Al foil and the ground plane.....	92
Figure 5.4. ESD calibration setup according to the IEC 61000-4-2, ESD gun is injected into the center of the plane which is a current target .....	93
Figure 5.5. Reference current waveform from an ESD gun discharging to ground .....	94
Figure 5.6. Impedance measurement process using a vector network analyzer (VNA). The schematic on the left shows the elements in the differential current path.....	95
Figure 5.7. Components of the impedance measurement setup.....	96
Figure 5.8. A short coaxial cable of 4 cm length is added to the VNA cable to measure the impedance between the metal piece and the metal rod attached to the short wire (30 cm long). ..	97

Figure 5.9. Locations of the metal rod (connected to the short ground wire) and the short coaxial cable (connected to the VNA cable) .....	98
Figure 5.10. The dynamic range of the VNA after calibration and port extension. One example measurement is shown to ensure the impedance data lies within the range between the open and short conditions.....	99
Figure 5.11. Impedance elements in the VNA setup .....	100
Figure 5.12. Impedance measurement for the long wire between the Al foil and the ground plane .....	101
Figure 5.13. The impedance of the long wire relative to the ground.....	101
Figure 5.14. ADS equivalent circuit for Z11 impedance measurement setup for a subject lying down on a bed and wearing a metal piece on his hand .....	103
Figure 5.15. Z11 Impedance between the metal piece on the subject's body at various postures, and the short wire connected to the Al foil .....	107
Figure 5.16. The position of the subject with respect to the edge of the hospital bed during impedance measurement while lying down on the bed (left: The metal piece on hand, Right: The metal piece on waist). .....	112
Figure 5.17. Comparison of the impedance of the human body measured in the literature and a capacitance with -20 dB/Dec relationship. ....	113
Figure 5.18. The impedance measured between the subject's skin and the short wire connected to the Al foil (comparison with the measurement for which the metal piece is mounted on the subject's body).....	114
Figure 5.19. The equivalent circuit of the ESD current measurement setup .....	116
Figure 5.20. ESD waveform for discharge from the hand while the subject is lying down on the bed (comparison with current estimation) .....	118
Figure 5.21. Initial peak of the ESD waveform at 6 kV discharge from the subject's hand, while he is lying down on the bed).....	119

Figure 5.22. Two phases of current waveform from an ESD gun. ....	124
Figure 5.23. Equivalent circuit representation of the spark gap during ESD from a wearable device.....	126
Figure 5.24. The variation of $K(t, l)$ with the body voltage at ( $t = 20 \text{ ps}$ ).....	129
Figure 5.25. Comparison of the measured peak ESD current for six test configurations and the IEC 61000-4-2 standard setup as a function of body voltage.....	133
Figure 5.26. Comparison between the ratio of the peak current from waist- to hand-worn discharges at each voltage and body posture.....	135
Figure 5.27. Effect of body posture on peak current (Top: Hand-worn metal piece, Bottom: Waist-worn metal piece).....	135
Figure 5.28. Estimated peak current using the developed equivalent circuit compared to the ESD gun results.....	136
Figure 5.29. Comparison of the peak ESD current derivative for 6 test configurations of a subject wearing a metal piece, and the IEC 61000-4-2 standard setup as a function of body voltage.....	138
Figure 5.30. Peak current derivative of waist-worn discharge from measurement compared to hand-worn discharges of the 3 body postures.....	139
Figure 5.31. Estimated peak current derivative using 100% Paschen's length from the circuit simulation.....	142
Figure 5.32. Peak current derivative of waist-worn discharge from simulation compared to hand-worn discharges of the 3 body postures.....	143
Figure 5.33. Estimated peak current derivative using 50% Paschen's length from the equivalent circuit simulation.....	144
Figure 5.34. The charge delivered to the ground during ESD from a wearable metal piece at various position and postures, compared to an ESD gun.....	146
Figure 5.35. Estimated charge transfer to the ground during ESD from a wearable metal piece compared to an ESD gun.....	147

Figure 5.36. Effect of shortening spark length on the waveform.....	148
Figure 5.37. Comparison between the estimated peak current at different spark lengths with Zhou et al.'s simulation [22] and Pommerenke's measurements [23] .....	149
Figure 5.38. Effect of gas constant on the peak current derivative at two spark lengths of 2.7 mm and 2 mm .....	151
Figure 5.39. Effect of increasing the wire inductance on the waveform .....	152
Figure 5.40. Effect of changing wire inductance on the Peak Current .....	153
Figure 5.41. Effect of radiation capacitance on the waveform .....	153
Figure 5.42 shows that after increasing the radiation capacitance to 4 times its initial value, a 6% decrease in $I_{max}$ can be observed. The effect on $dI/dt_{max}$ is negligible (about 1 %). .....	154
Figure 5.43. Effect of radiation capacitance on the waveform parameters.....	154
Figure 5.44. Effect of radiation resistance on the waveform .....	155
Figure 5.45. Effect of changing radiation resistance on the waveform parameters .....	155
Figure 5.46. Effect of increasing the body capacitance on the waveform .....	156
Figure 5.47. Effect of changing body capacitance on the peak current .....	156
Figure 5.48 shows that capacitance is linearly related to the total charge transfer, which is according to our expectations (2.4 times increase in charge transfer after capacitance is multiplied by 4). Variations of the spark length, as noted before, does not influence the area under the current waveform. ....	156
Figure 5.49. Effect of changing body capacitance on transferred charge .....	157
Figure 5.50. Effect of changing body resistance on the waveform (Left: Estimated waveform until 500 ns), Right: Estimated Waveform until 25 ns) .....	157
Figure 5.51. Effect of changing body resistance on the waveform parameters .....	158
Figure 5.52. Top: Comparison between simulation results with and without adding the short wire, Bottom: Zoomed view of the top figure to show the changes in the rising edge.....	159



Figure 5.53. Effect of the speed of approach and the spark length at 1.5 kV for dry and humid air, from Pommerenke [31] .....	162
Figure 5.54. Effect of the speed of approach and the spark length at 9.9 kV for dry and humid air, from Pommerenke [31] .....	162
Figure 5.55. Comparison of the 1.5 kV discharge in dry and humid air at various speeds of approach (subject lying down on the bed, metal piece on hand) .....	164
Figure 5.56. Comparison of the 9.9 kV discharge in dry and humid air at various speeds of approach (subject lying down on the bed, metal piece on hand) .....	165

# 1. Introduction

Wearable medical device market is expected to reach 34\$ billion by 2020 [1], owing to the growing need for treatment of chronic diseases for the ever-increasing aged population, particularly in the US. Examples of these devices are infusion pumps, wearable cardioverter defibrillators, health and fitness monitors. These devices are designed to remain attached to patients while performing daily activities. Some of these wearable devices (e.g., insulin pumps) are life-sustaining and the patient lives depend on their functionality, thus they need to be consistently attached to the patient's body. Since the body can be assumed as a weak conductor of electricity, the wearable device and the body can be assumed equipotential.

Discharges of accumulated charges while performing various activities can expose the device to an unwanted source of electromagnetic energy, called electrostatic discharge (ESD). During various routine activities such as walking on a carpet, static charges on the subject's body can be accumulated, discharges to the ground (e.g., touching a door knob), a significant amount of charge is released during the discharge process. This discharge current may enter the internal circuitry of the wearable device and transient disturbances and/or the damage to the integrated circuit may occur if the device is not protected against the ESD current.

In a hospital environment or at home, many routine activities result in the accumulation of electrostatic charge on a patient wearing a wearable medical device and other equipment such as beds and carts. For instance, walking on a carpet, sliding a patient with transfer

boards, sitting or lying down on a hospital bed result in charge buildup on the patient's body or hospital personnel. ESD events due to electrostatic charging of patients have resulted in medical device malfunctions such as data corruption and changes in the settings of cochlear implants [2], changes in the baseline sensor reading of intracranial pressure monitors [3], or controller reset in a ventricular assist device that resulted in two deaths and four injuries [4], [5]. Over the 10-year period of January 2006 to December 2016, the adverse event database of the U.S. Food and Drug Administration (FDA) [6] contains 1342 malfunction reports, resulting in 5 deaths and 46 injuries. Among these adverse events, 196 reports, consisting of all the deaths and 20 injuries, associated with wearable devices including infusion pumps, heart assist devices, and neurostimulators. These devices are labeled as class III, which require the highest reliability considerations among all classes of medical devices.

The family of standards for medical devices, recognized by the FDA, is the IEC 60601-1-2, and it calls for ESD testing according to the test method specified in the IEC 61000-4-2. To prevent device malfunctions, these ESD immunity standards need to represent the “reasonably foreseeable maximum severity” during usage [7]. A critical challenge is to identify and characterize the activities leading to severe discharges of a wearable medical device, in terms of the body postures, device locations, and the discharge setup. Moreover, hazard reduction measures need to be employed in healthcare facilities where the wearable medical devices are used. Therefore, the materials involved in these activities and the associated environmental conditions need to be identified.

### *1.1. Research Questions*

This study was mainly focused on answering two research questions as follows:

- 1) Does the existing ESD standard provide sufficient immunity against realistic discharges in the field for wearable medical devices? In other words, is the ESD test procedure for these devices severe enough to represent the reasonably foreseeable maximum voltage level during usage?

The first step to answer this question is to identify the activities that result in severe charging of a wearable medical device (exceeding the standard test levels). Then, the charging voltages while performing these activities need to be compared with the maximum test limit in the standard. The final step is to compare the current waveform resulting from the severe discharges identified in the first step, with the standard waveform. This comparison will explain whether the standard test method provides sufficient immunity against discharges during usage.

- 2) Can a circuit representation of the discharge events be developed to predict the resulting current waveform based on physical elements of the setup?

To answer this question, the electrical impedance of each element in the discharge setup including the human body in the specified posture and location on the body and the discharging structure. Then, the simplified RLC representation of the elements needs to be found and integrated with an electrical model of the spark. This prediction model can be used by manufacturers to virtually assess the immunity of wearable devices in the field.

## *1.2. Dissertation Outline*

The work presented in this dissertation consists of two main parts: the identification and analysis of a list of severe charging activities in a healthcare environment, and the measurement and the development of a circuit model for the discharges in the identified activities and configurations. Chapter 2 discusses the background of the study including electrostatic charging mechanisms, characteristics of ESD waveform, and the relevant standards on ESD control in healthcare and wearable medical devices. A review of literature is provided in chapter 3 for both electrostatic charging of human body and the analysis of the discharge waveform from a charged person. This chapter ends with a discussion of the research gaps in literature on both parts of the dissertation.

Chapter 4 presents our investigation of electrostatic charging conditions and activities of a human body in healthcare facilities. Chapter 5 describes the discharge configurations, ESD and impedance measurement setups, and the equivalent circuit model to predict the current waveform. The developed circuit model is then analyzed to investigate the effect of model parameters on the waveform, and the results are compared with the measurements in our setup, as well as previously published literature. The contributions of the work are explained in chapter 6. The appendix and references are provided in chapters 7 and 8.

## 2. Basics of Electrostatic Discharge (ESD)

ESD is the rapid transfer of electrostatic charge between two objects at different electrical potentials. This process could occur when the local electrostatic field between the two objects exceeds the electrical breakdown strength of the surrounding medium. ESD cannot be felt by people until the voltage exceeds almost 3kV [8], and a visible spark develops at much higher voltages.

Accumulation of electrostatic charge mostly occurs during contact and separation of two objects, a process known as *triboelectric charging*. Static charge buildup can also occur due to less common ways such as electrostatic induction (due to the electrostatic field from nearby charged insulators), ion bombardment, or contact with another charged object [9].

When a charged person touches a grounded electronic equipment, an ESD occurs that has a current level sufficient to burn internal circuitry or cause dielectric breakdown in the electronic equipment. If the discharge current directly enters the internal circuitry, it can destroy the electronic components resulting in an unrecoverable damage. ESD can also cause indirect damage due to the electromagnetic (EM) fields associated with the time-varying discharge current. The discharge current, which has a short duration (less than 100 ns), generates a transient EM field that couples into the traces in the circuitry, and induces voltages exceeding the noise margin of logic devices, leading to data corruption [10]. This type of damage is recoverable, however, in life-support applications, such as medical devices, even a temporary malfunction can jeopardize the patient's safety [4].

This chapter discusses the background information about ESD including triboelectric charging mechanism, characteristics of an ESD event (e.g., discharge current waveform and severity parameters), and a review of standards for ESD immunity of wearable medical devices.

### *2.1. Charge Buildup Mechanisms*

The process of generating electricity by friction is called triboelectric charging. Figure 2.1 illustrates a simplified charging mechanism of materials A and B before and after triboelectric charging. Both materials are neutral before making contact, as they have the same number of electrons and protons. After contact and separation (e.g., due to friction), one of the electrons on the outer orbital of material A moves to material B. Therefore, material A loses an electron and acquires a net charge of +1. Material B gains an electron and its net charge will be -1. A common example of triboelectric charging occurs when a person walks across a carpet and the friction between the shoe sole and the carpet causes charge buildup on the person. Simple daily activities such as walking on a carpet or vinyl tiles can generate voltages as high as 5kV [11].

There are many factors that influence the amount of charge transfer in a triboelectric charging process, such as the area of contact, the speed of contact and separation, the chemistry of materials (i.e., electronic affinity), surface cleanliness, and relative humidity (RH) [12]. Two critical parameters that are analyzed more often in triboelectric charging studies are the electron affinity [13]–[15] of the contacting materials (i.e., material combinations) and the RH level of the environment[16]–[18]. These two factors are explained in the next sections.

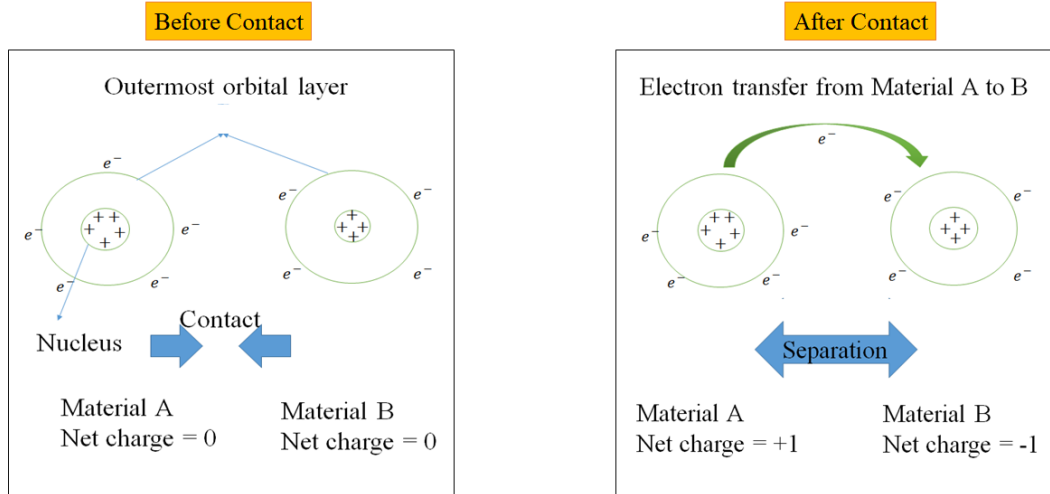


Figure 2.1. Electronic structure of materials A and B before (left figure) and after triboelectric charging (right figure)

## 2.2. Characteristics of ESD Events

ESD literature, often study severity of an ESD event in terms of the charging voltage, and the resulting current and transient electromagnetic field waveforms. This section presents a simplified electrical representation of the discharge process, and the common approach to characterize the severity of an ESD event.

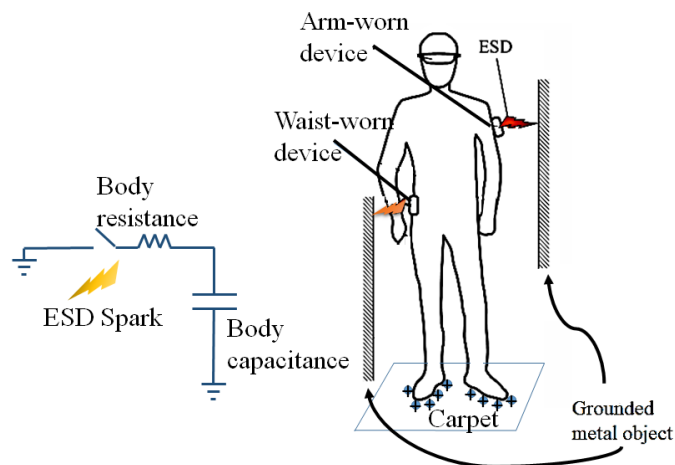
### 2.2.1. ESD Circuit Model

Figure 2.2 shows a person standing on a carpet with wearable devices mounted on his body. Due to triboelectric charging between his footwear and the carpet, static charges are accumulated on his body, and the wearable devices are at the same charging voltage of the person. Due to the insulating properties of the footwear and the clothing, the accumulated charges remain on his body until the person touches the ground. The person is considered an electrical capacitor. While touching a grounded metal object, an ESD spark occurs and



the accumulated charges in the capacitor (i.e., human body) transfer to the ground. The discharge path has a resistance, that is associated with the human body and the wearable device.

The charge transfer process during an ESD event is similar to charging and discharging of an RC circuit is shown in Figure 2.2 and Figure 2.3. During the charging process, the capacitors  $C_s + C_d$  are charged via a high voltage DC power supply and a resistance,  $R_C$ , as shown in the left side of Figure 2.3. The total electrical capacitance of the charging person is denoted by  $C_s + C_d$ , where  $C_s$  is the energy storage capacitor (capacitance of the human relative to ground), and  $C_d$  is the distributed capacitor (capacitance relative to the surrounding walls). Once the charge switch is on, the power supply charges the capacitor. Due to the high resistance of the charging circuit,  $R_C$ , (e.g., the resistance of the footwear) usually a long time is required for the capacitor to get fully charged (compared to the time spent during the discharge process). The voltage of an ESD event is the electrical potential across the capacitance of the object with a higher electrical potential than the other.



*Figure 2.2. ESD from wearable devices mounted on a charged subject to grounded metal objects*

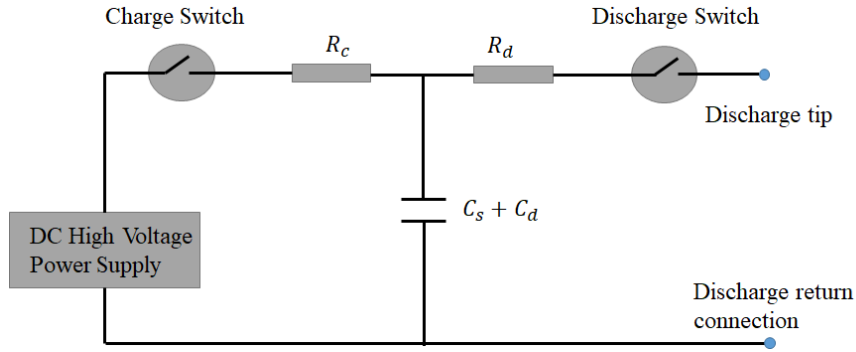


Figure 2.3. An RC circuit that describes the charging and discharging process during an ESD event

Once the capacitors are fully charged, and the discharge switch is turned on, the accumulated charges in the capacitor releases to the other object (at a lower electrical potential) via a discharge resistance  $R_d$  (right side of Figure 2.3). This resistance is different from the charging resistance  $R_C$ , since the discharge process involves a different current path than the charging process. For instance, when a charged human body is holding a key in his/her hand, touches a metallic door knob (at a lower potential than the human body), the accumulated charges on his/her body quickly transfers to the door knob via the key. In this example, the discharge current path involves the key held in the person's hand, while  $R_C$  is the resistance of the footwear.

### 2.2.2. ESD Current Waveform

Figure 2.4 shows an example of ESD current waveform caused by an ESD generator charged at 1kV. An ESD generator simulates an ESD event from a charged human body holding a metal rod and discharging to a vertical ground plane, known as the human metal model (HMM). The magnified portion of the peak is shown in the lower right corner. Three parameters of peak ( $I_{max}$ ), maximum time derivative (i.e.,  $\left(\frac{dI}{dt}\right)_{max}$ ), charge transfer during

the ESD event  $Q_{ESD}$ , and the rise time,  $T_r$ , are typically extracted from the waveform [19]. The rise time is defined according to the IEC 61000-4-2 standard for ESD immunity of electronic equipment, by extracting the time interval between 10% and 90% of the peak. The charge transfer  $Q_{ESD}$  can be calculated by integrating the area under the current waveform:

$$Q_{ESD} = \int_0^T i(t) dt \quad (1)$$

where  $T$  is the time at which current approaches zero (e.g., 500 ns) It has been shown in many ESD studies that susceptibility of a device to ESD failure depends on its design and a weighted combination of these parameters [20], [21]. Severity of an ESD event increases with the larger voltage,  $I_{max}$ ,  $\left(\frac{dI}{dt}\right)_{max}$ , and  $Q_{ESD}$ , and decreases with  $T_r$ . Unrecoverable damage to electronics is caused by sufficiently high  $I_{max}$  and  $Q_{ESD}$ , whereas, soft failures such as unexpected resets, and software issues are usually associated with sufficiently fast  $T_r$  and large  $\left(\frac{dI}{dt}\right)_{max}$  [22].

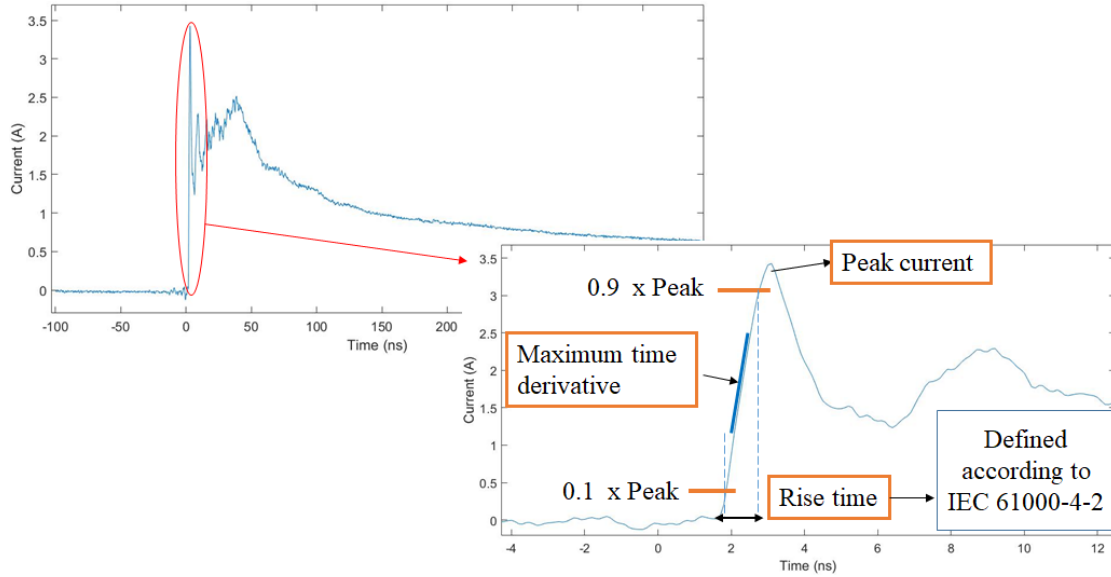


Figure 2.4. Severity parameters of an ESD current waveform

### 2.2.3. Contact and Air-Mode Discharges

In ESD studies, two types of discharges are often investigated: contact-mode and air-mode ESD. These two discharge conditions result in different waveforms given the same voltage levels, due to the presence of an air spark in the air-mode ESD. In contact-mode ESD, the discharge process occurs when the tip of the ESD gun touches the equipment under test (EUT), and there is no spark between the tip and the ground. However, the realistic discharges often involve a spark between the two approaching objects. The nonlinear behavior of the air spark is one of the most critical challenges of studies on air-mode ESDs, since the tests are not repeatable, due to its dependence on the environmental condition, approaching speed and the spark length [23]. Thus, the initiation of a realistic discharge process cannot be simulated as a switch, similar to Figure 2.3, due to the impedance of the air gap. Rompe and Weizel [24], developed a time-varying resistance model for the air spark, which has been shown to be effective in simulating ESD events:

$$r_{air\ gap}(t) = \frac{l}{\sqrt{2K_R \int_0^t i^2(\tau) d\tau}} \quad (2)$$

where  $K_R$  is a constant related to gas pressure, and  $l$  is the spark length. This model suggests that the spark acts as a time-varying resistance. The underlying assumption is that the conductivity of the spark depends proportionally on the dissipated ohmic energy [23]. If the spark occurs in a gas confined between two stationary planar electrodes, the spark length can be estimated from the Paschen's law:

$$U = 25.4l + 6.64\sqrt{l} \quad (2)$$

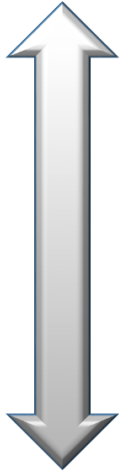
where  $U$  is the input voltage in kV and  $l$  is the spark length on cm. Changing the shape of the electrode will affect the spark length in Paschen's law. In fact, the spark length for sharper electrodes is longer than round ones. The Paschen's law estimation usually provides reasonable results for estimating the spark lengths from round electrodes, which is the common shape of air-mode discharges in ESD literature [22]. However, during some ESD events, the real spark lengths are smaller than the predicted value by Paschen's law [25], due to the statistical time lag (will be explained in section 2.4).

An air-mode ESD compared to contact-mode ESD, results in lower  $I_{max}$  at a given charging voltage (and the same discharge path), due to the resistance of the spark. For two air-mode ESD events at the same charging voltage (and the same discharge path), the one with shorter spark is more severe due to lower spark resistance, which results in higher  $I_{max}$  [26]. Moreover, since the rising edge of the ESD waveform (and the rise time) depends on the spark length and the applied voltage, the waveform with shorter spark length results in a faster rise time and larger  $\left(\frac{dI}{dt}\right)_{max}$ .

### 2.3. *Effect of Material Combination on Electrostatic Charging*

The amount of charge buildup is often related to the difference between the electron affinity of the materials involved in the triboelectric charging [13]–[15]. Electron affinity is a material property indicative of its tendency to gain or lose electrons. When different materials are brought into contact during a triboelectric charging process, the one with lower electron affinity loses some electrons and becomes positively charged, while the other gains the released electrons and becomes negatively charged. The electron affinity of materials is often shown in a table called *triboelectric series* (Table 1). For instance, if a nylon cloth is rubbed against a piece of paper, it acquires a positive charge, since it is upper than paper in the triboelectric series. On the other hand, paper gains negative charge during this triboelectric charging process. This table is also useful for comparing the relative magnitude of the charge transferred between pairs of materials. A pair whose materials are farther apart in the triboelectric series results in higher amount of charge transfer than a pair whose materials are closer. For example, a higher amount of charge is transferred between brass and glass compared with silk and wool.

Table 1. Triboelectric series table

Electric Charge	Material
 <p>Positive</p> <p>Negative</p>	Air
	Glass
	Human hair
	Nylon
	Wool
	Silk
	Aluminum
	Paper
	Wood
	Nickel, Copper
	Brass, Silver
	Gold, Platinum

#### 2.4. Effects of Ambient Relative Humidity on ESD

ESD events are more frequently reported during cold and dry environments [6]. It is commonly known that lowering RH levels results in stronger ESD events with higher voltage levels, most likely due to the higher surface resistivity of materials which results in stronger triboelectric charging. However, many materials exhibit the opposite trend or unaffected by RH level [27].

Adding moisture to the environment using humidifiers is a common practice in the electronic industry to reduce the risk of ESD in manufacturing and assembly areas [28]. In some electronic facilities, the RH level of the work areas need to be kept above a minimum threshold (e.g., 30%) as part of the ESD control program. Adding moisture to the air results in precipitation of a conductive layer (i.e., water) on the surface of materials. This moisture

layer contributes free charge carriers and in general, reduces the surface resistivity of materials [29]. Moreover, if the moisture layer extends to a grounded object, accumulated charge on the material can be dissipated to the ground prior to a discharge to another object.

Ambient RH can also affect the severity of an ESD event due to a phenomenon called *statistical time lag* [25]. Lowering RH can result in shorter spark lengths and stronger ESD events [23]. During an ESD event, a dielectric breakdown occurs in the medium between the two objects involved in the discharge event. This breakdown process occurs when the electrostatic field confined between the contacting edges of the two materials exceeds the dielectric strength of the medium (usually air). However, the breakdown process does not immediately occur, unless “seed electrons” are present on the surfaces of the contacting materials [25]. These electrons supposedly initiate the avalanche process. Thus, lack of sufficient seed electrons delays the onset of discharge [25]. Since during the discharge event, the two objects are constantly approaching, this delayed discharge results in a shorter spark length, and consequently, a more severe discharge occurs. This condition occurs at low RH levels due to insufficient seed electrons length [30][31]. However, in humid conditions, the electrons of the water molecules on the tip of the contacting objects act as seed electrons for initiating electron avalanche and formation of a spark. Therefore, spark length in humid conditions are expected to be longer than dry conditions, which results in less severe ESDs.

## 2.5. ESD Immunity Standards for Medical Equipment

ESD immunity standards in the electronics industry include component-level testing, system-level testing and material and factory standards [33]. The component-level testing deals with ESD immunity of packaged semiconductor components, and the material and



factory testing involve ESD control programs in the electronic manufacturing environment, such as the material conductivity of footwear, wrist-straps and grounding systems. This study, however, focuses only on system-level testing, which addresses the susceptibility of electronic systems to ESD malfunction after the manufacturing process, for instance during shipping, handling, and final usage.

U.S. FDA's regulations for medical devices is based on their assigned classifications. There are 3 classes for medical devices, based on the associated risks: class I (e.g., handheld surgical instruments), class II (e.g., powered wheelchairs), and class III (e.g., wearable cardioverter defibrillators, infusion pumps, and neurostimulators) [32]. Many of the wearable medical devices, such as wearable cardioverter defibrillators, infusion pumps, and neurostimulators are considered as class III medical devices, which require the highest reliability among all classes of medical devices.

According to the FDA's regulations, manufacturers of class II and III devices are required to demonstrate that the device is as safe and effective as a legally marketed device [33]. Manufacturers can prove effectiveness and safety of their products by testing according to selected voluntary standards recognized by the FDA. The IEC 60601-1-2 is a widely recognized collateral standard that provides general requirements and test methods for electromagnetic compatibility. Regarding ESD immunity of medical devices, this collateral standard requires compliance to IEC 61000-4-2 test method at certain voltage levels. Until December 31, 2018, FDA recognizes the 3<sup>rd</sup> edition of the IEC 60601-1-2 standard, in which ESD testing is required at  $\pm 6$  kV contact mode and  $\pm 8$  kV for air-mode discharges. For home use medical devices, FDA currently recommends that devices for which conformity is claimed to the 3<sup>rd</sup> edition, be tested to higher immunity test levels,

including maximum levels of  $\pm 8$  kV for contact discharge and up to  $\pm 15$  kV for air discharge mode for ESD testing. This higher voltage level for home use devices is due to the potential higher ESD risks compared to a hospital environment. Wearable medical devices are often classified as home-use devices since they need to remain attached to the patient's body during everyday activities. After December 31, 2018, the FDA recognizes the 4<sup>th</sup> edition of the IEC 60601-1-2. This edition specifies that manufacturers need to identify the pass/fail criteria during and after performing the compliance tests. These criteria are based on the consequences of degradation of the device performance or failure caused by the ESD test. Performance degradation is allowed during the test, as long as failure mode does not adversely affect the patient's health after performing the test. For instance, many manufacturers argue that it is acceptable if the device shuts down and require user intervention to restart.

The test levels specified in the 4<sup>th</sup> edition of the IEC 60601-1-2 standard are considered to be “reasonably foreseeable maximum”, not the absolute maximum. To demonstrate that the test levels are insufficient, electrostatic charging experiments need to be performed and large datasets need to be obtained to convince the standard committee and the manufacturers. Thus, higher test levels could be adopted in the next edition of this standard, which is scheduled to be published in 2024. However, medical manufacturers are already having difficulty meeting the 15 kV air discharge requirement in the 4<sup>th</sup> edition.

#### *2.6. IEC 61000-4-2 Standard Test Method*

The IEC 61000-4-2 standard specifies the test configurations for ESD testing of electronic equipment. An ESD generator is injected to the exposed ports and surfaces of an electronic equipment. The injected ESD pulse to the equipment under test (EUT) represents

the HMM discharge scenario as shown in Figure 2.5. The standard claims that “... this metal discharge situation is sufficiently severe to represent all human discharges in the field” [34].

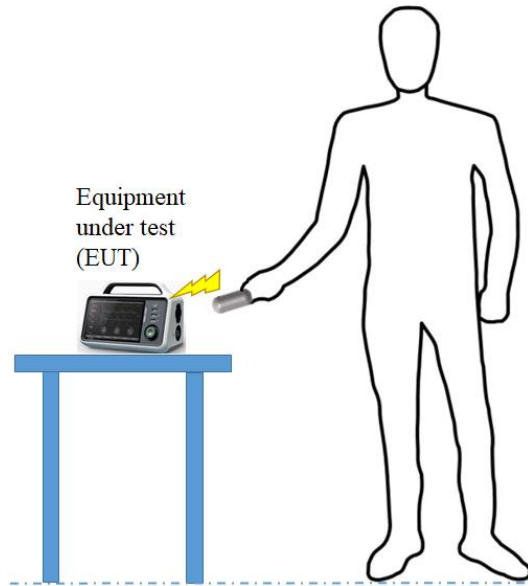


*Figure 2.5. ESD testing according to the human metal model*

The internal circuitry of the ESD gun is designed according to the electrical properties of a human body during an HMM ESD event. Figure 2.6 shows an RC circuit that simplifies the discharge process from a charged human body. The discharge path involves a capacitor,  $C_d + C_s$ , of 150 pF that represent the capacitance of a standing human body, and the resistance  $R_d$  refers to the person’s arm resistance combined with the resistance of the metal object in the person’s hand. In reality, the internal circuitry of the ESD gun is much more complex than a simple RC circuit, however, this model is still used as a simplified network representation of the ESD gun in the IEC 61000-4-2 standard.

Two types of ESD tests are applied to the EUT: direct contact and air-mode discharges. The direct mode requires the injection of the pulse once the tip of the ESD gun

makes physical contact with the EUT. Therefore, no spark occurs between the tip and the EUT. During air-mode tests, the gun approaches the device while holding the trigger, and a spark occurs between the tip and the EUT (Figure 2.7). Air-mode tests are injected to insulating parts of the EUT, while contact-mode tests are delivered to conductive exposed surfaces, peripheral ports, LCD or keypad. The tip of the gun for contact mode tests is sharp so that it can touch the EUT and no spark occurs between them. However, the tip of the ESD gun is rounded to facilitate the spark (Figure 2.7).

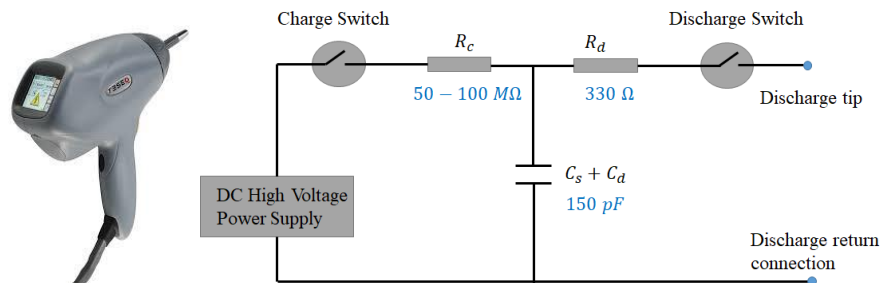


*Figure 2.6. An ESD gun (left) and its simplified equivalent RC network representation (right)*

If the ESD gun directly discharges to the insulating part without an air gap, the accumulated charges may not release to the EUT, unless an electric breakdown of the insulating material occurs. The dielectric strength of the air is typically less than other insulators, thus, if there is no air gap during an air-mode test, it is likely that the dielectric breakdown of the medium (the insulating material) does not occur. Therefore, the presence of an air gap is necessary for injecting to insulating materials.

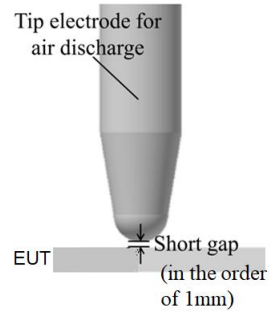


*Figure 2.7. Air-mode testing on an EUT using an ESD gun*

### 2.6.1. ESD Gun Calibration

The IEC 61000-4-2 provides the procedure for calibration of ESD guns to minimize the impact of environmental conditions on the results (Figure 2.8). Before attempting to perform ESD tests on an EUT, the ESD gun needs to be calibrated according to this setup. The ESD gun injects an ESD pulse to a current target, mounted on a vertical coupling plane (VCP). The current target is an SMA connector that is connected to a coaxial cable from an oscilloscope via an adapter. The impedance of the current target relative to ground is around  $2\Omega$ . The oscilloscope and cables are placed inside a metallic enclosure are behind the VCP to shield them from the electromagnetic coupling. This calibration setup is used for direct-contact discharges.

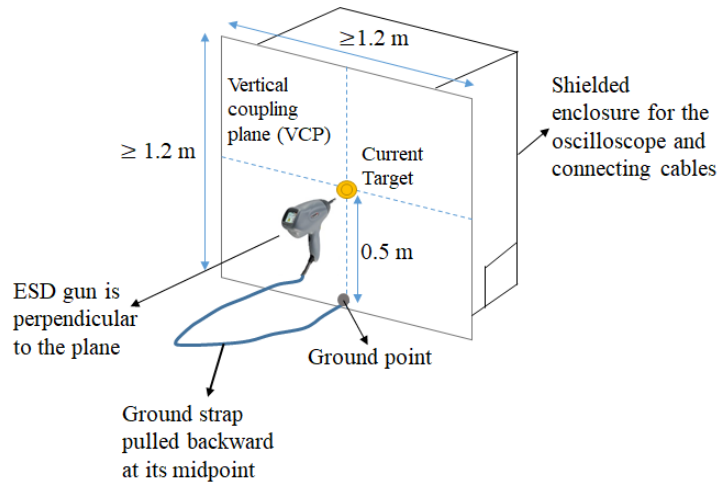


Figure 2.8. Calibration setup for an ESD gun

The IEC 61000-4-2 standard provides the current waveform parameters for ESD gun calibration, as shown in Figure 2.9 and Table 2. This waveform is different from the result expected from a simple RC network due to the pulse-generating and parasitic elements in the ESD gun [35].

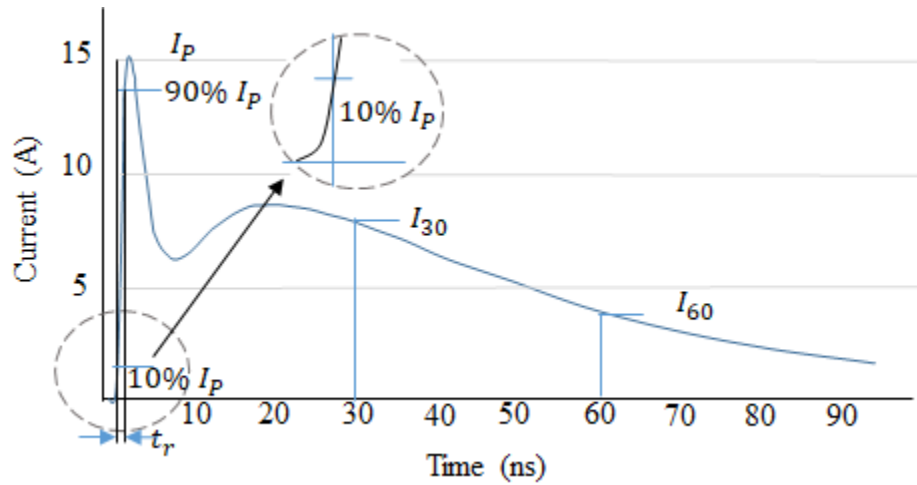


Figure 2.9. ESD current waveform specified in the IEC 61000-4-2 standard for direct-contact mode [34]

Table 2 shows the parameters of the waveform, including the peak current, and the current level at 30ns and 60ns after the initiation of the discharge event, as a function of the ESD voltage level. Peak currents are linearly increasing with the charging voltage since all the elements in the circuit are linear (i.e., RLC) and there is no spark in contact mode ESDs. It is important to note that the standard allows variation in the current waveforms of the calibration ranging between 15% to 30%, which could be due to the different construction of ESD guns and parasitic elements in the circuitry. For air discharge tests, no calibration waveform is provided due to the issues with repeatability of the tests.

After calibration of the ESD gun, ESD tests need to be performed on the EUT at voltage levels specified by relevant standards. For medical electrical equipment, the 4<sup>th</sup> edition of the IEC 60601-1-2 standard requires testing at  $\pm 8\text{ kV}$  for contact mode, and  $\pm 2\text{ kV}$ ,  $\pm 4\text{ kV}$ ,  $\pm 8\text{ kV}$ , and  $\pm 15\text{ kV}$ . The reason for including lower voltages in the air mode tests is that  $\left(\frac{dI}{dt}\right)_{max}$  increases at shorter spark lengths (which occur at low voltages).

*Table 2. ESD voltage and the parameters of the current waveform for contact mode discharges of an ESD gun in the calibration setup*

<b>Level</b>	<b>Indicated Voltage (kV)</b>	<b>First peak current of discharge( +/- 15%) (A)</b>	<b>Rise time (+/- 25%) (ns)</b>	<b>Current (+/- 30%) at 30 ns (A)</b>	<b>Current (+/- 30%) at 60 ns (A)</b>
1	2	7.5	0.8	4	2
2	4	15	0.8	8	4
3	6	22.5	0.8	12	6
4	8	30	0.8	16	8

### 2.6.2. ESD Test Setup

Two test setups for two types of EUTs are provided in the IEC 61000-4-2: floor standing and tabletop (no separate category for wearable EUTs). The common practice in

the electronics industry is to test wearable EUTs in the tabletop setup, as shown in Figure 2.10. In general, a portable device is addressed as ungrounded tabletop EUTs.

The ESD gun is injected either directly to the EUT using contact-mode or the air-mode discharges, or indirectly to a VCP located at 10cm away from the EUT. This indirect ESD testing represents the discharges from personnel to objects nearby the EUT. The indirect ESD test generates transient electromagnetic fields that can cause disturbances in the EUT. It is to be noted that indirect test is only performed in the direct contact mode.

For both direct and indirect tests, at least 10 single discharges need to be applied, with 1 second resting period between successive discharges. Both positive and negative polarities need to be applied to the EUT at each voltage level. The standard provides guidance for ESD testing both grounded and ungrounded EUTs in both categories: floor-standing and tabletop. When the ESD pulse is injected to a grounded EUT, the transferred charged from the ESD gun to the EUT will dissipate quickly to the ground. However, in the case of ungrounded EUT's, the charges might remain on the EUT after the injection of the pulse. Thus, ungrounded EUTs are connected to ground via 470  $k\Omega$  bleeder resistors to facilitate discharge.



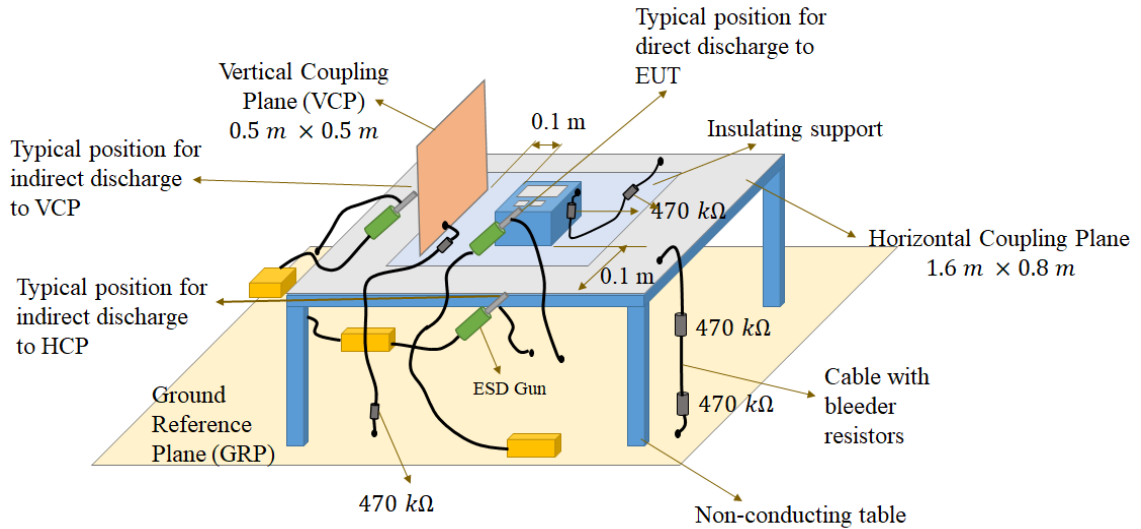


Figure 2.10. IEC 61000-4-2 standard ESD test setup for ungrounded tabletop EUTs [34]

The contact-mode discharge is only applied to the exposed points on the EUT. For a connector with a metallic shell, the discharge is only applied to the shell. ESD test should not be applied to ESD sensitive parts such as RF inputs, because they are not protected by ESD diodes due to their large stray capacitance, which will interfere with their high-speed operation.

ESD testing is usually performed in two stages: after the EUT assembly (prior to usage) and post-installation (in the usage environment). In general, ESD testing causes significant aging of EUT and cause them to fail much faster than those without any prior ESD testing. Therefore, post-installation ESD testing is not recommended according to the standard.

### 3. Literature Review

Since a wearable device is often attached to the user's body, the voltage level on the device is expected to be equal to the body's potential. Thus, to analyze the ESD risks associated with wearable medical devices, the characteristics of an ESD from a human body to ground via a metal object (i.e., in lieu of a wearable device) need to be studied. Two aspects of the ESD events are the charging voltage and the current waveform. This section discusses literature on both aspects. The first group discusses the extent of triboelectric charging of a human body while performing various routine activities and the effects of material combinations and RH levels during the activity on the voltage levels. The focus of the second group is on the characterization of the ESD waveform from a human body holding or wearing a metal piece.

#### *3.1. Human Body Charging*

The human body can be viewed as a weak conductor since it has almost 80% water content. However, footwear and clothing provide an insulating barrier that minimizes charge transfer to objects in contact with the body. Therefore, when triboelectric charging of a human body occurs during an activity, e.g., walking on a carpet, the accumulated charges dissipate slowly to the ground via the insulating footwear or neutralize via charge carriers in the air, unless the person touches a grounded object.

The triboelectric charging, however, is not the only parameter affecting the body voltage. The body capacitance, which varies according to the subject's posture and the footwear and flooring is related to the body voltage via  $Q = CV$ . For instance, the body posture while sitting on a chair with insulating sheet is different than standing up on a floor

(65 pF compared to 80 pF, measured by Talebzadeh et al. [38]) This lower capacitance results in a larger body voltage compared to previous studies, given the same amount of charge transfer ( $Q = C \downarrow, V \uparrow$ ). Therefore, the changes in body capacitance during activities need to be considered for analyzing the charging condition affecting a wearable device.

To conduct ESD testing according to the IEC 61000-4-2 test method, the manufacturer needs to determine the reasonably maximum foreseeable voltage level of ESD events in the usage environment. The 3<sup>rd</sup> and 4<sup>th</sup> editions of the IEC 60601-1-2 requires a maximum of 8 kV and 15 kV (air discharge tests), respectively. A manufacturer can adopt this standard, however, if the test voltages in the usage environment exceed this threshold, ESD malfunction might occur that may result in adverse events. Therefore, a manufacturer needs to analyze the usage environment specific to their product for the reasonably maximum foreseeable voltage levels. For a wearable medical device, the usage environment can be a healthcare facility or the patient's home. Therefore, the electrostatic charging of the person while performing routine activities in these usage environments need to be examined to investigate whether 15 kV is a reasonably maximum foreseeable voltage level. Therefore, the body voltage level during routine activities performed by device users need to be examined in a controlled setting (i.e., reproducible conditions).

The largest voltage level on a human body reported in literature is around 40 kV [36]. However, the corona discharge from the body (e.g., nose, ears) usually does not allow voltage level to reach this limit [36]. However, obtaining the absolute maximum body voltage during rare activities does not help in updating the standard test levels. Only if the voltage levels for a large fraction of the electrostatic charging tests in the usage environment of the device exceeds the standard test limit (15 kV), the voltage levels in the

standard will be proven inadequate. This section discusses the literature on triboelectric charging of human body, with an emphasis on routine activities under reproducible environmental conditions by users of wearable medical devices.

A number of papers developed simplistic human body models to study triboelectric charging during various activities that involve friction between the body and insulating materials. The most common activity studied for electrostatic charging is walking. Ficker [37] studied triboelectric charging due to walking on a resistive flooring. He developed a variable capacitance model of the human body, based on the distance between each foot and the ground.

The amount of charge accumulated on the body during walking was found to be dependent on the step height as a function of time, the surface area of the foot and the dielectric strength of the footwear. It was also found that during this charging process, the amount of charge accumulated on the person's body over time asymptotically approaches a constant value known as the saturated potential. This means that the amount of charge has an upper bound if the same activity is repeated over time. However, the voltage ranges are much lower than the test levels of the IEC 60601-1-2, therefore, walking may not be considered as a critical charging activity.

Pirici et al. [38] measured the triboelectric charging of a human body while exiting a car -seat, and developed a physical model to predict the body voltage over time. The high voltage rise (as high as 16kV) that occurs when exiting a car was found to be related to change in body capacitance at the seat/clothing interface. During the separation from the car seat, the capacitance of person's clothing relative to the seat changes from 8 nF inside

the car to 1 pF outside the car, which results in an increase in the body voltage and ESD occurrence when a passenger leaves a car.

A number of studies investigated the risk of ESD in data centers through a series of laboratory experiments on human body charging in different RH levels, activities and material combinations [11], [39], [40]. These studies investigated triboelectric charging in four operating envelopes shown in Figure 3.1, while walking, removing a garment and sitting on an office chair. The amount of charge generated during these activities performed by a subject was measured at the operating points shown in Figure 3.1. The materials used for footwear and flooring ranged from electrically insulating to conductive. It was found that using conductive footwear and flooring significantly reduce charge buildup (2 to 5 for garment removal, and 2 to 7 for sitting on a chair). These studies suggest that data centers that operate in the widest range of RH (i.e. A3 and A4) need to be equipped with conductive flooring and user's footwear need to be conductive, to mitigate the risk of ESD.

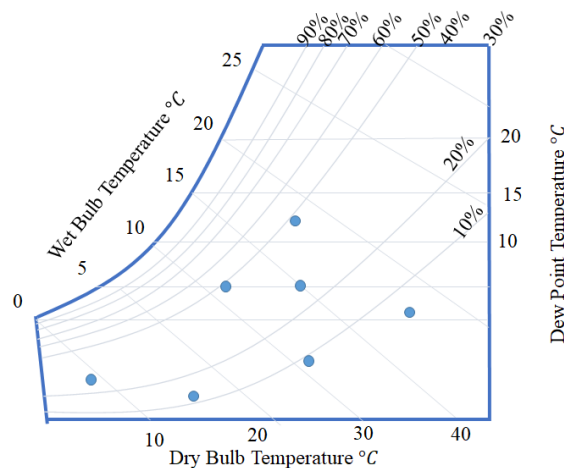


Figure 3.1. The RH and temperature conditions for seven points tested in Talebzadeh et al.'s study [29]

Talebzadeh et al. [39] measured triboelectric charging voltage while removing a sweater. The voltage waveform during the sweater removal experiment showed that the peak body voltage occurs at the moment of dropping the sweater. At this point, the accumulated negative charges on the body are no longer neutralized by the positive charges on the garment, thus the body voltage increases abruptly.

The aforementioned studies were not specific to any usage environment since they focused on routine everyday activities of a human body that can result in electrostatic charging. However, the usage environment for wearable medical devices can be a healthcare facility, where different charging activities than those mentioned previously, need to be considered. Hospital staff and patients perform a variety of activities that involve friction between large portions of the human body on insulating items and result in significant charging of the human body. For instance, handling and exchanging blankets on hospital beds, transferring a patient from a stretcher to a bed, rolling medical carts and wheelchairs, sitting and lying down on a hospital bed or the patient table in an imaging system (e.g., X-Ray, MRI). Since the magnitude of triboelectric charging depends on the area of contact, the human body charging is expected to be more severe in a healthcare facility than other environments.

The results of the aforementioned studies on charging level of a human body could be well applicable for the consumer wearable electronics. However, the criticality of wearable medical devices, in comparison with consumer electronics, is the consequences of failure. An ESD malfunction in wearable medical devices, can result in interruption of delivery of therapeutics or monitoring of vital signs of the patient, which can lead to adverse events such as injury or death. Therefore, the analysis of electrostatic charging for wearable

medical devices need to be considered in a wide range of activities and environmental conditions. The body capacitance of the patients during clinical activities such as lying down or sitting on the bed with respect to the hospital bed, affect the amount of body voltage. To our knowledge, only a few studies exist on analysis of triboelectric charging in healthcare environments, and a majority of them are only reports or observations, rather than a systematic design of experiments to explore the extent of the problem. In a study by Holdstock and Wilson [41], the extent of the electrostatic charging of personnel while exchanging hospital-grade bedding materials from a hospital bed was analyzed. Rubbing and separation of textile fabrics cause charge buildup on the fabrics and the nurse who handles them since the person is separated from the ground via insulating footwear or flooring. Bedding materials used in this experiment were modacrylic, and normal and flame-retardant cotton and polyester blankets. Bed removal was performed using two methods of pulling the sheets off the bed and folding them. Then one of the subjects holds the item of bedding close to his body, and the maximum voltage level on his body was recorded using an electrostatic voltmeter. The results for the voltage levels on bed frames showed that folding method results in lower values than pulling, which can be attributed to the lower area of contact between the blankets in the latter approach. The highest recorded voltage level resulted from pulling a combination of modacrylic and polyester blankets, which lead to over 20 kV on the bed frame and over 38 kV on the subject holding the folded blanket. Treatment of the blankets with fabric conditioners was found to reduce the voltage levels. The results indicate that bed frames and hospital personnel should be earthed to avoid charge buildup and minimize the risk of ESD. Other recommendations included

using low resistance bedding material, treatment with antistatic agents or low-friction removal of bedding, instead of pulling method.

The main objective of Holdstock et al.'s study [41] was on the ignitability of blankets due to electrostatic charging, however, this problem is not common in today's healthcare facilities due to the limited use of flammable anesthetic agents.

Viheriakoski et al. [42] performed an observation of electrostatic risks in a hospital in Finland. A survey was performed among the hospital personnel about the ESD nuisance in winter and hospital items with which most discharge experiences occurred. It was found that most of the personnel experienced a discharge event when touching patient beds and metallic parts of elevators. This study also reported voltages above 20 kV on personnel and more than 30 kV on a patient bed. This study only reported the voltage measurement results, rather than the personnel activities and the environmental conditions that led to the observed voltage levels.

In another similar observation [43], body voltage of the hospital staff was monitored during normal activities such as standing up from a chair or handling a patient blanket in an operating room. More than 20 kV was measured on hospital staff, while the RH level was about 10%, the personnel was wearing insulating footwear. This study suggested minimizing the ESD risk by covering the operating rooms with static dissipative flooring and the personnel need to wear static dissipative footwear.

The analyzed reports and studies on the triboelectric charging of human in healthcare applications were mostly observations of charge buildup in hospitals, rather than systematic laboratory research. The only systematic studies on human charging that was



found in the literature were focused on data centers [11], [39], [40], and only considered three activities of walking, garment removal and sitting/rising from a chair. Although these triboelectric charging activities are valid for any environment, activities that are specific to hospitals and cause higher voltage levels (e.g., lying down on a hospital bed) need to be considered. The only systematic study aimed at triboelectric charging activities in hospitals was Holdstock and Wilson's [8] study. However, this study only focused on an activity (i.e., blanket handling) that causes charge buildup on the hospital staff. Although nurses and personnel can interact with wearable devices and their body voltage is important, it is more useful to analyze the charging voltage levels of patients (who wear these devices) during clinical activities.

### 3.2. *ESD Current Waveform from a Charged Human*

Reviewing the literature shows four main scenarios for discharge events involving wearable devices: 1) When a person picks up the device, ESD might occur while touching the device. This is essentially the HMM scenario if the person is holding a metal object and touching the device with it. 2) ESD might occur when removing a device from the body and placing it on the ground. This condition involves a discharge between the device, charged at the electric potential of the body, and the ground. 3) When the person is wearing the device and accidentally touches a grounded object (without a direct contact with the device), the resulting ESD event creates transient electromagnetic fields that may couple into the circuitry and cause malfunction. This is an indirect type of ESD which is less severe than the first two scenarios that result in direct discharges. 4) When the wearable device directly touches a grounded object, an ESD might occur. This type of ESD is called brush-

by scenario. 5) While removing a garment, a discharge event might occur between the layers of clothing and the device itself. The most severe discharges among the remaining scenarios depend on the impedance of the discharge path and need to be investigated. In this research, only the brush-by and the HMM scenarios are investigated. This section presents a review of the literature for these scenarios.

For simulation of the discharge current, the electrical impedance between the human body and the ground need to be known. The setup shown in Figure 3.2 can be used to measure the impedance of the body seen at the point of discharge, i.e., hand, using a vector network analyzer (VNA). The impedance for ESD modeling,  $Z(s)$  is provided as a function of frequency, typically in the range of 1 MHz to 1 GHz. The measured impedance can be directly used to estimate the discharge current  $I(t)$  from the Ohm's relationship in the frequency domain,  $I(s) = \frac{V(s)}{Z(s)}$ , and performing an inverse Fourier transform of  $I(s)$ . Another approach for current estimation is to identify an RLC representation of the system and solve the circuit model for current.

The discharge event for contact mode tests can be simulated by a switch. In other words, the body voltage can be assumed to change from a constant value to zero in a stepwise manner at the moment of discharge. In contrast, this switch assumption does not work in air mode tests, in which the spark resistance and its rise time need to be integrated into the circuit model via the Rompe-Weizel's resistance model. This calculation is often performed via a SPICE simulator. More discussion about the details of the current estimation and the impedance measurement setup are provided in chapter 5.

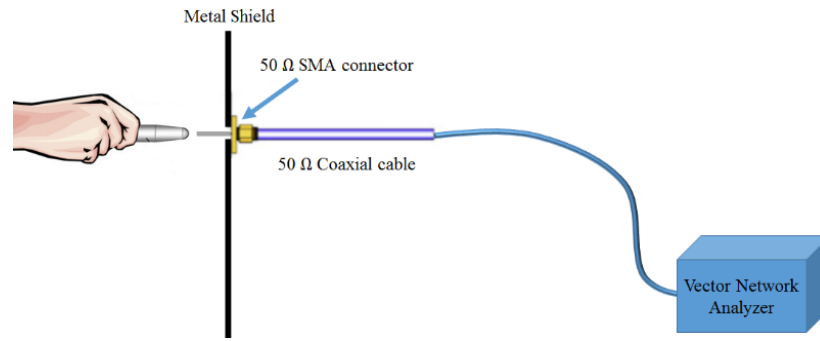


*Figure 3.2. Setup for impedance measurement (between the body and the grounded metal shield)*

Many studies on human ESD are focused on the first ESD scenario, i.e., HMM. Pommerenke and Aidam [44] investigated the discharge current from a charged human in a standing posture, holding various metal pieces with different arm postures (stretched out and bent), and compared the results with the currents from ESD simulators. The ESD current from a person charged at 1 kV was calculated using the impedance data over a range of frequencies (300 kHz to 3GHz), and the results were compared with the measurement data. Due to the body low voltage, the spark was simulated as a switch. This over-simplification of the arc behavior resulted in the overestimation of the peak current. This article also calculated the current waveform for 5kV air-mode discharge of a human, using the Rompe-Weizel's model for spark resistance. however, no current measurement was performed for this input voltage. Since ESD generators have a fixed rise time (about 0.7 ns to 1 ns), the spark length for 5kV ESD from the human was selected to match the rise time of the ESD gun. the current waveform has 1 ns rise time. Since no current measurement was performed, the validity of the rise time assumption could not be justified.

While the calculation showed that the human ESD can result in discharge current up to  $10\text{ kV/A}$ , the ESD simulator, calibrated according to the standard IEC 801-2 (an earlier version of the IEC 61000-4-2), produced a much lower value of  $3.75\text{ kV/A}$ .

Pommerenke [23] measured the discharge current from a human holding a small rod charged spheroid rod and simulated the results using 3 common spark resistance models of Rompe-Weizel law, Toelpler and electron avalanche model, at 1.5 kV to 10 kV). The simulation model for human ESD was based on method of moments and a 2D model of a spheroid that represents the hand metal configuration. One of the main advantages of the method of moments (MOM) in solving the ESD simulation of human discharge is the ease of computation compared to the conventional methods such as finite element methods. The spark length was found to have a significant influence (up to 3 orders of magnitude) on the peak current and its maximum derivative. Estimations using Rompe-Weizel's law was found to be closer to the measured data.

Jobava et al. [45] measured the ESD current from a human body holding a small metal rod and developed a computer simulation to estimate the ESD waveform using the Rompe-Weizel's model and a 3D model of a spheroid configuration. The reason for this 3D model was to evaluate the electromagnetic fields resulting from the ESD events.

Using the method of moments in the time domain, a simulation model was developed to estimate the discharge current and the transient electromagnetic field from a voluminous object (i.e., spheroid). At 10 kV charging voltage, the discharge current from a charged human holding a metal rod (8 mm diameter, 75 mm long) was measured and compared with the simulation model of a spheroid. A range of spark lengths between 0.5 mm to 3 mm was considered to estimate the current and electromagnetic fields using the

Rompe-Weizel's spark resistance model. In contrast to previous ESD studies, the gas constant in the spark resistance model was varied at each spark length, based on current measurement. Good agreement between the spheroid simulation and measurement results for the current waveform parameters was obtained. The main finding of this study was the strong influence of spark length on the severity of the current waveform. Measurements of Jobava et al. [45] found that for the same charging voltage of 10 kV, and the discharging geometry,  $I_{max}$  and  $\left(\frac{dI}{dt}\right)_{max}$  varied by more than 1 and 3 orders of magnitude, respectively when the spark length was varied from the Paschen's estimated value (2.7 mm) to about 18% of its value (0.5 mm).

Kagawa et al. [46] measured and simulated human ESD in contact-mode, while a subject's finger touches a grounded metal plane (Figure 3.3). This study developed an equivalent circuit model (Figure 3.3) to predict the discharge current from a subject's fingertip (skin and with aluminum foils attached) and holding a metal bar. Using the measured body impedance (from the fingertip to the larger vertical plane), and a switch assumption for the spark (due to the low body voltage, less than 1 kV) the ESD current was estimated from equation 1, considering the circuit shown in Figure 3.3:

$$i(t) = -\frac{1}{2\pi} \int_{-\infty}^{+\infty} \int_{-\infty}^{+\infty} \frac{v_s(\zeta)}{Z_W + Z_B(j\omega)} \cdot e^{j\omega(t-\zeta)} d\omega d\zeta \quad (1)$$

where  $v_s(\zeta)$  refers to the fourier transform of the spark voltage,  $Z_w$  is the impedance of the cable, and  $Z_B(\omega)$  is the impedance of the human body. The ideal switch assumption, in which the body voltage is assumed to drop to zero in a stepwise manner, was found to be invalid particularly for the case of discharge via the subject's bare fingertip. For the other two discharge situation where aluminum foil was attached on the fingertip,

the reconstructed spark voltage waveform was close to a switch, however, the body voltage did not reach zero after the discharge.

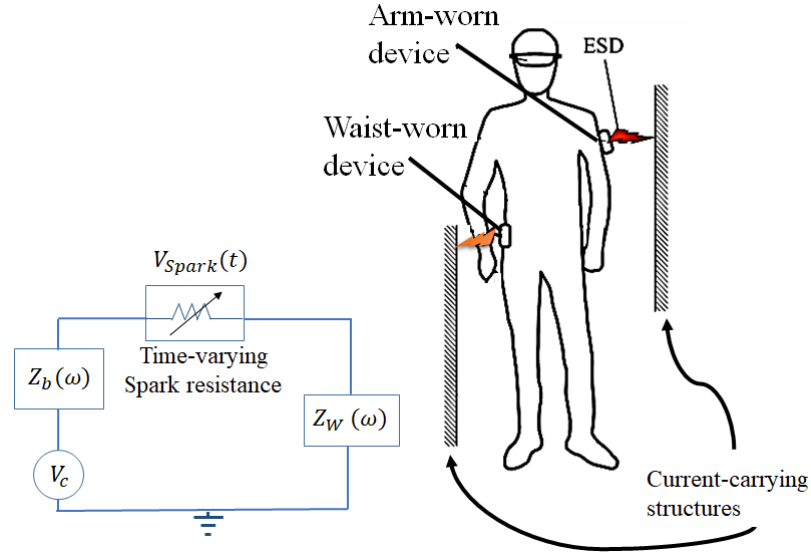


Figure 3.3. Human ESD measurement setup (top) and an equivalent circuit (bottom)

Mori et al. [47] investigated the effect of speed of approach on human ESD tests according to Figure 3.3. The discharge current was measured and simulated in air discharge tests at 200V to 1000V. It was found that the speed of approach has a negligible effect on the current waveform at 200 V, while at 800 V, faster approaches resulted in a shorter rise time and larger  $\left(\frac{di}{dt}\right)_{max}$ . Moreover, the validity of the Rompe-Weizel's spark resistance law was investigated in the vicinity of the peak current. The spark voltage was found using the measured current waveform, and the spark resistance was calculated at the peak current. At this point, spark length was calculated using the Rompe-Weizel's law and the field strength  $(V_C/\delta)$  was found to be close to the breakdown value reported for air in the literature ( $V_C$  is the applied voltage and  $\delta$  is the spark length). This field measurement confirmed the validity of the Rompe-Weizel's law at the vicinity of the peak current.

In an attempt to verify the applicability of the spark resistance formula, Taka and Fujiwara [48] measured the discharge current from a charged subject in the setup of Figure 3.3, at 200V and 2kV. To verify the applicability of Toepler's and Rompe-Weizel's law for spark resistance, the relationship between the spark conductivity (found from current measurement), and transferred charge (for the validity of Toepler's law) and ohmic dissipation energy (for the validity of Rompe-Weizel's model) was found. The dotted lines belong to the spark law approximation before the peak current. It is found for both Toepler (left figure) and Rompe-Weizel's law (right figure), the measurement only fits with the dotted lines (derived from the spark's resistance law) before the peak current. Thus, the spark resistance laws are meaningful at a few nanoseconds before the peak current. Moreover, at a higher voltage level, the deviation from the spark resistance law approximation increases. This observation has been mentioned in Pommerenke's study [23] and was attributed to channel widening at larger spark lengths.

All the research studies discussed so far considered the HMM discharge scenario specified in the IEC 61000-4-2 standard where a standing subject holds a metal rod and discharges it into a ground plane. For a wearable device, the effect of various body locations for the discharge, and postures of the person, at a range of realistic voltages (e.g., 2 kV to 8 kV) need to be analyzed. The first study to investigate the brush-by scenario was performed by Ishida et al. [49]. In this study, the human subject was charged to 1kV and discharge to a ground plane via a small square metal piece mounted on the subject's head, arm or waist. For each device location, 20 air discharge tests were performed to a large vertical plane, and the peak currents were compared with the HMM scenario (i.e., handheld metal bar) and the ESD gun calibration setup. The average peak current from the waist-

worn device was found to be about 4 times larger than the ESD calibration (according to IEC 61000-4-2 standard), 1.5 times larger than arm-worn, 1.3 times larger than head-worn, and 1.5 times larger than HMM scenario. The energy of the discharge current was also simulated and a similar behavior was observed for the waist-worn scenario. The authors claimed that the trend in the peak current and energy consumption can be analyzed using the resistance and reactance of the human body for different scenarios. For the range of 2 MHz to 10 MHz, the resistance and reactance of the waist were the lowest compared to other body locations, which confirms the finding for the trend of peak current and energy consumption. However, this range was a very small range of the impedance spectrum (2 MHz to 8.5 GHz), and this trend in the impedance of the waist may not be applied to all the frequencies. Therefore, the visual comparison between the different configurations does not seem valid to interpret the trend of peak current and the energy consumption. Other limitations of Ishida et al.'s study [49] were its focus only on standing posture, and the applied voltage of 1kV, which is not sufficient for analyzing the effect of spark on the waveform at higher voltages.

Yoshida [50] measured the air-discharge ESD current when a charged person touched a grounded electrode, using wearable devices held by the person. Using a high voltage DC power supply, the person was charged to 1 kV, 2 kV, 4 kV and 6 kV. The air discharge current from the fingertip of a charged person was measured. Analysis of the discharge current waveforms showed that as the ESD voltage increases, the shape of the waveform shows more peaks; for instance, at 6 kV the waveform shows two small peaks after the initial impulse, while the waveform at 1 kV shows only a single impulse [50]. No further discussion on the underlying reasons was provided.



Oganezova et al. [6] developed a 3D model of human body discharging to a grounded structure via a body-worn metal piece mounted on wrist, head, waist, and arm in different body postures. The discharge current was estimated using the method of moment, assuming a homogeneous dielectric with frequency-dependent permittivity for the outer surface of the human body. The discharge current, however, was not measured directly. The authors calculated the discharge current using the measured body impedance for the brush-by scenarios. They assumed a 1 kV charging voltage and simulated the spark with a switch having 1 ns rise time for voltage drop. The discharge current was obtained via the convolution of the inverse Fourier transform of the measured impedance. The simulated currents, however, were not in a good agreement with current measurements (i.e., calculated from measured impedance). This could be due to the inaccuracies in the permittivity assumptions for the human model.

The most recent study on the characterization of wearable devices was performed by Zhou et al [51]. The goal of the study was to investigate whether the IEC 61000-4-2 provides sufficient immunity for wearable devices. The discharge current waveforms from head-worn, waist-worn, wrist-worn, and arm-worn metal pieces were compared with the HMM scenario at 1 kV, 5 kV, and 10 kV, as well as ESD gun discharge to the metal piece. It was also found that despite the nonlinear resistance of the air spark, the peak current from the brush-by scenario is still larger than the 3.75A/kV limit of the IEC 61000-4-2 standard, even at 10kV charging voltage. To estimate the air discharge current waveform for each scenario, impedance measurement was taken from the subject at the discharge point, and an equivalent circuit of human body impedance based RLC elements was developed. At 1kV, the RLC circuit was employed with a switch assumption for the spark,

to estimate the discharge current waveform. The peak current was found to be overestimated (about twice as high as the measurement). At 10kV, the Rompe-Weizel's law was employed to reconstruct the discharge current waveform, assuming the spark length equal to the Paschen's law. This assumption was made based on the slow speed of approach during the experiment.

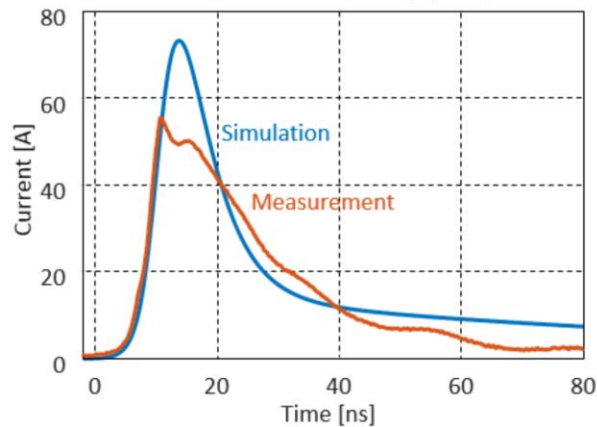


*Figure 3.4. Comparison between the measurement and simulation of the discharge current at 10kV brush-by scenario in Zhou et al. s study [22]*

To provide additional evidence on the characteristics of brush-by discharges compared to the IEC 61000-4-2 setup, soft failure testing was performed on a wearable LCD module. The voltage threshold for observing soft failure in the waist-worn brush-by discharge scenario was 6 times smaller than ESD gun testing according to the IEC 61000-4-2 standard (injecting the pulse into the DUT). Based on the peak current and maximum current derivative results, the paper claimed that the test configuration specified in the standard may not sufficiently severe to represent discharges in the field for wearable devices.

### 3.3. *Research Gaps*

This section discusses the research gaps in the literature on ESD from wearable devices. At first, the limitations of the studies on the electrostatic charging of a human during routine activities, to assess the ESD risks associated with wearable medical devices are presented. Then, the literature studies on ESD waveform from wearable devices are reviewed and the main gaps related to their applicability to medical applications are discussed.

#### 3.3.1. The Literature on Electrostatic Charging of a Human Body

The first research question in this study was on evaluating whether the test levels in the IEC 60601-1-2 is sufficient for wearable medical devices. To address this question, the reasonably foreseeable maximum electrostatic voltages on wearable device users while performing charge generating activities need to be analyzed. The electrostatic voltage on a person depends on the environmental conditions (e.g., relative humidity (RH), combinations of materials), and the characteristics of the activity (e.g., area of contact). A few reports in literature noted that common activities in a healthcare facility, such as rolling carts and beds, and preparing bed sheets [41]–[43], [52], can result in significant charge buildup on the patient’s (or the hospital staff’s) body, exceeding 20 kV. However, the reported data were mainly recorded observations rather than systematic studies in a laboratory environment.

Although these studies already show that voltage levels exceeding the maximum test limit may occur in hospitals, these recorded observations cannot be used to justify changes in the IEC 60601-1-2. In fact, a large dataset of body voltages exceeding the test limit that occur during reproducible conditions can prove that the test limit is not sufficient.

In addition to literature studies on human charging, there are many routine activities that particularly occur in hospitals and involve significant frictional contact between the patient and insulating fabrics but have not been studied in the electrostatic literature. Transferring a patient with a sliding board, sitting and lying down on a hospital bed involve significant friction and a large area of contact between the patient's clothing and blankets, which may result in significant triboelectric charging. To obtain a large list of potential activities, conducting surveys among the personnel of a hospital is a practical solution.

While the peak voltage during an activity is the most common indicator of the electrostatic risk mentioned in literature, the time required for the dissipation of the accumulated charge to ground need to be taken into account as well. Talebzadeh et al. [38] evaluated the ESD risks associated with various charging activities by comparing their charge decay time constant. Longer dissipation times indicate a higher risk of ESD since there will be more chances of a discharge event at a voltage level that may not be safe for the equipment.

In section 5, our investigation of the triboelectric charging conditions in a hospital environment, during a set of activities that have not been analyzed in literature, is presented. This investigation provides a large dataset of body voltages and the charge decay constants for four charging activities performed by patients and hospital personnel. The effect of the associated materials and RH levels are discussed on the voltage results.

### 3.3.2. The Literature on ESD Waveform of a Wearable Device

To address the first research questions of this study, the ESD waveforms associated with the discharges of a wearable medical device need to be investigated and compared

with the test specification of the IEC 61000-4-2 standard. This standard recognizes only two types of floor-standing and tabletop EUTs. In the absence of a test procedure for wearable devices, manufacturers perform the ESD testing in the tabletop configuration. However, the tabletop configuration differs from the realistic discharge scenario due to the presence of the human body (i.e., electrical impedance and geometry at the point of discharge). Due to this difference, the discharges of an ESD gun (according to the IEC 61000-4-2) may not represent the severity of realistic discharges of wearable devices during usage.

Regarding the severity of the HMM test, the IEC 61000-4-2 standard claims that "...this metal discharge situation is sufficiently severe to represent all human discharges in the field". However, literature studies (e.g., [22], [49], [53]) more severe ESDs can occur depending on the EUT location on the body, given the same voltage level [7]. For instance, for a waist-worn device, a larger portion of the body is close to the ground, which increases the body capacitance relative to the ground and results in a larger discharge current [51]. Therefore, the realistic discharges of wearable devices from different body parts need to be characterized and compared with the standard ESD pulse in the tabletop configuration.

Studies on human impedance (e.g., Amoruso et al. [54]) has shown that the differences in the test setup, geometry in the vicinity of the discharge point and changes in body posture can result in different impedance, which will affect the ESD waveform. In all previous studies on ESD from a wearable device, the same body posture (i.e., standing on the floor) and the discharging structure (large vertical plane) was investigated. However, other postures such as lying down or sitting on a bed may result in higher voltage level, due to the lower body capacitance in these postures. To our knowledge, these two postures have

not been studied in ESD literature. Moreover, the discharging structure in realistic ESD events may not be a large metal plane, which is the common structure in ESD literature. In the example of a patient lying down on a hospital bed, the current-carrying structure is the metallic side-rails of the bed. Another example of the discharging structure can be wires or cables attached to the wearable device. Using a large plane for the discharging structure simplifies the current prediction model since the plane has only a negligible resistance. However, the realistic discharging structures can have non-negligible impedance and may result in radiation loss that needs to be included in the equivalent circuit model.

In studies that involved ESD guns, or any other charged object in HMM scenario [23], [45], a setup was designed to measure the spark length. Spark length measurement data was used to reconstruct the discharge current waveform or investigate the effect of spark length on ESD parameters. In a spark measurement setup [23], the object approaching the ground needs to move in a straight path. However, in human ESD applications, measurement of the spark length is challenging due to the geometry factors and arbitrary trajectory of hand movement. In the case of other body parts such as the waist, this measurement issue will be more sophisticated. Therefore, in these studies, the spark length is assumed to be equal to the Paschen's value. This assumption seems to be valid if the speed of approach is very slow and graphite is added to the electrodes (to provide seed electrons and prevent statistical time lag).

Characteristics of the spark strongly depend on the voltage level of the ESD event. Therefore, analyzing the waveform at a low voltage level of 1 kV, cannot provide information about the waveform at higher voltages, due to the nonlinear behavior of the spark. Thus, the ESD events from a wearable device need to be investigated in a range of

realistic voltages expected for a device user during routine activities. Most studies measured ESD at single ESD voltages of 1kV [44], [46], [49] or 5kV body voltage [44], while only Zhou et al. [22] and Pommerenke [23] considered a range of voltages from 1kV to 10kV. It is to be noted that Mori et al. [47] also investigated the air-mode discharges in HMM scenario in a range of voltages (200 V to 1 kV), however, these voltage levels are much lower than realistic voltages during an ESD from a wearable device in the field.

Zhou et al. [22] and Pommerenke [23] provided the trend of the waveform severity parameters including  $I_{max}$  and  $\left(\frac{dI}{dt}\right)_{max}$  were as a function of the applied voltage, and the spark length. Pommerenke [23] measured the spark length and the waveform parameters, however, only the HMM scenario was investigated. Zhou et al. [22] measured the waveform parameters only for HMM and waist-worn brush-by scenario, but did not measure the spark length. Therefore, an estimation of the effect of spark length on these two parameters were provided. The severity parameter of other discharge configurations such as wrist-, arm-, and head-worn discharges were not compared with the waist-worn and HMM scenarios.

Analysis of the transferred charge was only shown in Zhou et al. [22] for waist-worn and HMM scenarios. Despite the importance of transferred charge in the characterization of ESD risks, specifically, its effect on permanent damage to electronic components [55], [56], this parameter was not investigated by other authors.

Another limitation of the previous ESD studies on wearable devices was their interpretation of the waveform parameters for different discharge configurations. Ishida et al. [49] compared waist-worn discharges to other configurations and used impedance

measurements for various device locations to confirm the peak current results. However, their comparison of the body impedance was only limited to a short range of frequencies from 2 MHz to 10 MHz. The impedance results showed fluctuations in the rests of the frequency spectrum, which complicated the impedance comparison. Zhou et al. [22] argued that the higher peak current for waist-worn brush-by scenario compared to other configurations is due to its higher capacitance relative to the ground plane (i.e., lower impedance) resulting from the smaller distance between the body and the plane. However, impedance measurements in these configurations were not compared to verify this hypothesis.

The second research question of this study is about the development of a current waveform prediction model based on the physical parameters of the setup. This model can be used to characterize the effect of various setup parameters on the resulting waveform. For instance, if a discharge setup consists of several wires each with different impedance terms, the model can predict the effect of changes in each element. Moreover, if the human body is represented with conventional parameters (e.g., RC network), the effect of body location and posture on the waveform can be interpreted by changes in these parameters. Studies on wearable devices have developed current prediction models only for the simple setup of HM or brush-by scenario. Kagawa et al. [46] and Mori et al. [47] directly used the measured impedance to calculate the ESD waveform. Zhou et al. [22] and Pommerenke and Aidam [57] developed an RLC representation for the human body to match the measured impedance results. Although the equivalent circuit based on random elements provide a good match to the impedance data, this approach may not be useful if the discharge setup is more complicated than a standing person discharging to a vertical plane.



The accuracy of the prediction model is a critical factor that has not been adequately addressed in ESD literature. Zhou et al.'s [22] prediction for current waveform on waist- and arm-worn brush by scenarios showed nearly 40% error in peak current compared to measurement. This large error could be due to the variation in the spark length (less than Paschen's length), or inaccuracies in impedance modeling using RLC elements. An additional source of uncertainty is the gas constant  $K_R$  in the Rompe-Weizel's model. Jobava et al. [45] used a range of values from  $0.5 \times 10^{-4} \text{ m}^2/\text{V}^2\text{s}$  to  $4 \times 10^{-4} \text{ m}^2/\text{V}^2\text{s}$  depending on the applied voltage. Zhou et al. used the smallest value of this range, so that the maximum current derivative of the waveform matches with measurement. Investigating the changes in this gas constant can show the impact of this parameter on the waveform.

## 4. Electrostatic Charging Activities in a Hospital

As mentioned in previous chapters, the IEC 60601-1-2 provides test levels for medical devices based on reasonably foreseeable maximum voltages that the standard claims to be observed in a hospital environment. However, literature studies and reports have noted that the test voltages in the standard may not be sufficient. However, the literature on human charging reported observations or examined a limited set of activities, which may not be reproducible.

This chapter is focused on developing an experimental study to obtain a large data set of severe charging activities in a hospital, and the associated material combinations and environmental conditions. The results of this study can inform healthcare facilities and standard organizations about precautions for critical activities and associated material combinations that increase the risk of ESD events in these environments. More importantly, it addresses the first research question in this study, on whether the test levels in IEC 60601-1-2 is sufficient for ESD immunity if wearable medical devices.

The experiments were performed at 3 levels of low RH (10%, 20%, and 30%), and a range of materials combinations commonly used in hospital environments to obtain a distribution of the peak body voltage levels. The effect of RH level and material combinations on the peak voltage level are investigated and risk mitigation strategies are provided for healthcare facilities.

#### 4.1. *Methods*

The authors initially visited a local hospital to perform electrostatic measurements and identify potential charge generating activities and the associated materials and equipment for further investigation in a laboratory analysis. Moreover, a survey on electrostatic risks (provided in the Appendix) was distributed among six hospital staff in the radiation oncology department which is mainly an outpatient facility within the hospital. Except for one person who did not recall any static shocks, the remaining subjects reported slight jolting sensations during various activities in the hospital. Subject noted that contact with handles (4 responses) sliding boards (3 responses), plastic surfaces (3 responses), bed frames (2 responses), charging stations (1 response) and buttons (1 response) resulted in a static sensation. Among these apparatus, sliding boards, which are used for transferring a patient from one bed or stretcher to another one, have not gained any attention in the electrostatic literature. Analyzing sliding board features in the market revealed that some vendors commonly claim that their boards have an antistatic coating that dissipates the accumulated static charge to minimize the risk of ESD. These findings indicate that sliding boards are well-known for their high risk of electrostatic charging in hospitals.

Based on the results of the survey, electrostatic measurements and initial observations in the hospital, the following set of activities were identified for pilot studies in the laboratory environment at controlled RH levels: sweater removal, sitting and lying down on a hospital bed, rolling a medication cart and a wheelchair, walking on the floor, and patient transfer using a sliding board. This section provides a description of the climate

chamber, voltage measurement setup, and the experimental equipment for the electrostatic charging activities.

#### 4.1.1. Climate Chamber

It is well-known that the RH level has a considerable effect on electrostatic charging [58]. In general, the risk of electrostatic charging increases at lower RH levels, mainly due to the lower electrical conductivity in dry conditions [59]. Therefore, the worst-case of electrostatic charging condition is more likely to occur at lower RH levels, typically below 30% RH [58][60]. A climatic chamber (3m x 5m) was designed to control the RH level during the charging experiments using a dehumidifier and reduce the RH level of the intake air.

The experiments were performed during winter to ensure that the intake air has low RH (< 30% RH). By controlling the settings of the dehumidifier and an air conditioner, the RH level inside the climate chamber was controlled in 3 levels of 30%, 20%, and less than 10%. A hygrometer was used to measure RH level in the chamber with  $\pm 3\%$  accuracy. The walls and the ceiling of the chamber were made of Styrofoam, to prevent heat loss to the surrounding environment. A thin layer of Al foil tape (<0.1 mm) covered the walls, which served as the electrical ground.

#### 4.1.2. Voltage Measurement Setup

The human body voltage during the activities inside the climate chamber needs to be monitored, in order to obtain the peak voltage and the time decay constant from the voltage waveform. A surface DC voltmeter with 25 Hz sampling rate was employed to capture the voltage waveform during the activities. The voltmeter returned the electrostatic voltage on a surface based on the distance between the voltmeter and the surface, and the amount of

the electric field between them. Since the maximum voltage level that can be measured using the voltmeter was 20 kV, which may be low for the identified activities, the design was modified to extend the measurement limit to 40 kV. Figure 4.1 shows the modified voltage measurement setup in the climate chamber. A metal plate is placed at 5 cm distance of the voltmeter and is connected to a metal probe via a 2m long wire. Once a charged subject holds the metal probe in his hand, an electric potential at the same level of the body voltage is induced on the metal piece. The voltmeter measures the voltage potential induced on the metal piece, and return the data to a handheld monitoring device, which is connected to a laptop via a USB cable. Due to the capacitance of the 2 m long wire connected to the metal probe relative to the ground and the walls, the voltage readings needed to be adjusted accordingly. Since the capacitance of the wire relative to the ground and walls was 30 pF,  $C_w$ , and the human capacitance,  $C_h$ , was approximately 100 pF (measured using a capacitance meter), the voltage readings were multiplied by the ratio of the capacitances:  $\frac{C_w+C_h}{C_h} = \frac{100 \text{ pF}+30 \text{ pF}}{100 \text{ pF}} = 1.3$ . Although the maximum measurement limit of the voltmeter was 40 kV, the maximum limit of body voltage that could be measured with the setup is 52 kV, since the measurements on the voltmeter had to be multiplied to 1.3.

Before starting any experiment, the voltage readings were calibrated using a high voltage power supply. To minimize the high-frequency noise, and unexpected device resets (due to frequent discharges of the probe to ground), multiple ferrites are used on the cables from the voltmeter to the monitoring device and to the laptop (Figure 4.1).

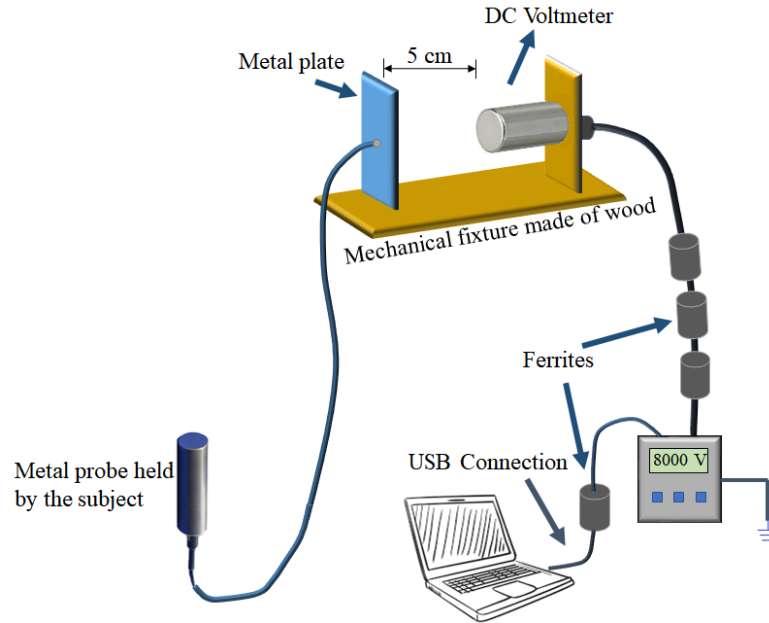


*Figure 4.1. Voltage measurement system in the climate chamber*

#### *4.2. Experimental Apparatus and Materials*

The main equipment in our voltage measurement setup includes flooring, footwear (which affects charge decay to the ground and triboelectric charging with the flooring [11]), blankets and sweaters. The materials for each activity need to represent those commonly used in a hospital. An initial list of representative materials were prepared, and the list was later shortened after performing preliminary tests.

Four types of medical-grade flooring, consisting of two types of tiles and two types of carpets were initially selected to perform preliminary experiments. Nine types of typical footwear ranging from boots and deck shoes to sneakers were initially selected. The conductivity of flooring and footwear are critical in voltage levels on the human body. However, it is not practical to measure the conductivity of the flooring and footwear materials due to their complicated shapes. Therefore, the selection of the final set of

materials was based on the voltage level on the body while performing preliminary experiments. Three types of footwear (1 running shoes, and 2 deck shoes), were selected from the initial set that resulted in the highest body voltage levels. Four common types of blankets were selected including 100% cotton, 65% polyester & 35% cotton, 100% nylon, and 50% polyester & 50% nylon. Four types of sweaters were selected including 100% cotton, 100% polyester, 50% wool & 50% nylon, and 50% wool & 50% acrylic.

Two male subjects with similar weights (160 lbs) and different heights: 5'7" and 5'11" performed the experiments in the chamber. Both subjects were wearing clothes made of 100% cotton (shirt and pants). To monitor the voltage waveform during the activity, the subject held the metal probe (from the voltage measurement setup) in his hand. Before starting the experiments, they had to touch the ground (via a wire connected to the main ground in the chamber, or the Al foil covering the wall), to ensure that the charge from the previous experiment has been released and the body voltage is zero. The blankets and other insulating materials used in the activities were rubbed against the Al foil covering the wall to dissipate the accumulated triboelectric charges to the ground.

The relative humidity of the tests was set at the lowest possible range (<5% RH), which could potentially lead to the highest voltage levels compared to other RH levels in the chamber. However, in the last experiment on sliding boards, three RH levels of 30%, 20%, and 10% were analyzed to determine the effect of RH variation on charging voltage levels. The air temperature was set at 25C, using an air conditioner inside the chamber. All the required material for the experiments such as the blankets, footwear, and flooring were kept inside the chamber for more than 24 hours at the RH level needed for the experiments.

### 4.3. *Measurement Results and Discussions*

This section provides an investigation of the effect of various material combinations and RH levels on the voltage level and the time decay constant for each activity via histograms and boxplots.

#### 4.3.1. Walking and Rolling a Medication Cart

According to the literature [40], [61] and observations in a hospital, the most common charging activities performed by a person are walking on a carpeted floor and rolling a medication cart (or a wheelchair). Preliminary experiments using various combinations of flooring and footwear showed that the maximum body voltage level during these activities may not exceed 2 kV. Since the voltage levels are too low compared to the maximum test voltage level in the standard (15 kV), these two activities were not considered for further evaluations.

#### 4.3.2. Sweater Removal

Sweater removal is one of the routine activities during which static shock is reported in cold days [39], [40]. The sweater removal experiments were performed similarly to Talebzadeh et al.'s study [40]. A subject removed his sweater and dropped it on the ground while holding the voltage probe in his hand. His body voltage was monitored while performing the activity as shown in Figure 4.2. When the subject takes off his sweater at the beginning of the activity, triboelectric charging occurs between the sweater and the underneath clothing (100% cotton), which results in a slight increase in body voltage. Then the subject completely removes the sweater and drops it on the floor. At this moment, the peak voltage occurs due to the separation of charges between the subject's hand and the sweater. After dropping the sweater, the body voltage decreases exponentially, due to the



dissipation of the charge to the ground via the footwear and flooring. In the final step, the subject touches a grounded object nearby (e.g., Al foil on the walls) to abruptly release the charges to the ground.

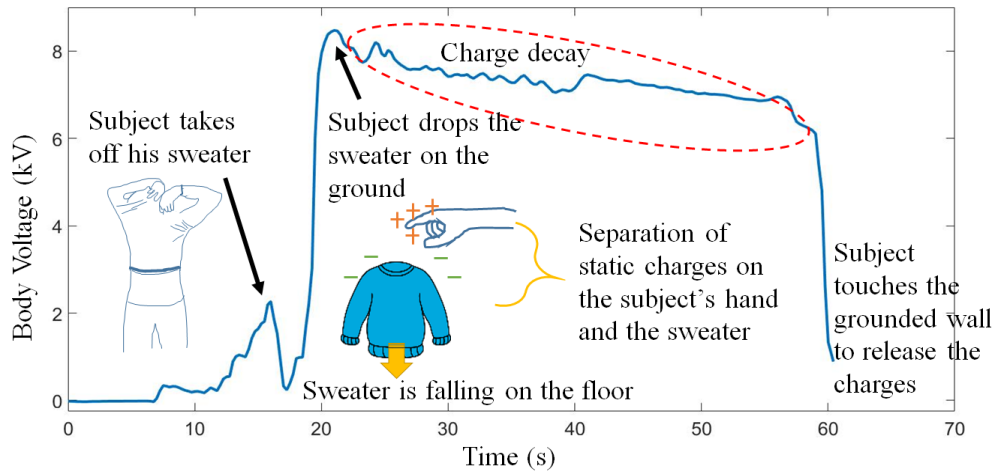
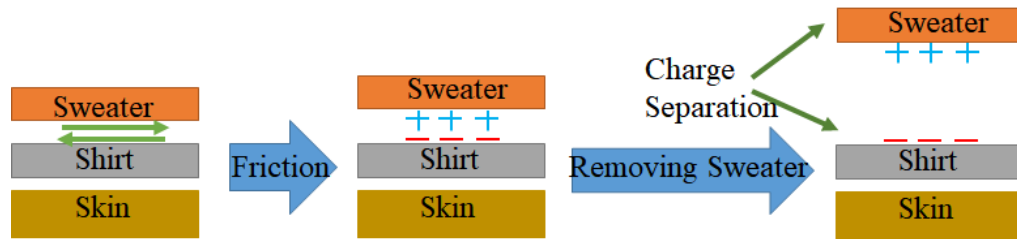


Figure 4.2. An example of a body voltage waveform during sweater removal experiment.

*The polarity of static charges is shown arbitrarily.*

Figure 4.3 shows a basic illustration of the triboelectric charging process in the sweater removal experiment. While the subject is trying to remove the sweater, there will be friction between the sweater and the underneath clothing, which results in liberation of static charge in both items. Once the sweater is dropped on the floor, the static charges remain on both items and cause an abrupt increase in body voltage due to the separation of the charges. The polarity of the static charges depends on their relative electron affinity, which could be derived from the triboelectric series table [58]. The positive charge on the sweater and negative charge on the shirt in Figure 4.3 are selected arbitrarily.



*Figure 4.3. Triboelectric charging of the sweater and the body while rubbing the sweater against underneath clothing*

This experiment was performed by two subjects, and four different sweaters, two medical grade flooring and 3 different footwear were used, resulting in 48 experiments. The order of the experiments (i.e., material combinations and subjects) was randomized, to minimize the bias in the results.

Since the goal of the study is to identify the severe electrostatic voltage ranges, the RH level at the chamber was set to the lowest possible level of 5%. For each experiment, the peak voltage and the time decay constant were extracted from the voltage waveform. The histogram of the peak body voltage during the sweater removal activity and the boxplot of the voltage distribution (Figure 4.4) shows that the voltage level for the majority of the experiments or the interquartile range (IQR) is between 10 kV to 14 kV, and the median is 12.1 kV. These experiments were performed using a range of typical footwear, flooring and sweater material, which do not represent all the possible combinations that might occur in a hospital environment. However, the results of this controlled study showed that even using this limited range of materials, in 7 out of 48 experiments (14% of all the combinations), the peak body voltage during sweater removal exceeded 15 kV, which is the maximum ESD test level specified in the IEC 61000-4-2 standard. Among these 7

experiments, 4 tests were performed using a sweater made of 50% wool & 50% nylon, 2 tests with 50% wool & 50% acrylic, and one with 100% polyester.

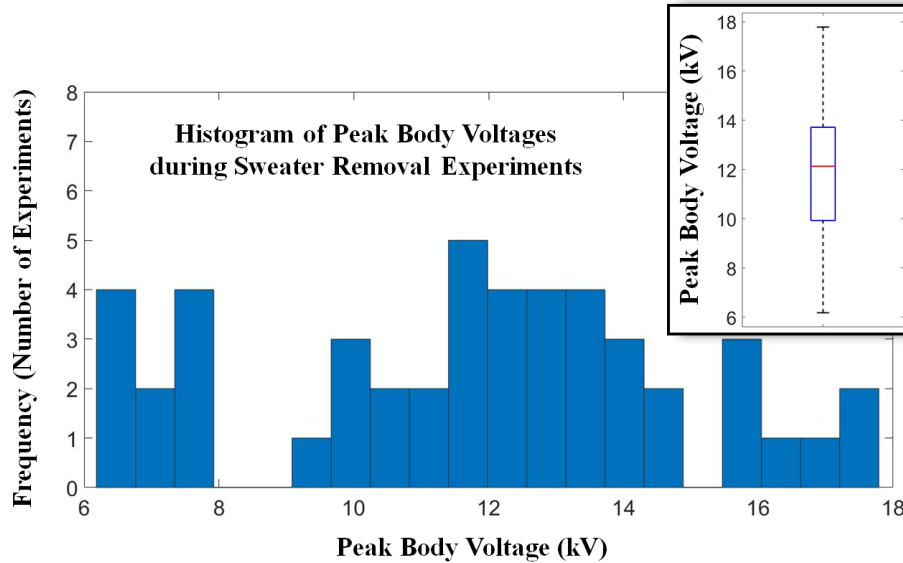


Figure 4.4. Histogram and the boxplot of the Peak body voltage while taking off the sweater

To obtain the charge decay time constant,  $\tau$ , an exponential curve fit ( $V(t) \propto e^{-t/\tau}$ ) was fitted to the decay portion of the voltage waveform, starting from the peak value until the abrupt voltage drop. Similar procedure was performed in Talebzadeh et al.'s study [40]. The histogram of the time constants for all the 48 experiments is shown in Figure 4.5. Longer time constants indicate a higher ESD risk, since body voltage stays longer at levels that may not be safe for ESD immunity of medical equipment. The voltage decay can be due to two competing factors: dissipation for the accumulated charge from the shoe sole to the ground, and neutralization of the charges on the body with the charge carriers in the air surrounding the subject. It is expected that charge dissipation is the dominant cause of decay, due to the negligible concentration of the charge carriers in the air at low RH.

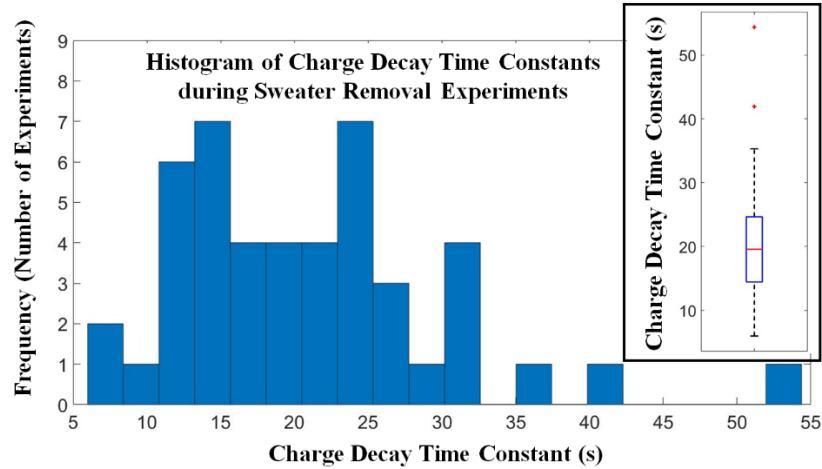
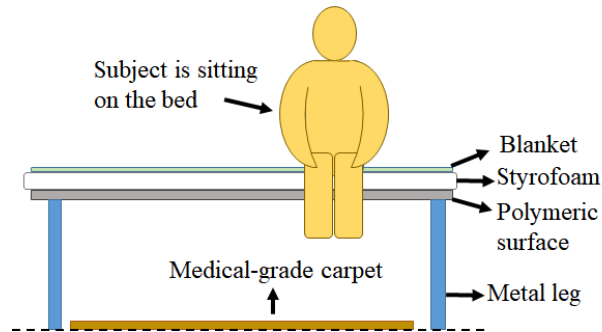


Figure 4.5. Histogram and the boxplot of the charge decay time constant during sweater removal

#### 4.2.3. Sitting on and Rising from a Bed

A common charge generating activity that patients perform while visiting a healthcare facility is sitting on a hospital bed and rising from it. To evaluate the electrostatic risks associated with this activity, a bed was designed to represent the structure of a typical hospital bed (Figure 4.6). A Styrofoam layer (~ 4 cm thickness) and a blanket covered the surface of the bed (2 m x 1 m). A medical grade flooring (1 m x 1 m) covered the floor. At the beginning of the experiment, the subject was standing on the carpet near the bed, while his body voltage was near zero. Then, he sat on the bed, and the voltage rose due to the triboelectric charging between clothing (pants) and the blanket. Triboelectric charging also occurred between the shoe soles and the carpet, while the subject was moving his feet on the floor to raise his shoes and sit on the bed. At the moment of sitting, the separation of static charges between the shoe soles and the carpet resulted in a peak voltage, as shown in Figure 4.7 (the polarity of the charges on the subject and the carpet reflect the sign of the body voltage). Next, the subject stayed on the bed in sitting posture for about 20 seconds,

which resulted in dissipation of the accumulated charges to the ground via the bed (blanket and the Styrofoam), in an exponential waveform seen in Figure 4.7.



*Figure 4.6. Experimental setup designed for sitting activity*

After about 20 seconds, the subject touched the grounded walls, to discharge the remaining accumulated static charges to the ground. Then he rose from the bed and stood up on the floor for about 30 seconds. While rising from the bed, triboelectric charging occurred due to the friction between his clothes (pants) and the blanket. At the moment of standing on the floor, there was a peak in body voltage due to the separation of the charges on his clothes and the blanket (Figure 4.7). While the subject was standing on the floor, the accumulated charges dissipated to the ground via the floor. This charge decay phase was much faster than the first decay while sitting on the bed, probably because the foam and the blanket on the bed are better electrical insulators compared to the flooring and footwear. The results of the charge decay time constants for these two phases will confirm this assumption.

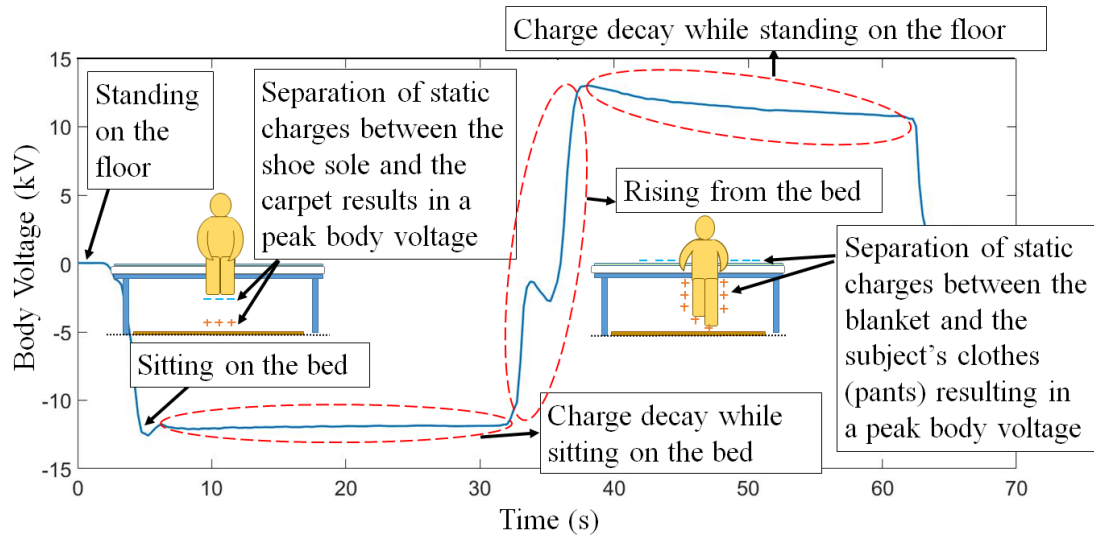
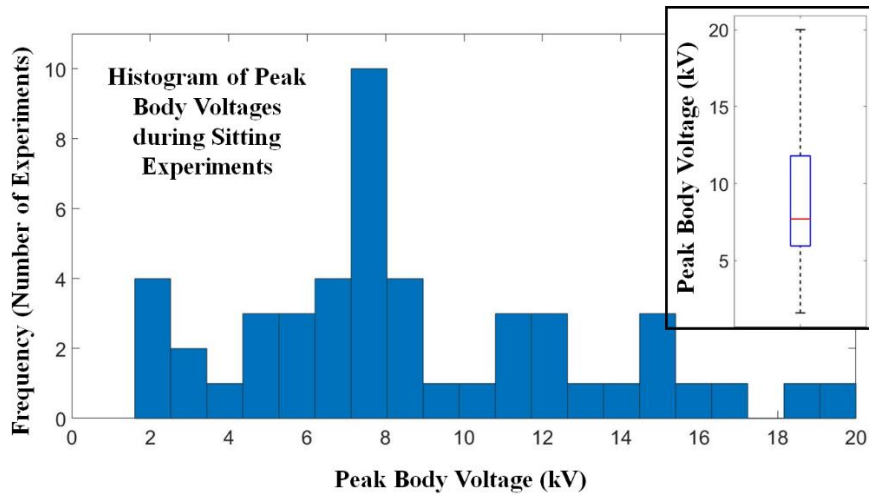


Figure 4.7. A typical voltage waveform during the sitting activity; Polarity of the static charges are shown arbitrarily.

Two subjects performed 48 experiments using 4 different sweaters, 2 medical grade flooring, 2 types of footwear (1 running shoes, and 1 deck shoes) and 4 types of blankets to cover the bed. Both subjects were wearing clothes (pants and shirts) made of 100% cotton. The number of experiments performed by subjects was less than the total number of possible combinations (64 experiments), and the order of the combinations was randomized to minimize the bias in the results. The RH level at chamber was set to the lowest possible level of 5%.

Since each experiment resulted in two peak voltages (one after sitting on the bed and the other after rising from it), only the maximum absolute value of the two peaks is analyzed. The histogram of the peak body voltage during the sitting and rising activity (Figure 4.8) shows that the IQR is ranging from 6 kV to 12 kV. Among 48 sitting experiments, 5 tests (10% of the combinations) resulted in voltages beyond 15 kV (maximum ESD test voltage in the IEC 61000-4-2 standard), all of which included 100%

cotton blanket. In comparison with the sweater removal, sitting experiments have resulted in a relatively lower range of voltages (12 kV median for sweater removal compared to 7.7 kV). This could be due to the lower contact area of friction between the clothing and blanket compared to sweater removal.



*Figure 4.8. Histogram and the boxplot of the peak body voltage for sitting experiments*

According to Figure 4.9 and Figure 4.10, the time constant for sitting is about 1 order of magnitude longer than standing posture (224 seconds median for sitting compared to 36 seconds for standing). The decay time constant for sweater removal was about 20 seconds which is in the same range of the standing posture, as expected. The reason for this difference is probably the larger area of frictional contact while sitting and the fact that Styrofoam and the blanket covering the bed are stronger insulators (i.e., with higher resistance) than the footwear and flooring.

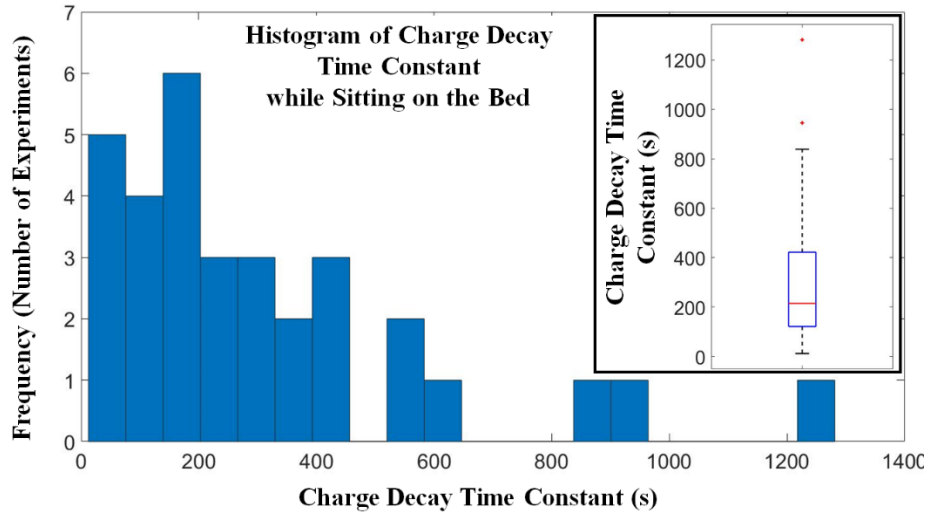


Figure 4.9. Histogram and the boxplot of charge decay time constant for sitting experiment

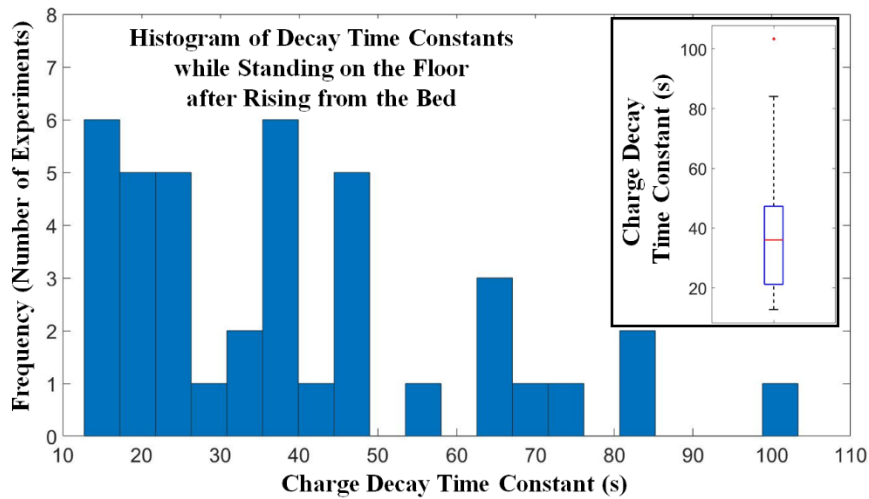
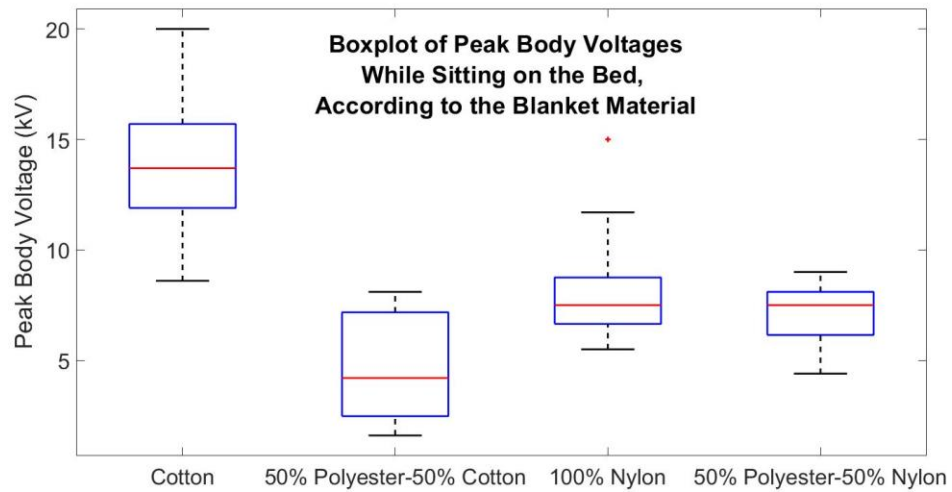


Figure 4.10. Histogram and the boxplot of decay time constant for standing posture

The effect of the material combinations on the peak voltage is explained in Figure 4.11. The goal of this analysis is to investigate the effect of blankets on hospital beds and provide suggestions for healthcare facilities regarding the electrostatic risks of using certain fabrics for blankets. The type of sweaters worn by patients in a hospital cannot be



controlled, therefore, each group in the boxplots contain various combinations of sweaters, footwear, and the flooring associated with a certain blanket material. The worst-case charging voltage among all material combinations in this test, results from blanket made of cotton (median value 13.7 kV) and the least charging voltage belong to 50% cotton-50% polyester blanket (median 4.2 kV).



*Figure 4.11. Boxplots of peak body voltage during sitting experiment for various types of blanket material*

#### 4.2.4. Lying down and Rising from a Bed

This phase of the experiments was performed similarly to the sitting experiments; however, the subject was lying down on the bed as shown in Figure 4.12. At the beginning of the experiment, the subject was standing on the carpet near the bed, while his body voltage was near zero. Then he sat and lay down on the bed and his body voltage rose due to the triboelectric charging between clothing and the blanket. Similar to the sitting experiment, the friction between the shoe soles and the carpet (at the moment of raising the feet) resulted in triboelectric charging of both materials. At the moment of lying down on

the bed, the separation of static charges between the shoe soles and the carpet resulted in a peak voltage, as shown in Figure 4.12. The polarity of the body voltage depends on the relative electron affinity of the shoe soles and the carpet, which can be obtained from the triboelectric series table. The negative charges on the body reflect the sign of the peak voltage in the waveform.

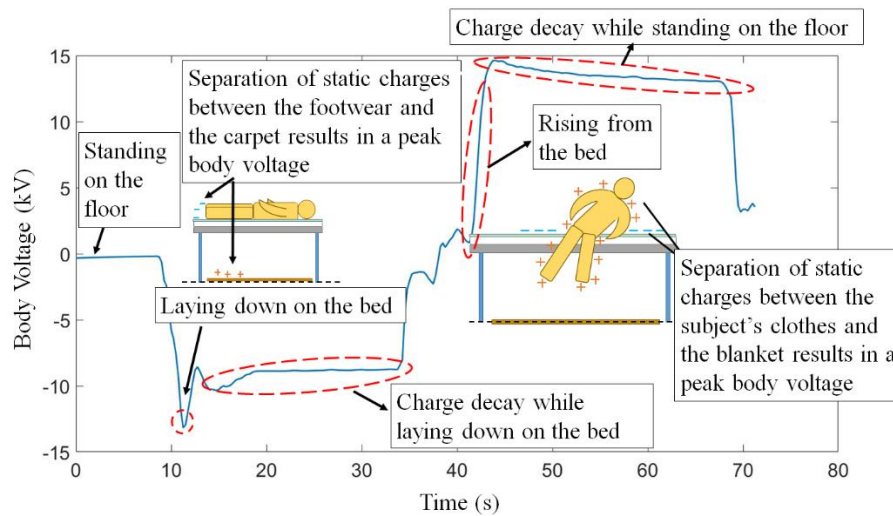
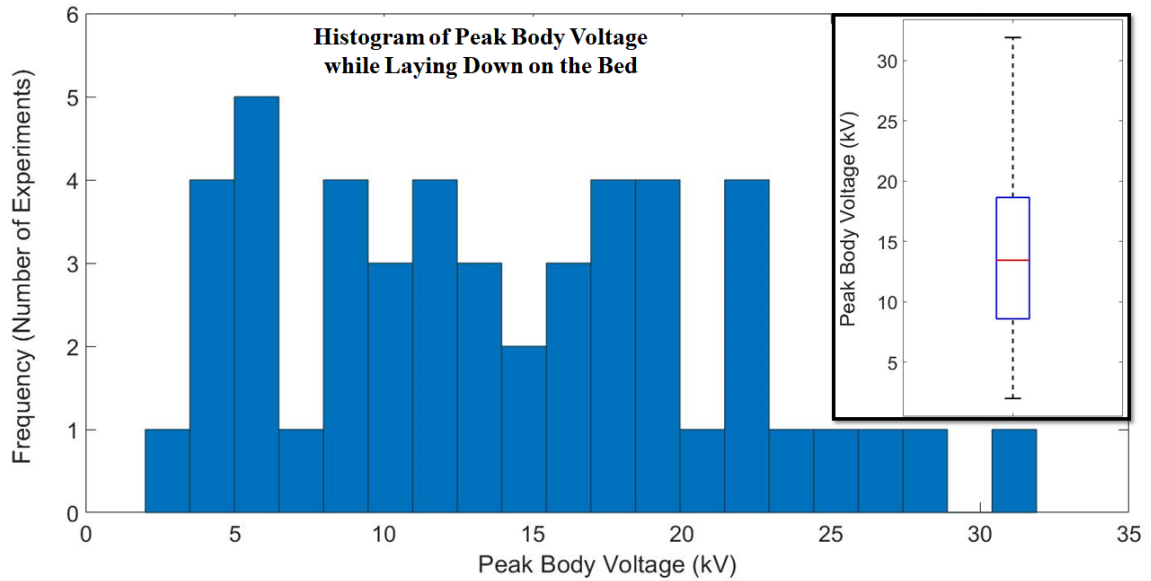


Figure 4.12. A typical voltage waveform while the subject is lying down on and rising from the bed; Polarity of the static charges are shown arbitrarily.

The subject stayed in the lying down posture for about 20 seconds. In this stage, the triboelectric charges on the body dissipated to the ground via the bed (blanket and the Styrofoam), in an exponential curve seen in Figure 4.12. In the next step, the subject touched the grounded walls to discharge the remaining static charges on his body to the ground. Then he rose from the bed and stood up on the floor for about 30 s. While rising from the bed, the friction between his clothes and the blanket resulted in triboelectric charging of the two materials. At the moment of standing on the floor, there was a peak in body voltage due to the separation of the charges on his clothes and the blanket (Figure

4.12). While the subject was standing on the floor, the accumulated charges dissipated to the ground via the floor. This charge decay phase was much faster than the first decay while lying down on the bed because the time decay constants estimated for the sitting experiments showed that the foam and the blanket on the bed are better electrical insulators compared to the flooring and footwear.

The experimental conditions, including the material combinations and the RH level, was exactly the same as sitting experiment. Since each experiment resulted in two peak voltages (one after lying down on the bed and the other after rising from the bed), only the maximum absolute value of the two peaks is analyzed. The histogram of the peak body voltage during the sitting and rising activity (Figure 4.13) shows that the IQR is between 9 kV to 19 kV. Compared to the sweater removal and sitting experiments, the median of the voltage levels for laying experiments is larger than the previous experiments (13.6 kV for laying compared to 7.7 kV for sitting and 12.2 kV for sweater removal). Moreover, Figure 4.13 shows that nearly half of the experiments (23 out of 48) resulted in the peak voltages exceeding 15 kV. This higher voltage level could be attributed to the larger distance between the subject's body and the ground, which results in lower capacitance of the body relative to the ground for the same amount of charge, and therefore, the body voltage becomes larger as well ( $Q = C \downarrow, V \uparrow$ ). Moreover, the contact area between clothing and the blanket is larger for lying down experiments compared to the sweater and sitting experiments, which results in larger triboelectric charging.



*Figure 4.13. Histogram and the boxplot of the peak body voltage while lying down on the bed and rising from it*

The histogram in Figure 4.14 shows the range of time constants for lying down on the bed. The median of the time constant is 66 seconds, which is longer than sweater removal, but shorter than sitting. The longer dissipation time for lying down than standing on the floor is mainly due to the larger resistance of the Styrofoam and the blanket compared to the flooring and footwear materials. The shorter time constant compared to sitting (almost 4 times) can be attributed to the larger body area in contact with the blanket and therefore the lower resistance of the charge dissipation path. Assuming a common relationship of  $\tau = RC$ , where  $R$  is the resistance of the dissipation path and  $C$  is the body capacitance, lowered resistance results in a shorter time constant for lying down compared to sitting posture. This finding also confirms that the neutralization process via charge carriers in the air is not as effective as charge dissipation to the ground. Considering that the area of the body in contact with air while sitting is larger compared to lying down, the neutralization

process is expected to be faster for sitting, however, the time constants shows the opposite trend. Therefore, the faster decay while laying is probably due to the larger area of contact with the blanket and lower resistance of the dissipation path.

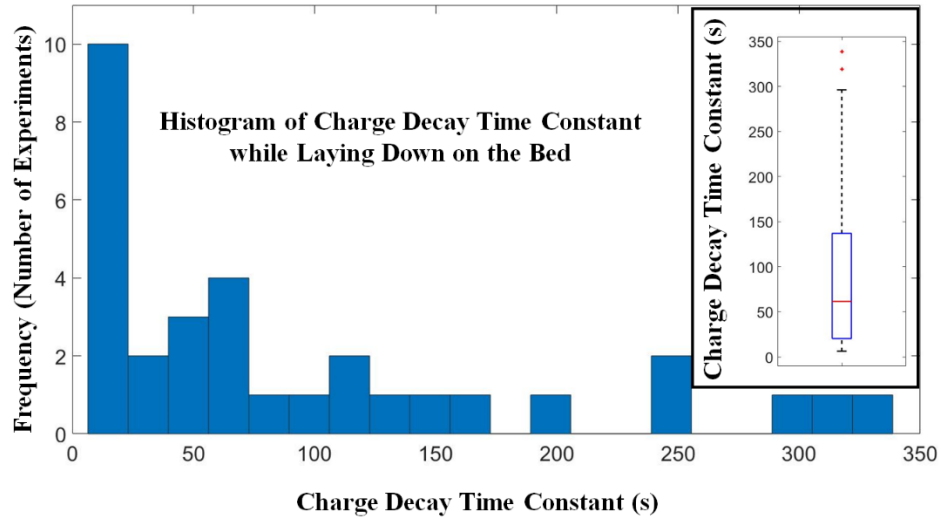


*Figure 4.14. Histogram and the boxplot of the charge decay from the body to the ground while lying down on the bed*

Among 48 experiments, 22 tests resulted in voltages beyond 15 kV. It was found that in 14 out of the 27 tests, the bed was covered with the 100% cotton blanket. In the remaining 13 tests, nylon and polyester blankets were used to cover the bed. Figure 4.15 shows the effect of blanket the material on the peak voltages during the activity. Similar to sitting experiments, the largest median of the voltages belongs to the cotton blanket (20.5 kV), while the least voltages were observed using 50% cotton – 50% polyester blanket (median 5.6 kV).

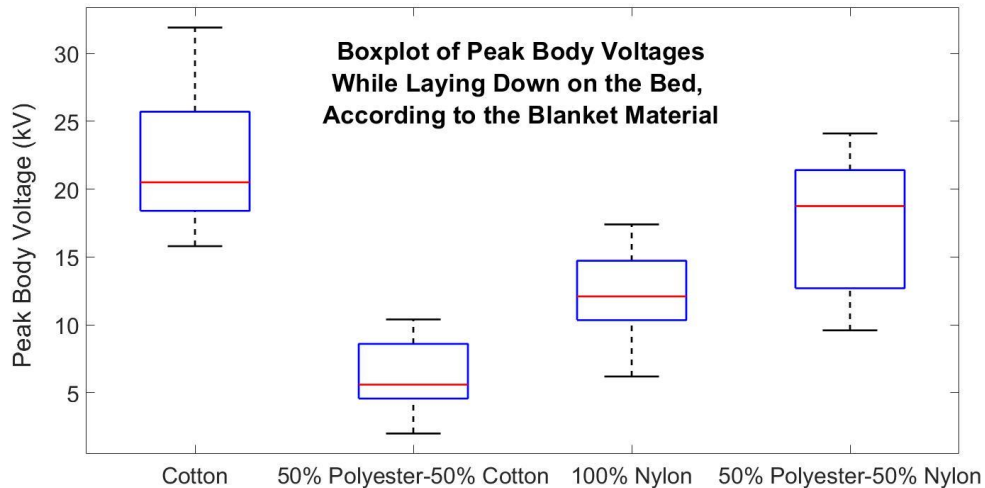


*Figure 4.15. Boxplots of peak body voltage during sitting experiment for various types of blanket material*

#### 4.2.5. Patient Transfer Using a Sliding Board

Patient transfer is a common activity performed by hospital personnel to transfer patients with disabilities or damaged spinal cord to various areas of the facility or from a stretcher to a bed. Figure 4.16 shows the two-step process for transferring a patient (subject 1) to another bed using a sliding board. The two beds are covered by a blanket (same material) and located close to each other. A sliding board is placed between the two beds and a sliding sheet is on top of the board. The patient (subject 1) is initially lying down on the sliding sheet and the nurse (subject 2) is standing on the left side of the bed in Figure 4.16. Then the nurse takes a firm grip on the sheet and pulls it toward himself to move the patient to the next bed. Once the patient is located on the next bed, the nurse removes the sliding board under the sheet.

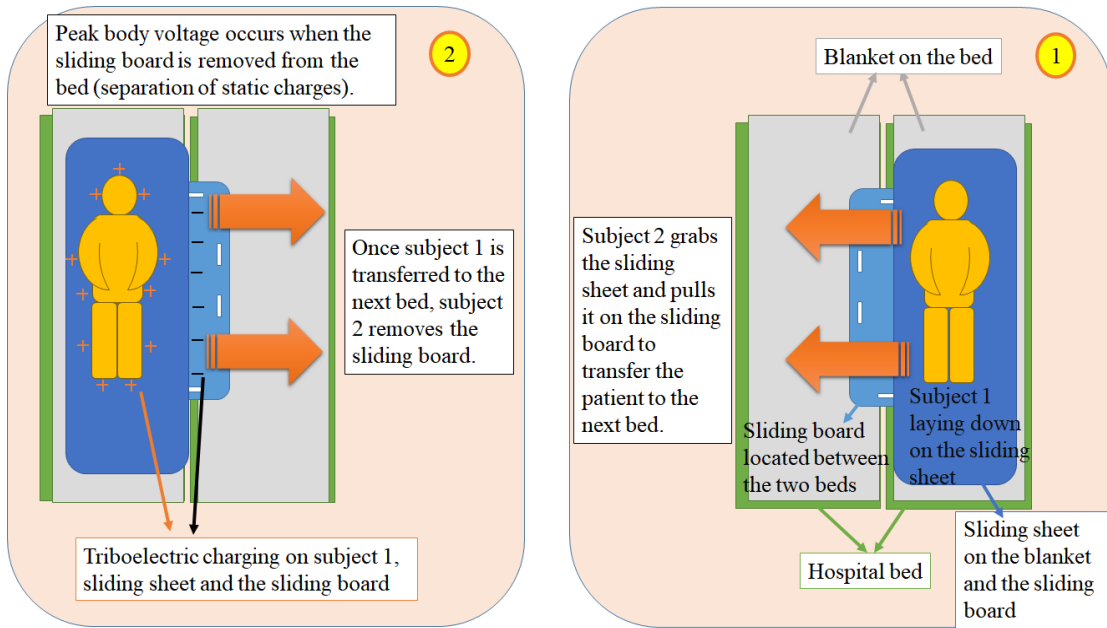


Figure 4.16. Patient transfer process using a sliding sheet and a board in two stages

Figure 4.17 shows an example of the voltage waveform for subject 1 during a typical patient sliding experiment. While the patient is sliding on the sheet and the board underneath, the friction causes triboelectric charging of his clothing, the sliding sheet, and the board. A slight increase in voltage occurs once the patient is transferred to the next bed, however, the peak voltage occurs when subject 2 grabs the sliding board and removes it from the bed, due to the separation of the charges between the patient and the sliding board.

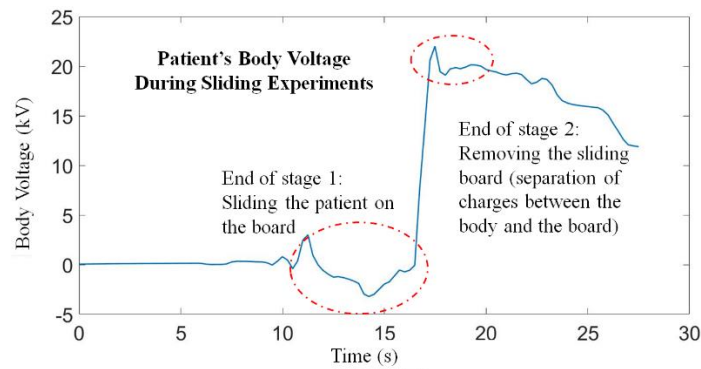


Figure 4.17. Patient's body voltage profile during the transfer process

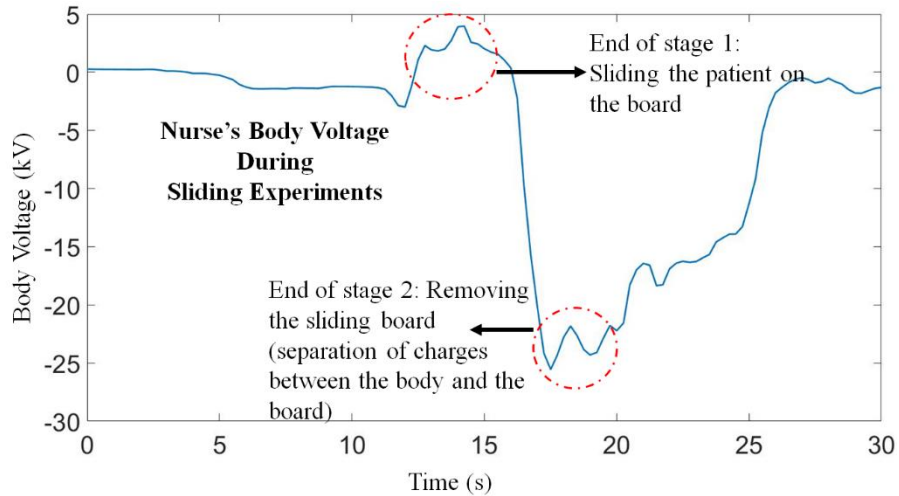
Since this experiment involves two subjects, it is useful to measure the voltage level of subject 2 who is handling the triboelectrically charged sliding board and the sheet, as well as subject 1 (i.e., patient). This assessment can show whether the nurse's voltage range is sufficiently high to exceed the ESD immunity level of medical devices. This analysis shows the ESD risks associated with the interaction of a nurse with medical equipment near the bed or wearable devices.

Figure 4.18 shows an example of the voltage measurement on the nurse's body, for the same experimental conditions of Figure 4.17. During the transfer experiment, the nurse holds the voltage probe while grabbing the sliding sheet and sliding it on the board with both hands. Triboelectric charging of the sliding sheet and the board while transferring the patient, results in slight charging of the nurse's body, however, the peak current occurs at the moment of touching the sliding board underneath the patient and pulling it off the bed. The sliding board is triboelectrically charged during the sliding process, therefore, the nurse's voltage (i.e., absolute value) abruptly increases at the moment of touching the board. The peak body voltage is close to that of the patient's, but with the opposite polarity.

The material combination in the sliding experiments is more complicated than previous tests due to the addition of the sliding board and the sliding sheet. Moreover, obtaining a voltage waveform for both subjects require performing each material combination twice. Considering these additional elements in the setup, all potential combinations is not practical. Therefore, this experiment was performed in two stages. The focus of the first stage was to measure the voltage levels for the patient (subject 1) and the nurse (subject 2) during a limited combination of materials, using the same sliding board at a constant RH level. The second stage consisted of a wider range of combinations to



analyze the effect of RH and material combinations on the patient's body voltage (i.e., subject 1) only, using various materials for the blanket, sliding sheet and the board.



*Figure 4.18. A typical voltage waveform for the nurse during patient transfer using the sliding board and the sheet*

The first stage of the experiment, which was focused on comparing nurse's voltage to the patient's voltage, involved 4 materials for the blanket and the sliding sheet (between the patient and the sliding board) including 100% cotton, 50% polyester & 50% nylon, 65% polyester 35% cotton, and 100% polyester. The sliding board was a regular board without antistatic coating. Each experiment was performed twice to measure the voltage on both subjects. The relative humidity level was set at 20%. A total of 50 experiments were conducted for each subject.

Figure 4.19 shows the histogram of body voltage for both subjects during the 1<sup>st</sup> stage of the sliding experiments. The absolute magnitude was selected for the nurse's voltage. The IQRs for both subjects are in the range of 12 kV to 18 kV. A two-sample t-test did not reject the hypothesis that the data in both populations come from independent

random samples from normal distributions with equal means and equal variances ( $p$  –  $Value = 0.15$ ). This similarity between the two samples come from the fact that the charge accumulated on the patient should be almost equal to the charges on the sliding board due to triboelectric charging while transferring the patient.

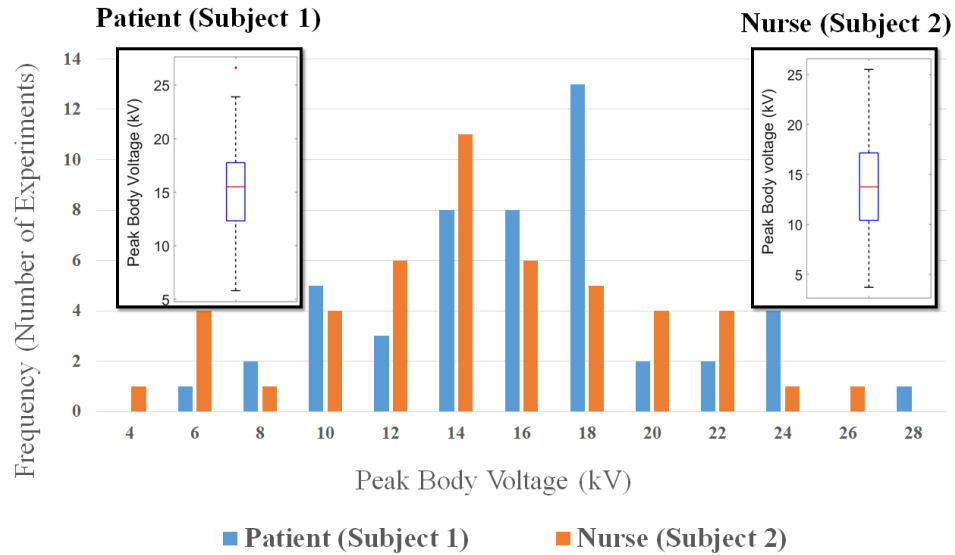


*Figure 4.19. Histogram and the boxplot of the peak body voltage distribution for both subjects (stage 1 of the experiment)*

In the second stage of the experiment, six different materials were used as the sliding sheet and the blanket covering the bed: 100% cotton, 65% polyester & 35% cotton, 50% polyester & 50% nylon, 100% polyester, 100% nylon. Four sliding boards were used, two regular board and two with an anti-static coating. It is to be noted that the size of the blankets and the sliding boards and the sheets were similar. The RH level was varied at 30%, 20%, and 10%. Body voltage was only measured on subject 1. This stage of the experiment consisted of 209 combinations of various materials at 3 RH levels.

To perform a statistical comparison between the data in each RH level, the histograms of the peak body voltages were obtained as shown in Figure 4.20. The histograms show that nearly half of the peak voltages at 3 RH levels (108 out of 209 data points) exceed 15 kV.

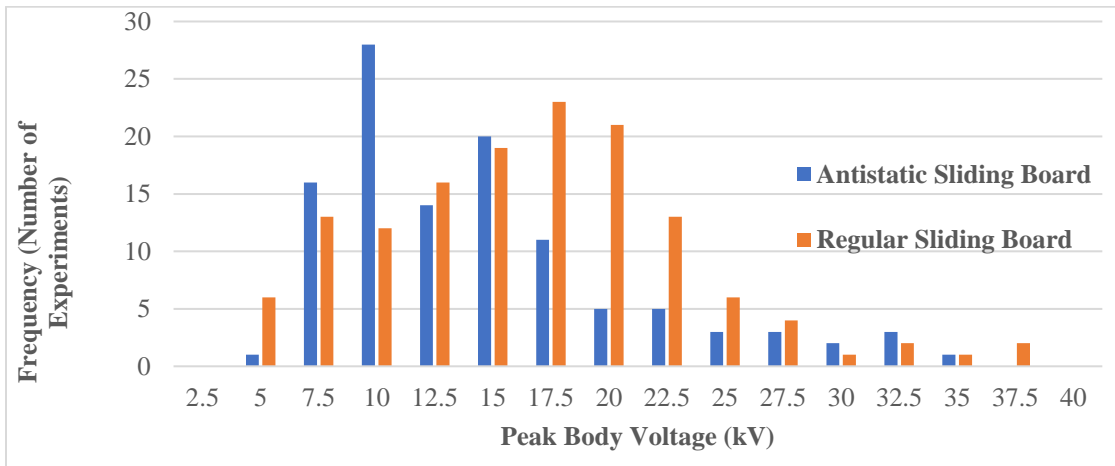


*Figure 4.20. Comparison between the histogram of peak body voltage during sliding experiments at 3 RH levels*

It is expected that triboelectric charging increases at lower RH levels. However, the boxplots of the results in Figure 4.21 show that the median of the results at 10% RH (10 kV) is lower than 20% RH and even 30% RH, while some of the outliers at 10% RH, exceed 50 kV. The median at 20% RH (15.7 kV) is larger than 30% RH (12.7 kV), which is according to expectation. This trend in the triboelectric charging data could be due to the complex properties of the blanket and sheet material. The main point in this analysis is that even at 30% RH, which is a common RH level in healthcare facilities during winter, many experiments (14 out of 41) resulted in triboelectric voltages larger than 15 kV.

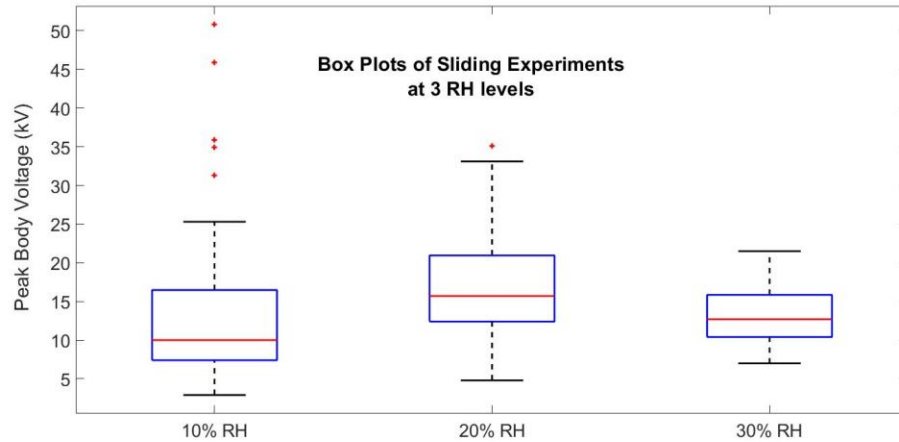


Figure 4.21. Boxplots of peak body voltage at 3 RH levels

Four sliding boards were used in this experiment, two with antistatic coating and two without the coating. To investigate the effect of the coating in reducing the triboelectric voltage generation, the histograms and the boxplots of the two conditions are analyzed in Figure 4.22. The antistatic coating on the sliding boards shifts the distribution of peak voltages to left. According to Figure 4.23, the median of the peak voltages for regular boards is 15.4 kV, and the maximum voltage reaches 50.8 kV. However, the antistatic coating reduces the median of the peak voltages to 11.7 kV, while the maximum voltage reaches 33 kV. The peak voltages above 15 kV are less frequent while using antistatic boards compared to regular ones. For experiments with the antistatic coating, 33% of the voltages exceed 15 kV (37 out of 113), however, this percentage for regular boards is 55% (78 out of 142). A student t-test analysis rejected the hypothesis that the two population (with and without antistatic coating) come from independent random samples with equal means and variances at 5% significance level ( $p - Value = 0.0085$ ). These results confirm that the reduction in the peak voltages using antistatic coating is statistically significant.

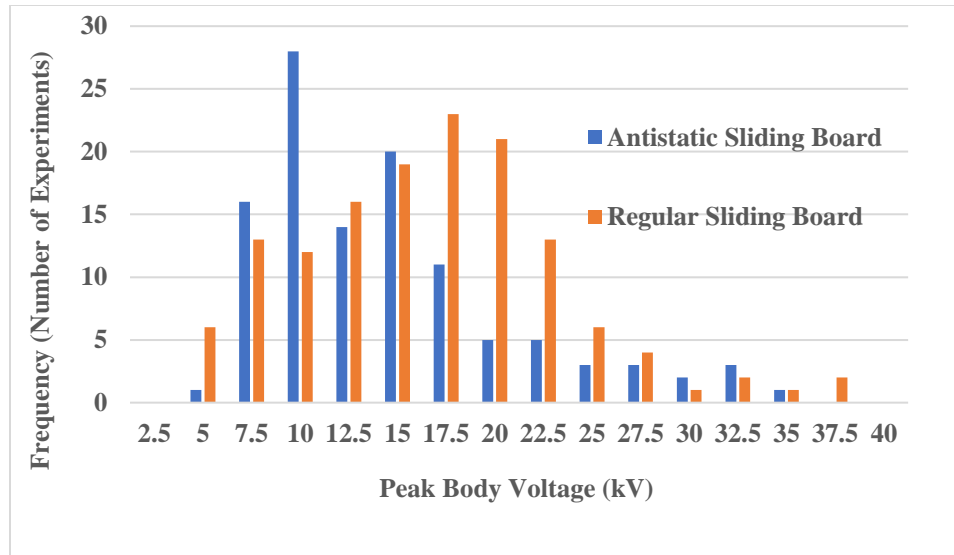
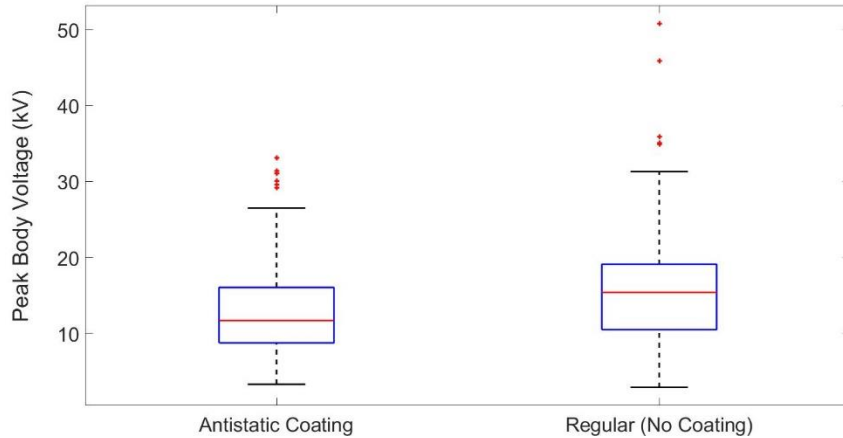


Figure 4.22. Histogram of the results with and without the antistatic coating

Despite lowering the median of the voltages by 24%, the histogram and the boxplot show that the antistatic coating still cannot reduce the voltage levels below 15 kV. This finding means that using antistatic coating does not reduce the risk of ESD to a safe level for medical equipment, since voltages above 15 kV have been observed in this study.

The results of this study are obtained from newly purchased boards with a fresh antistatic coating, however, in a hospital environment, the coating probably wears off due to usage and the static dissipation property of the board will be lost eventually. Therefore, the difference between the two types of boards will become less significant due to usage, and antistatic coating will not reduce the voltage levels over time.



*Figure 4.23. Comparison between the boxplots of the peak voltages with and without antistatic coating*

Figure 4.24 classifies the voltage results of each sliding board based on the RH level. In all the RH levels, the median of the voltage levels for boards with the antistatic coating is less than the regular boards: 40% reduction at 10% RH, 20% reduction at 20% RH, and 35% reduction at 30% RH. The difference between the two types of sliding boards is significant at 10% RH and 30% RH (based on a 5% significance for t-test statistic). This comparison shows that the effectiveness of the coating is still not sufficient to reduce the voltages to a safe level for the ESD susceptibility of the equipment.

The effect of material combinations on voltage levels is analyzed via the boxplots in Figure 4.25. Considering both types of the sliding board and 3 RH levels, the experiments were categorized according to the combination of the blanket on the bed and the sliding sheet. Material combinations in Figure 4.25 are designated by letters A to H and sorted according to the difference between the electron affinity of the constituents as shown in the last column of Table 3. The reason for this classification is that the triboelectric charging generation between two materials generally depends on their relative position in

the triboelectric series table [62], which sorts the materials based on their electron affinity. However, the median voltages in Figure 4.25 do not increase in most cases according to the electron affinity of the combinations. This could be due to the complexity of the triboelectric charging process in these experiments which includes friction between several materials including the sliding sheet, blanket on the bed and the sliding board. Another potential reason is that the real electron affinities of the fabrics used in this study might be different than the referenced table [22], due to a mixture of various compounds and treatments with chemical agents.

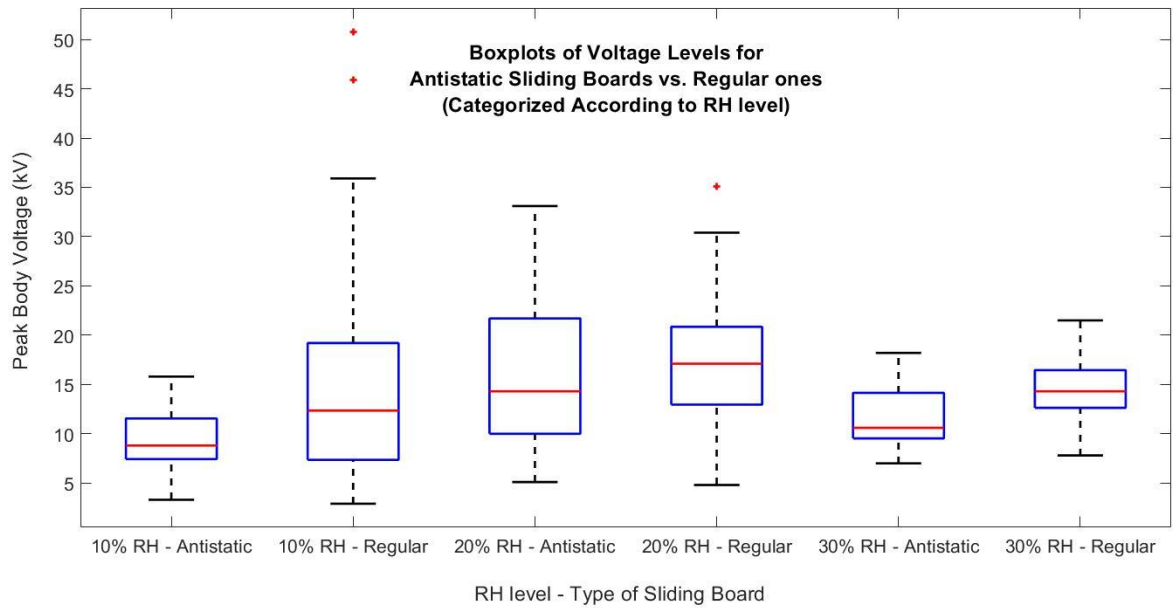


Figure 4.24. Comparison between the distribution of the voltage levels for different types of boards at 3 RH levels

The boxplots in Figure 4.25 also show that for all the combinations except H, the IQR of the voltage distribution includes 15 kV, and the maximum voltage levels in all cases exceed this test limit. The largest median of the triboelectric voltages occurred for F (median 17.9 kV) and G (median 16.5 kV), where sliding sheets made of 100% nylon were

used with blankets made of 100% cotton or 50% cotton & 50% polyester, respectively. In both sitting and lying down experiments, blankets made of 100% cotton, which is the most common material for bedding in hospitals [63]–[65], also resulted in the highest triboelectric voltages.

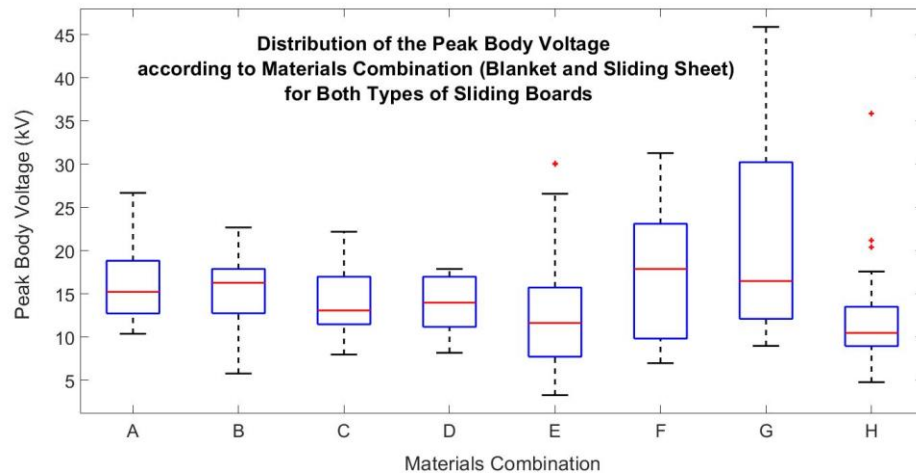


Figure 4.25. Effect of the combination of the blanket and sliding sheet on the peak body voltage. The blue dashed line represents the maximum ESD test voltage level.

Nylon is the most common material for sliding sheets [66], [67], [68], due to its low friction compared to cotton or polyester sheets, which makes patient transfer easier for hospital personnel and the patients. However, our results show that their lower friction leads to high triboelectric voltages ( $> 15$  kV), which could subsequently result in severe discharges to medical equipment in contact with the patient and personnel. This discrepancy between the expectation and our measurement could be due to the complex pattern of movement and sliding of various objects involved in the experiment, and the physics of triboelectric charging of fabrics.



Table 3. The median of the voltages and the difference between the electron affinity of the material combinations for each designated letter

Designated Name	Material Combination: Blanket and Sliding Sheet	Median of Peak body Voltage (kV)	Difference Between Electron Affinity [62] (nC/J)
A	Nylon-Nylon	15.2	0
	Cotton -Cotton		
	Polyester-Polyester		
B	Cotton - (50% Polyester & 50% Nylon)	16.3	5
	Cotton - (50% Polyester & 50% Cotton)		
C	Polyester - (50% Polyester & 50% Cotton)	13.1	10
	(50% Polyester & 50% Cotton) - (50% Polyester & 50% Nylon )		
D	Cotton - Polyester	14	15
E	(50% Polyester & 50% Nylon) - Nylon	11.6	20
	(50% Polyester & 50% Nylon) - Polyester		
F	Cotton- Nylon	17.9	25
G	Nylon - (50% Polyester & 50% Cotton)	16.5	30
H	Polyester - Nylon	10.5	40

### 4.3. *Conclusions*

In this study, a survey was performed among the staff of a local hospital and performed electrostatic measurements in several patient rooms to obtain a list of activities resulting in severe triboelectric voltages. Seven activities routinely performed in a hospital environment were identified and preliminary experiments were conducted to find out the activities resulting in the highest voltage ranges. Four out of seven activities found including sweater removal, sitting on and lying down on a bed, and patient transfer using a sliding board were selected for subsequent pilot studies in a wide range of material and environmental combinations. Using a combination of common types of medical-grade materials, the distribution of the peak body voltage while performing these activities was obtained. Nearly half of the sliding and lying down experiments resulted in peak body voltages exceeding 15 kV, while this percentage for sitting and sweater removal was 10% and 14% respectively. The finding of these study on charge levels of patients in a hospital indicate that 15 kV air discharge test level specified in the IEC 60601-1-2 may not be adequate for wearable medical devices.

Although electrostatic voltages exceeding 20 kV have been occasionally observed in hospitals in previous literature, a large portion of the activities examined in this study exceeded the maximum test limit in the IEC 60601-1-2. The major strength of the present work is that a set of activities were found based on a survey and on-site investigations, and a large dataset of material combinations and environmental conditions (nearly 400 experiments) were obtained for three activities (sitting an lying down on the bed, and sliding experiments) that have not been analyzed in literature.

It was surprisingly found that the most common fabrics used for sliding sheets (i.e., nylon) and blankets (i.e., cotton) result in the highest electrostatic risk. The highest median voltage while performing sitting and lying down was observed when the bed was covered with cotton blankets (13.7 kV and 20.5 kV, respectively). In both cases, the lowest median voltage was observed when a blanket made of 50% cotton – 50% polyester was used to cover the bed (4.2 kV and 5.6 kV, respectively). During sliding experiments, the highest median of voltages (17.9 kV) was observed when a cotton blanket was used with a nylon sliding sheet. Considering the fact that cotton blankets and nylon sliding sheets are the most common materials used in hospitals nowadays, these results indicate that the composition of these fabrics needs to be modified to develop materials to lower the electrostatic risks. For instance, treatment with conditioners as suggested by Holdstock and Wilson [41], or using blankets made of 50% cotton – 50% polyester can be a potential solution.

The analysis of charge decay constants showed that time required for dissipation of the accumulated charge to the ground while the subject is lying down or sitting on the bed is almost one order of magnitude longer than standing on the floor, most likely due to the insulating properties of the blanket and the mattress. Thus, the dissipation of the electrostatic voltage on the subject lying down or sitting on the bed is long enough to increase the chance of an ESD event upon contact with nearby medical equipment. For instance, after a patient is transferred to a bed using a sliding sheet and a board, a nurse must quickly attach electrodes of medical sensors and various electronic equipment to the patient's body. The combined effect of the high triboelectric voltage of the patient's body and the long decay time required for charge dissipation while sitting or lying down on the hospital bed can be destructive to ESD-sensitive equipment nearby or in direct contact with

the patient. In fact, one of the common reports of electrocardiogram malfunction is attributed to static charges on the patient's body, when the electrodes are attached to the skin [69].

The distribution of voltage levels shows that ESD events exceeding 15 kV can still occur even at common RH levels in hospital rooms during winter. While performing sliding experiments at 30% RH, 36% of the tests (15 out of 42) resulted in peak body voltages exceeding 15 kV. Our analysis implies that lowering the minimum limit of the RH levels in hospitals from 30% to 20% can increase the risk of ESD by 27% according to the median of the body voltage in these two RH limits. A relevant standard concerning RH level in hospitals is the ASHRAE 170, which recently lowered the minimum limit from 30% RH to 20% RH in its Addendum D. Considering the risk of triboelectric charging at 20% RH, we recommend healthcare facilities to keep the RH level to above 30% as a useful ESD risk mitigation strategy.

Antistatic coatings on the sliding boards reduced the median of the voltage levels by 24% (averaged over 3 RH levels), however, peak voltages exceeding the maximum ESD immunity test limit of equipment still occurs. Considering that the degradation of the antistatic coating on the sliding boards due to overuse, the risk mitigation programs in hospitals should not rely on using these types of boards. Moreover, designers of these boards need to develop improved chemistries for the coating to enhance their charge dissipation property. Moreover, using dissipative bedrails for hospital beds instead of plastic ones used nowadays can accelerate charge dissipation to the ground.

We recommend manufactures and standard developing organizations to increase the maximum voltage limit for ESD testing from 15 kV to 25 kV, specifically for bed-side

medical devices. This high voltage limit ensures that the ESD events do not cause any disturbances in these safety-critical devices, due to common activities performed by patients. Moreover, this limit is essential for ESD safety of wearable medical devices which need to be used in patient's homes. Although healthcare facilities can adopt standards and guidelines to reduce the electrostatic risks, wearable medical devices are used in environments where no ESD control program can be practically implemented. Therefore, the only practical approach to minimize the risk of ESD malfunctions in these devices is to improve their ESD robustness by increasing the maximum ESD test limit.

## 5. Current Measurement and Equivalent Circuit for ESD from Wearable Medical Devices

The previous chapter showed the charging levels during three charging activities in a hospital environment including sitting and lying down on a bed and transferring to a bed with a sliding board. Since these activities result in the severe charging that exceeds the maximum test limit of the IEC 60601-1-2 standard, the discharge events while performing these activities represent severe ESD events of wearable medical devices. It is likely that the patient's wearable device is discharged to the grounded bedframe, rather than a larger vertical plane as suggested in the literature. Therefore, the discharging structure in these severe ESD events is the hospital bed.

The focus of the present chapter is on the ESD events associated with the body postures identified in chapter 4 for the activities resulting in severe electrostatic charging (sitting and lying down on a hospital bed, and standing on the floor). The severity of the waveforms are compared with the calibration waveform specified in the IEC 61000-4-2 standard. The discharge current during ESD testing of wearable devices is most likely lower than the current during calibration of the ESD gun, as the calibration is performed by injecting an ESD pulse into a grounded metal sheet. Thus, the current from the calibration becomes an upper bound for the discharge current injected by an ESD gun into the EUT. If the real discharge current is even larger than the upper bound, then the differences between the geometry of the usage scenario and the standard testing are expected to lead to insufficient ESD testing.

Using impedance measurement in each discharge configuration, an equivalent circuit model that consists of the physical elements of the setup and the Rompe-Weizel's spark resistance model is developed. The effect of various parameters of the setup, such as the device location on the subject, body posture, spark length and gas constant for the Rompe-Weizel's spark law is investigated on the waveform parameters. The changes in the waveform parameters according to device location and body posture are explained in terms of the physical elements of the setup. Finally, the effects of relative humidity (RH) and the speed of approach on the estimated waveform is analyzed using published data on the RH dependence of the spark length.

This model will help device manufacturers to evaluate the performance of their product for various body postures and locations on the body in a virtual manner. It also informs standard developing organizations such as the FDA and the IEC 60601-1-2 standard committee about whether the ESD test method in the IEC 61000-4-2 is sufficient for wearable medical devices.

This chapter provides the discharge configurations in section 5.1 and the ESD measurement setup in section 5.2. To predict the discharge current, an equivalent RLC model is proposed and verified using measurement data. To develop this model, the impedance data for each element in the discharge configuration is initially measured. The procedure and setup for impedance measurement are described in section 5.3.1. The equivalent RLC circuit for each element of the impedance setup is provided in section 5.3.2. Then, using the developed circuit model for the impedance of each element, the measurement and estimation results for impedance between the subject and the discharging structure is provided in section 5.3.3. The fitted RLC elements for the impedance model of

each test configuration are presented in section 5.4. In section 5.5, the ESD current waveform obtained from the measurements and the equivalent RLC circuit are compared with the IEC 61000-4-2 standard waveform. Section 5.5 discusses the waveform of each test configuration and provides explanations for the trend of the results according to the physical elements of the setup. Section 5.6 presents a discussion on the sensitivity of the waveform on the various model parameter and circuit elements. Section 5.7 discusses the effect of RH on the waveform using published data. Conclusions are provided in section 5.6.

### *5.1. Discharge Configurations*

The goal of this study is to measure and simulate the discharge current waveform from a charged person wearing a small metal piece on his body (in lieu of a wearable medical device). According to the activities identified in chapter 4, three body postures for severe charging activities are lying down and sitting on a hospital bed and standing on the floor near the bed. Two positions for the metal piece on the subject's body are considered: his hand (wrist) and waist. Therefore, 6 configurations are investigated as the realistic discharge scenarios for a wearable medical device.

The metal piece worn on the subject's body was a square metallic plate of 5 cm × 5 cm dimensions (i.e., a realistic watch size), which had an 11.5 mm diameter hemispherical tip (Figure 5.1). The rounded tip of the rod facilitated the generation of a spark during the discharge event.



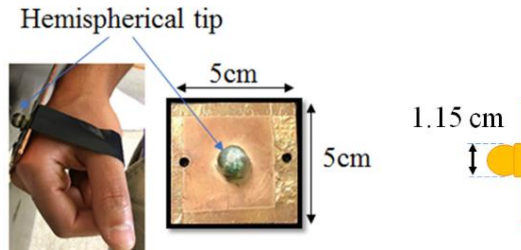


*Figure 5.1. A square metal piece used in lieu of a wearable medical device*

It is assumed that the ESD occurs when the tip of the metal piece mounted in the subject's body accidentally touches the grounded metal frame of the hospital bed. Figure 5.2 shows the ESD measurement setup for the charged person lying down on the hospital bed and the metal piece worn on his hand. The same setup was used for sitting and standing postures and the metal piece worn on the subject's waist. The subject lying down on the bed, discharged the metal piece into a small metal rod (about 10 cm long and 10 mm in diameter) connected to a short wire. The metal rod was attached to a short wire (about 30 cm-long) connected to the Al foil layers under the bed that represent a grounded bedframe of a hospital bed. Connecting the short wire and the metal rod to the Al foil is necessary since it enables measurement of the discharge current to the bedframe via a current clamp over the wire. Addition of the wire, however, results in radiation loss and extra apparent inductance, which makes the setup more complicated than those studied in literature for HMM or brush-by discharge scenarios. In the simulation model, the waveform with and without the wire will be analyzed.

A large ground plane (1m × 1.5 m) under the bed was connected to the Al foil with a 1 m-long wire. This long wire was added to ensure the bed-frame and the ground are at the same potential. The ground plane under the bed emulates the flooring system, which is often made from reinforced concrete. The electrical characteristics of a human body were

simulated with a resistor,  $R_b$ , and a capacitor,  $C_b$ , in series, which refer to the resistance of the discharge path from the metal piece to the Al foil, and the capacitance of the body relative to the Al foil, respectively. The assumption RC series for simulation of the human body is the most common model used in ESD standards [34], [70].

The electrical characteristics of the rest of the components in the setup were determined by impedance measurement. Section 5.3 discusses the impedance measurement and determination of the RLC parameters for each element in the six discharge configurations using impedance measurement. These RLC parameters will be used to estimate the current waveform at four voltage levels and the results will be compared with current measurements to evaluate the accuracy of the simulation model (section 5.4). The developed model will later be used to analyze the waveform at various spark lengths (sections 5.5.2 and 5.6.1).

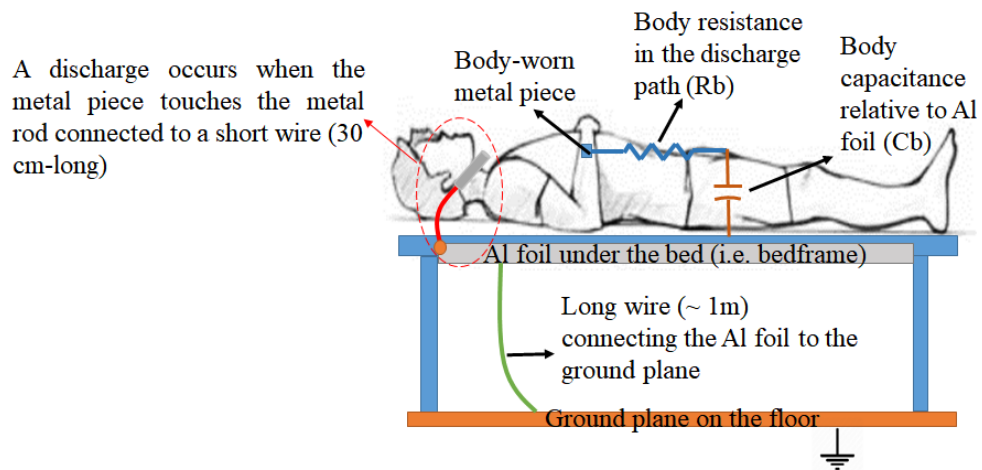


*Figure 5.2. ESD event from a charged subject lying down on a bed, wearing a body-mounted metal piece (in lieu of a wearable device)*

## 5.2.ESD Setup and Measurements

Figure 5.3 shows the experimental setup developed to measure the discharge current. The subject is initially charged by a high-voltage power supply to voltages of 2 kV, 4 kV, 6 kV, and 8 kV, to be consistent with the test levels specified in the IEC 61000-4-2 standard. This choice of voltage levels allows comparison with the ESD gun results (in contact-mode).

To reduce the current from the power supply, a  $100\text{ M}\Omega$  current-limiting resistor was added to the wire. While the subject was holding the wire from the power supply in his right hand, the metal piece was mounted on his left hand or waist. To ensure the accuracy of the power supply, the voltage levels were double checked with a surface DC voltmeter and the same levels were obtained. Since the body is a weak conductor, the voltage on the metal piece mounted on the subject's left hand the voltage of the subject's right hand (in which he holds the wire from the power supply) can be assumed to be the same. Due to the low capacitance of the body ( $\sim 100\text{ pF}$ ), the time required for the body to reach the voltage level set by the power supply is extremely short (time constant of charging the body capacitance via the current-limiting resistor is  $\tau = RC \approx 100 \times 10^{-12} \times 100 \times 10^6 \Omega = 0.01\text{s}$ ). Thus, the voltage potential of the whole body becomes the same as the power supply's charging level, immediately after touching the wire. Therefore, there is no need to hold the wire for a long time to keep the voltage at the same level of the power supply.

To initiate the discharge, the subject held the wire from the power supply in his right hand for about 10 seconds (to ensure the body has reached the voltage level). Then, he touched the metal rod connected to the short ground wire to release the accumulated charge via a spark. The discharge path is from the metal piece to the Al foil, and from there to the ground plane on the floor. The subject did not let go of the wire from the power supply throughout the experiments, to ensure that the body voltage remained the same after the discharge. A small piece of foam (10 cm × 5 cm × 2 cm) was used to hold and mechanically secure the current clamp and the metal rod on the bed so that they could not move when the subject touched the rod (with hand or waist) during each discharge event.

To capture the discharge current, an F65 current clamp was used around the metal rod that was connected to the short wire. Since the sensitivity of the current clamp reduces at frequencies below 1 MHz, a deconvolution method was employed to correct for the frequency response in this frequency range [71].

The oscilloscope was placed inside a metal shield to protect it against electromagnetic wave coupling due to the ESD events. To protect the oscilloscope from the high current level of the ESD, a pulse attenuator (20 dB for 2 kV and 4 kV, and 40 dB for 6 kV and 8 kV) and an ESD protection were used. Many ferrites were placed on the coaxial cables connected to the oscilloscope to suppress noise coupling.

Once the subject extends his arm or moves his waist toward the metal rod to initiate the discharge, a spark occurs between the hemispherical tip of the metal piece and the rod. The length of the spark is a critical parameter that determines the peak current and rise time. Since the measurement of the spark length in the setup was not practical, ESD tests were performed at a slow speed of approach (about 2 cm/s) to ensure that the spark length

is close to the value predicted by Paschen's law. Moreover, pencil marks were added to the surface of the hemispherical tip of the metal piece to increase electron emission, and thereby minimize the statistical time lag [25]. The circuit model will be used to obtain waveforms for shorter spark length using Rompe-Weizel's spark resistance law [24]. To enhance the connection between the metal piece mounted on the subject's body and the skin, a few water droplets were added at the metal piece location. Temperature and relative humidity were measured at 25C and 25% RH, respectively. Results of these experiments will be discussed in section 5.4.

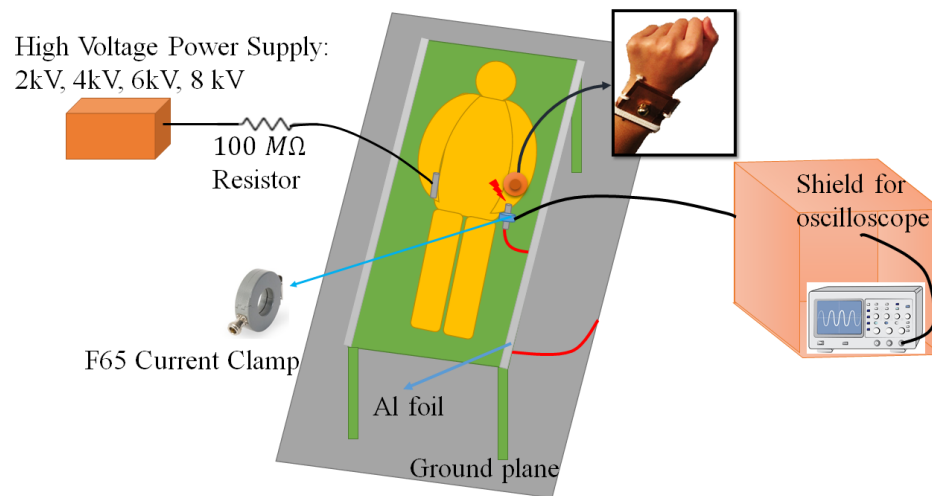


*Figure 5.3. ESD current measurement setup while the subject is lying down on the bed. A short wire is attached to the Al foil, and a longer wire connects between the Al foil and the ground plane.*

Before starting the discharge experiments for wearable devices, ESD gun tests were performed according to the IEC 61000-4-2 standard. In the calibration setup of the IEC 61000-4-2 standard (Figure 5.4), an ESD gun directly injects a pulse into a current target with about 2 Ω impedance. These ESD tests were performed in 4 voltage levels of 2 kV, 4

kV, 6 kV and 8 kV. The severity parameters of each waveform, including  $I_{max}$ ,  $\left(\frac{dI}{dt}\right)_{max}$  and  $Q_{ESD}$  were extracted for comparison with the six discharge configurations of the wearable device.



*Figure 5.4. ESD calibration setup according to the IEC 61000-4-2, ESD gun is injected into the center of the plane which is a current target*

Figure 5.5 shows the ESD current waveform when an ESD gun charged at 1kV, discharges to the current target in the calibration setup (a metallic enclosure that holds the oscilloscope) in contact mode. The waveform for this experiment matches the IEC 61000-4-2 specifications (3.75 A/kV, 0.8 ns rise time, 2A at 30 ns and 1A at 60 ns). The rest of the results and comparison with discharges from a metal piece will be discussed in section 5.5.

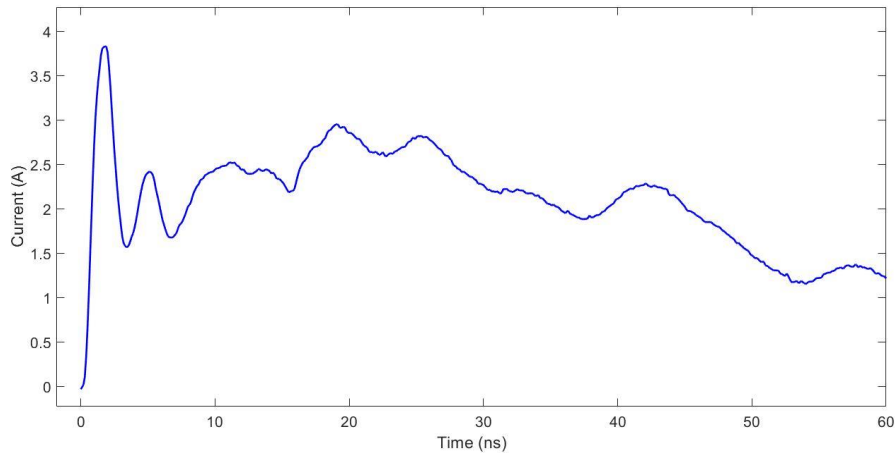


*Figure 5.5. Reference current waveform from an ESD gun discharging to ground*

### *5.3. Impedance Measurements and the Equivalent Circuit*

The simulation model for this ESD event consists of the elements of the ESD measurement setup, including the human body at various postures (while the metal piece is worn on waist or hand), air spark and the current carrying structures (a hospital bed with metallic frame). While both the discharging person and the current carrying structures are linearly dependent with voltage, the air spark needs to be modeled with a nonlinear relationship specified by Rompe-Weizel's spark resistance law. Thus, all but the spark can be modeled using a linear equivalent circuit made of RLC elements

The equivalent circuit for ESD current prediction is developed based on the impedance of each component in the setup. The impedance of the human body and the wires in the discharge path, including the short wire between the Al foil and the discharge location, and the long wire between the Al foil and the ground plane on the floor need to be measured.

Reflection ( $Z_{11}$ ) impedance between the human body and the discharge wire was measured using a vector network analyzer (VNA), as shown in Figure 5.6. Only one port of the VNA is used to capture the  $Z_{11}$  impedance between the metal piece on the body and the metal rod connected to the discharge wire (i.e., the impedance of the “differential” current between the body and the discharge wire). More details of the VNA connection is provided in Figure 5.6 and Figure 5.7.

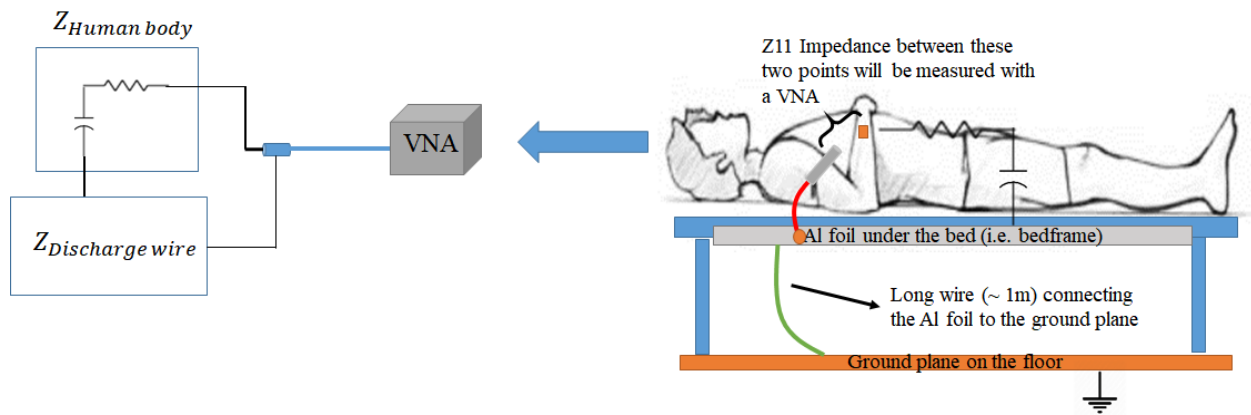


*Figure 5.6. Impedance measurement process using a vector network analyzer (VNA). The schematic on the left shows the elements in the differential current path.*

### 5.3.1. Impedance Measurement Setup

To capture the impedance between the human body and the wire, a short shielded coaxial cable (4 cm-long), shown in Figure 5.7, was connected to the VNA cable. The tip of the inner conductor of the short coaxial cable touched the hemispherical tip of the metal piece mounted on the subject’s body, while the metal rod touched the ground of the coaxial cable. In fact, the current path was from the tip of the coaxial cable to the human body, toward the Al foil, and then from the short wire and the metal rod to the shield of the coaxial cable. This path is depicted on the left side of Figure 5.6. Many ferrites are placed on the



VNA cable to attenuate the common mode currents on the surface of the shield of the short coaxial cable.

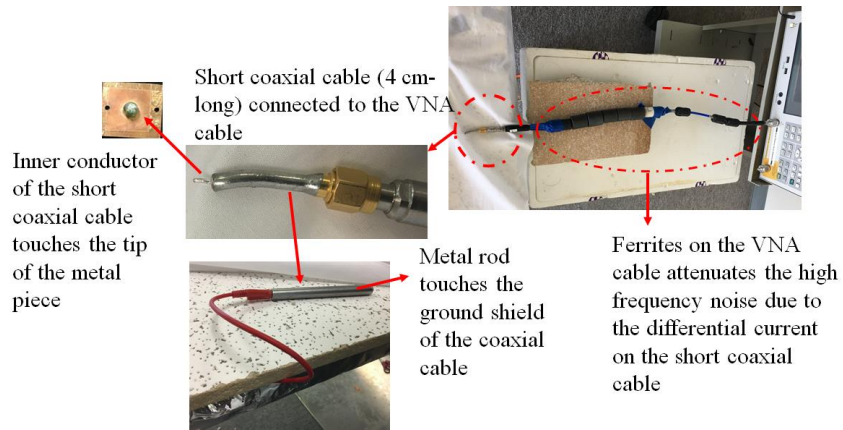


*Figure 5.7. Components of the impedance measurement setup*

Figure 5.8 displays more details of the connection between the metal piece mounted on the subject's body and the short wire connected to the Al foil under the bed. The VNA measured  $Z_{11}$  (reflection) impedance using the current that flows in the current path shown in Figure 5.6.

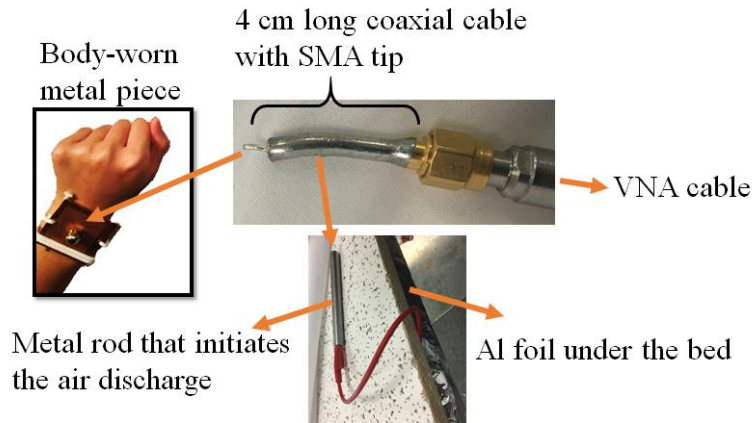
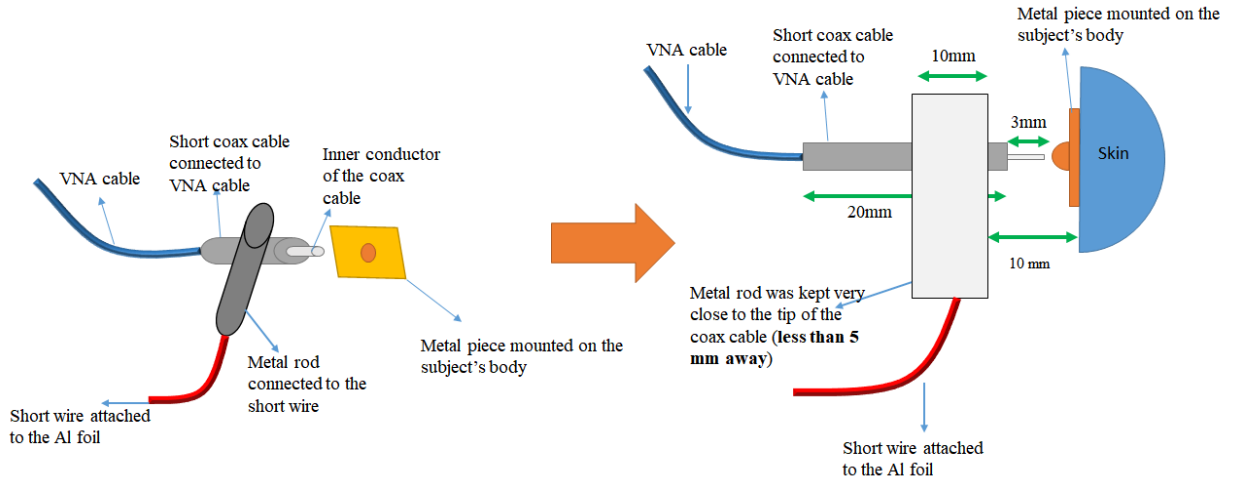


Figure 5.8. A short coaxial cable of 4 cm length is added to the VNA cable to measure the impedance between the metal piece and the metal rod attached to the short wire (30 cm long).

During the impedance measurement, the subject kept the metal rod very close to the edge of the ground shield of the short coaxial cable connected to the VNA cable (less than 5mm away) to minimize the parasitic inductance on the shield, however, it did not make contact with the metal piece. The distance between the metal rod and the metal piece was kept at about 10mm. Figure 5.9 shows the details of the measurement setup at the tip of the coaxial cable.

Before starting the impedance measurement, the VNA (model E5071C) was calibrated using the following settings: log magnitude format, applied power 10 dBm, 1601 points data, and range of frequencies: 1 MHz to 3 GHz. After calibration of port 1, the short coaxial cable was added to the VNA cable and port extension was performed in *short* condition (i.e., the inner conductor and the ground of the cable were connected with a piece of copper tape). In the format settings, the Smith chart was selected, and the port extension

was manually added equal to the length of the cable (about 40 cm) until a small circle was displayed at the left side of the Smith chart.



*Figure 5.9. Locations of the metal rod (connected to the short ground wire) and the short coaxial cable (connected to the VNA cable)*

After performing port extension, the dynamic range of the VNA with the cables was obtained, as shown in Figure 5.10. All the measurements were found to lie within the two extremes of impedance for open and short conditions. One example of the measurements is shown in Figure 5.10 for comparison (all other measurements are discussed in detail in the next sections). The measurement shows the impedance between the Al foil and the ground plane on the floor, wherein the tip of the short coaxial cable touches the Al foil and the ground of the coaxial cable touches the ground plane on the floor. Impedance measurement results for the six test configurations (3 body postures and 2 device locations) and the equivalent RLC circuit are provided in section 5.4.

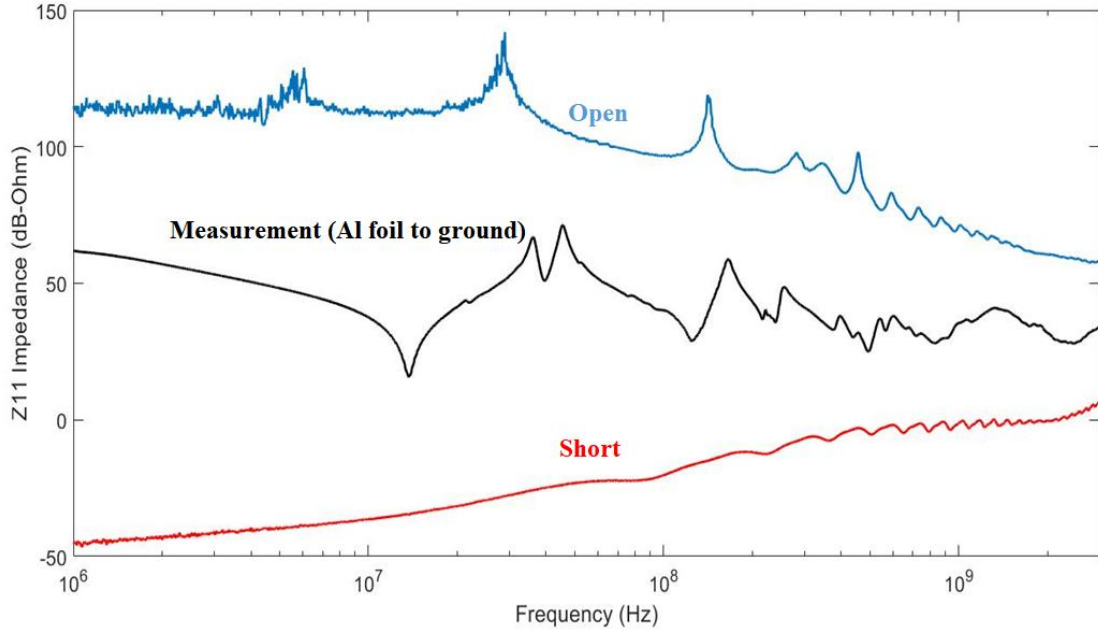


Figure 5.10. The dynamic range of the VNA after calibration and port extension. One example measurement is shown to ensure the impedance data lies within the range between the open and short conditions.

### 5.3.2. Equivalent Circuit Elements of Impedance Measurement Setup

Figure 5.11 shows various elements in the impedance measurement setup. The human body is simulated with a resistance,  $R_b$ , and capacitance relative to the Al foil,  $C_b$ , connected in series. In each of the six discharge configurations, the associated values for  $R_b$  and  $C_b$  will be found by fitting the simulation results to the measurements.

There is an additional capacitance between the subject and the wall and ground,  $C_{bw}$ , which will be assumed. A capacitance meter estimated this capacitance around  $35 \text{ pF}$ . The inductance of the short wire (labeled (1) in Figure 5.11) is denoted by  $L_w$ . The 1 m-long wire from the Al foil to the ground plane (labeled (2) in Figure 5.11), is represented by an inductance  $L_l$  and the capacitance of the Al foil relative to the ground  $C_l$  is connected in

parallel. Due to the radiation loss of the Al foil, a series RC connection is added between the Al foil and the ground ( $R_{rad2}, C_{rad2}$ ). This assumption is according to radiation loss in an antenna [72]. Based on previous experiments, these two parameters were selected as  $R_{rad2} = 150\Omega$  and  $C_{rad2} = 20\text{ pF}$ .

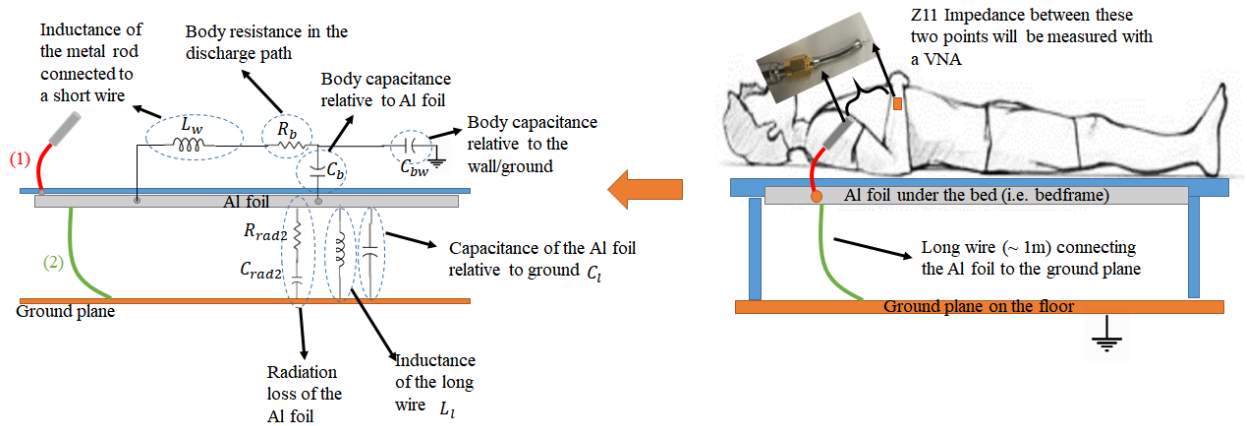


Figure 5.11. Impedance elements in the VNA setup

The capacitance and inductance elements between the Al foil and the ground plane can be determined by analyzing the  $Z_{11}$  impedance of the long wire at low frequency (below 100 MHz). The measurement was performed by connecting the tip of the inner conductor of the short coaxial cable to the long wire, while the shield (ground) of the coaxial cable touches the ground plane (Figure 5.12).

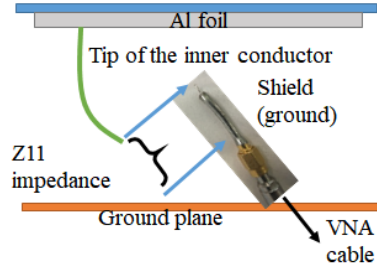


Figure 5.12. Impedance measurement for the long wire between the Al foil and the ground plane

Figure 5.13 shows the impedance result for the long wire, which indicates a series RLC at low frequency. Using the low-frequency impedance, the capacitance is estimated as:

$$\frac{1}{C_l \times 2\pi f} = 10^{\frac{61.9 \text{ dB}}{20}} \rightarrow C_l = 128 \text{ pF} \quad (5.1)$$

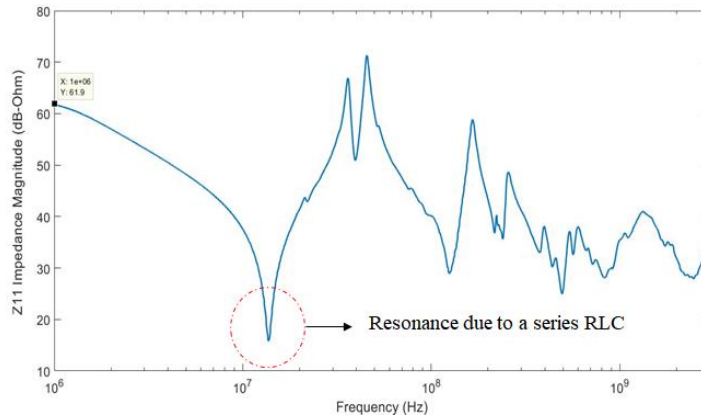


Figure 5.13. The impedance of the long wire relative to the ground

Using the resonance frequency at 13.8 MHz, the inductance  $L_l$  can be estimated as:

$$\frac{1}{2\pi\sqrt{L_l C_l}} = 1.38 \times 10^7 \rightarrow L_l = 1.04 \mu\text{H} \quad (5.2)$$

Using parallel LC from the Al foil to the ground ( $L_l$  and  $C_l$ ) results in a resonance at about 13 MHz. This can be obtained from the following expression for the resonance frequency of a parallel LC (1100 nH and 130 pF respectively):

$$f_r = \frac{1}{2\pi\sqrt{L_l C_l}} = \frac{1}{2\pi\sqrt{1100 \times 10^{-9} \times 130 \times 10^{-12}}} = 13 \text{ MHz} \quad (5.3)$$

Since this resonance was not seen in the measurement, a small series resistance  $R1 = 5\Omega$  was added to the parallel to suppress the Q factor of the resonance at 13 MHz. Addition of this non-physical element is a consequence from modeling a physically large system by a simple equivalent circuit.

Series RC elements labeled as  $R_{rad1}$  and  $C_{rad1}$ , representing radiation loss was connected in parallel to the inductance of the short wire,  $L_w$ . Moreover, a small capacitance was assumed between the metal piece and the Al foil in the range of 1 pF to 10 pF. The updated RLC elements that were used in simulation are shown in Figure 5.14. It is to be noted that the series elements need to be in parallel with the inductance, since radiation and conduction (through inductance) are two separate paths for the discharge current.

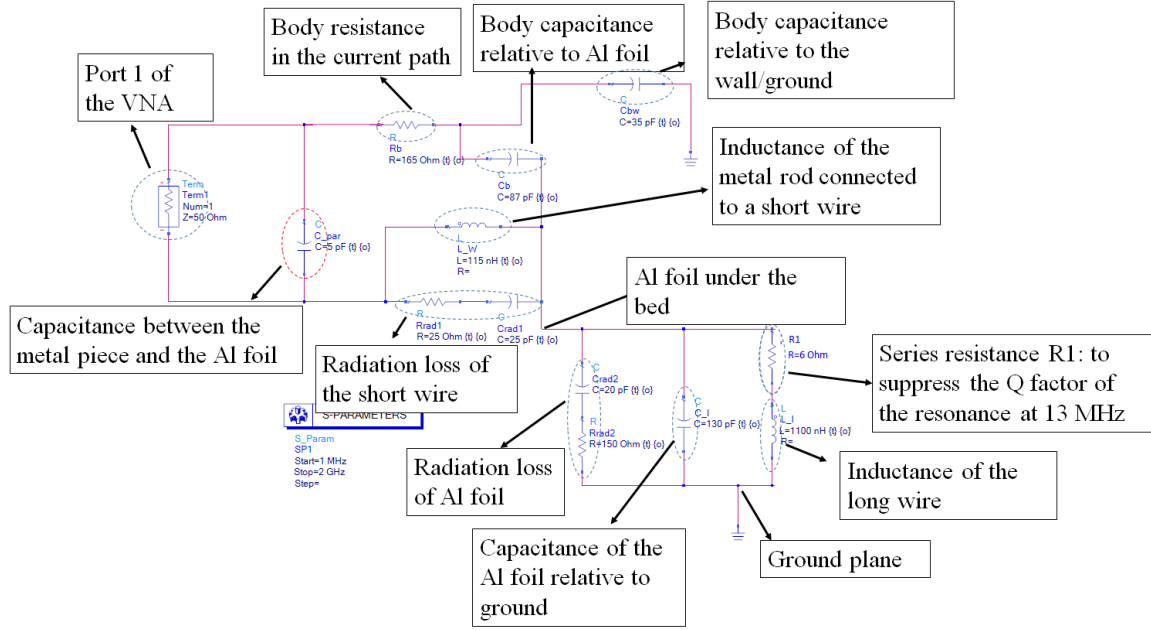


Figure 5.14. ADS equivalent circuit for  $Z_{11}$  impedance measurement setup for a subject lying down on a bed and wearing a metal piece on his hand

Thus far, the associated values of some of the elements in the equivalent circuit were directly measured by impedance measurement including  $R_{rad2} = 150 \Omega$ ,  $C_{rad2} = 20 \text{ pF}$ ,  $C_l = 130 \text{ pF}$ ,  $L_l = 1100 \text{ nH}$ ,  $R_1 = 200 \Omega$ ,  $R_2 = 1 \Omega$ ,  $C_w = 35 \text{ pF}$ . For the rest of the elements including the resistance of the subject  $R_b$ , capacitance relative to the Al foil  $C_b$ , the inductance of the short wire,  $L_w$ , and the radiation elements of the short wire  $R_{Rad1}$  and  $C_{Rad1}$ , the best fit need to be obtained to match the measured impedance. These parameters are expected to be different for each of the six discharge configurations.

The circuit simulation was performed using Advanced Design Systems (ADS), which is an electronic design software. The tuning tool and the optimization cockpit of ADS were employed to obtain the best fit from the RLC circuit to the VNA measurement in each test configuration. At first, the tuning tool was used to find the range of parameters and then



the fitted RLC values were found using the optimization cockpit. The optimization method was gradient descent and the goals were defined as the impedance values of the measurement (magnitude of  $Z_{11}$ ) at 12 frequency points of 1 MHz, 4 MHz, 10 MHz, 200 MHz, 300 MHz, 400 MHz, 600 MHz, 800 MHz, 1 GHz, 1.1 GHz, 1.5 GHz, 2 GHz. The rest of the parameters were optimized within the range specified in Table 4.

*Table 4. Range of optimization for RLC parameters of the equivalent circuit*

	$R_b$ (Ohm)	$C_b$ (pF)	$L_w$ (nH)	$R_{Rad1}$ (Ohm)	$C_{rad1}$ (pF)	$C_{Par}$ (pF)
Min	50	50	100	10	10	0.5
Max	200	300	300	50	50	5

The range of values for the circuit elements in Table 4 can be justified using literature data and physical approximations. The radiation parameters  $R_{Rad1}$  and  $C_{rad1}$  are within the range of previous experiments performed by our group. Body resistance  $R_b$  in the IEC 61000-4-2 standard is 300 Ohm. This value is based on a hand-held rod in the HMM scenario (no dimensions provided). However, the metal piece in this experiment, is probably smaller in size than the hand-held rod. Thus, the resistance is expected to be less than 300 Ohm.

Body capacitance relative to the bed frame  $C_b$  depends on the body posture, as a larger area of contact with the bed (lower distance between the body and the Al foil) increases the capacitance. Thus, it is expected that lying down posture results in a higher capacitance than standing or sitting posture. Considering that the body capacitance for a standing

person in the IEC 61000-4-s is assumed 150 pF, the range of  $C_b$  values in Table 4 seem valid.

The inductance of the short wire,  $L_w$ , can be estimated from the self-inductance formula of a single wire in free space as defined below [73]:

$$L = 2l \left( \ln\left(\frac{2l}{d}\right) \left(1 + \sqrt{1 + \left(\frac{d}{2l}\right)^2}\right) - \sqrt{1 + \left(\frac{d}{2l}\right)^2} + \frac{\mu}{4} + \left(\frac{d}{2l}\right) \right) \quad (5.4)$$

where  $l$  is the wire length, and  $d$  is its diameter. In the discharge setup, the length of the short wire was around 20 cm, and its diameter was about 3 mm. The estimated  $L_w$  is 200 nH. Thus, the range of values for this element in Table 4 seem reasonable.

The maximum capacitance of the metal piece relative to the Al foil,  $C_{par}$ , can be estimated by assuming the capacitance between two parallel plates:

$$C = \frac{\epsilon_0 A}{d} \quad (5.5)$$

where  $\epsilon_0$  the permittivity of air ( $8.85 \times 10^{-12} \frac{F}{m}$ ),  $A$  is the area of each plate and  $d$  is the distance between the two. The maximum capacitance occurs when the metal piece is parallel (i.e., horizontal) with respect to the Al foil. The maximum value for  $C_{par}$  can be 5 pF.

### 5.3.3. Impedance Measurement Results

This section provides the impedance measurement data and the estimated results using the equivalent RLC circuit described in section 5.3.2. The equivalent RLC elements for the setup were described in section 5.3.2.

Figure 5.15 shows the  $Z_{11}$  impedance magnitude measured between the metal piece worn by the subject and the short wire attached to the Al foil, in a log-log format. It shows the comparison between the simulation using ADS and the measurement using VNA, for 3 postures of lying down, sitting on the bed and standing on the floor, considering both locations of the metal piece (i.e., hand and waist).

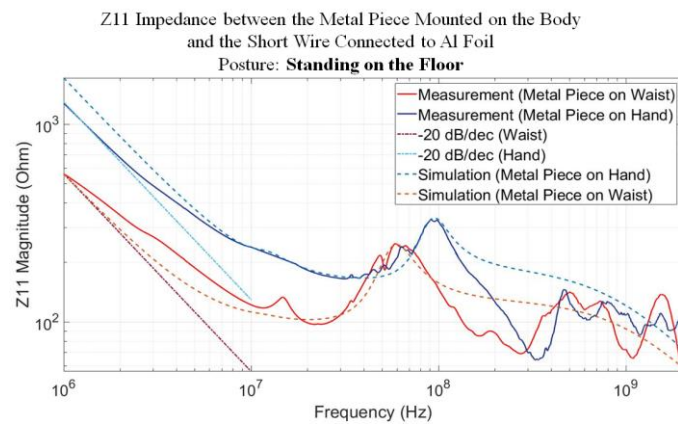
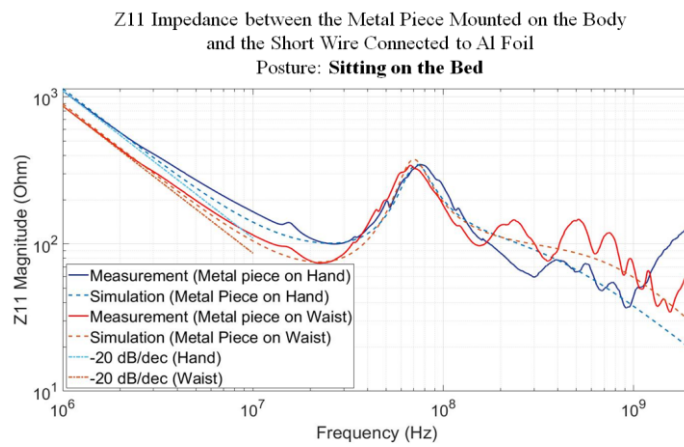
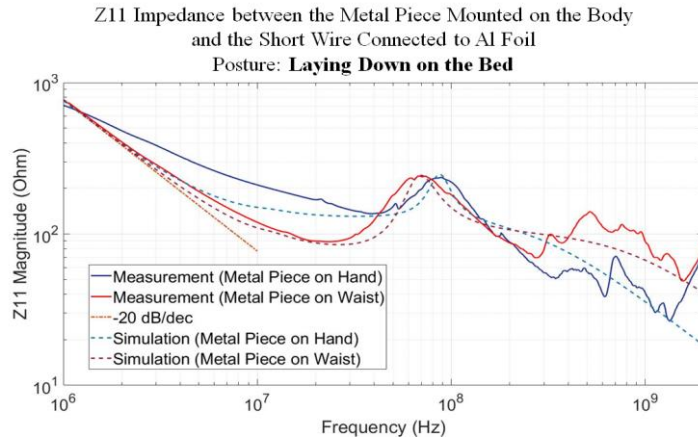


*Figure 5.15. Z11 Impedance between the metal piece on the subject's body at various postures, and the short wire connected to the Al foil*

The simulation results shown in Figure 5.15 have a reasonable agreement with the measurements, however, there are differences between the two at higher frequencies (after 100 MHz). A number of reasons can explain these differences. As the frequency increases, the assumption of lumped elements for the impedance model may not be valid anymore and deviations from the measurements become more pronounced. In fact, at higher frequency ranges, the human body needs to be modeled with a transmission line, which will be a more complex simulation. In fact, the body can be modeled with discrete elements with finite delay between different segments. This deviation could also be attributed to the parasitic elements (capacitance and inductance) between the tip of the inner conductor and the shield of the short coaxial cable (or tip of the metal piece on hand and the metal rod) as shown in Figure 5.9. It is critical to note that the values of the equivalent circuit are only semi-physical. Thus, not every variation can be directly explained. The goal is to have an approximate circuit that predicts the current, not to fully justify each component and value.

In each of the measurement plots, a line representing capacitive behavior (20 dB/Dec) is drawn a tangent to the impedance results at 1 MHz. This line is added to confirm the capacitive assumption for the impedance model of the human body, which will be discussed in section 5.4.2.

#### 5.3.4. Analysis of the Impedance Measurement Results

The list of fitted parameters of the equivalent circuit used in the simulation for each configuration is provided in Table 5. A common trend for  $R_b$  among all configurations is the lower resistance for waist-worn than the hand-worn tests. The location of the metal piece on the body affects the current path and therefore, the resistance of the body changes accordingly. Therefore, the body resistance from the waist (i.e., shorter path) is expected

to be less than the hand. It was found that the fitted  $R_b$  was close to the impedance magnitude in the first resonance at around 20 MHz. This result reflects the resonance behavior expected for a series RLC circuit consisting of  $R_b$ ,  $C_b$ , and  $L_w$ .

It is expected that the fitted values of the body capacitance relative to the Al foil  $C_b$  does not change with respect to the metal piece location on the body, and only depends on the body posture. However, the results of Table 5 shows that in all configurations,  $C_b$  is larger when the metal piece is worn on the waist compared to hand. This unexpected result can be explained by a closer look at the measurement setup for the two positions of the metal piece, shown in Figure 5.16. The position of the subject relative to the Al foil on the edges of the table changes for the two positions of the metal piece, which results in this difference in body capacitance. It is to be noted that the non-physical element of the equivalent circuit,  $R_1$ , was removed for current prediction, since it was added to suppress the Q factor of a low the resonance frequency that did not affect the current waveform (below 100 ns). Thus, all the elements of the equivalent circuit for current prediction can be assumed based on the physics of the model.

When the metal piece was mounted on the subject's hand, the subject had to lay down in the middle of the table and extend his hand to reach the coaxial cable from the VNA and the metal rod. However, when the metal piece was mounted on his waist, the subject had to position himself very close to the edge of the table, in order to reach the metal rod and the tip of the coax cable. Therefore, during waist measurement, the subject's body was closer to the Al foil (on the edge), which resulted in a lower impedance and larger capacitance at low frequency (1MHz).

Table 5. List of the fitted parameters of the equivalent circuit for impedance measurement

Posture	Metal Piece location	$R_b$ (Ohm)	$C_b$ (pF)	$L_w$ (nH)	$C_w$ (pF)	$R_{Rad1}$ (Ohm)	$C_{Rad1}$ (pF)	$C_{Par}$
Lying down on the bed	Hand	132	173	65	34	10	47	5
Lying down on the bed	Waist	84	170	135	34	23	39	2
Sitting on the bed	Hand	101	101	205	35	44	20	4.3
Sitting on the bed	Waist	75	140	233	35	44	20	3
Standing on the Floor	Hand	165	87	115	35	25	25	2
Standing on the Floor	Waist	102	250	170	35	29	44	1.6

For the hand-worn configurations, the metal piece on the subject's wrist was about 20 cm away from the edges (arm was extended above the table to reach the tip of the coaxial cable), while during waist measurements, the metal piece on the body was about 5 cm away from the Al foil on the edge of the table. Thus, the larger capacitance of the body relative to the Al foil during waist impedance measurement can be attributed to the proximity of the metal piece to the Al foil on the edge of the hospital bed. This difference was largest when the subject was standing on the floor near the bed. The distance between the metal piece on the subject's waist and the edge of the bed was less than 10 cm, while for hand-

worn configuration, this distance was more than 30cm. Note that during ESD current measurement, the position of the subject relative to the edges of the hospital bed was the same. Therefore, the fitted parameters are valid for ESD current prediction.

For all the postures, the inductance of the wire,  $L_w$ , for the waist-worn configurations is larger than the hand-worn configurations. The reason could be attributed to the changes in the wire shape when the subject positions himself close to the edge of the bed during waist-worn configurations. When the subject is in the middle of the bed, the wire is completely extended outward and becomes relatively straight, however, when the subject positions himself close to the edge of the bed to reach the metal rod, the wire will not be completely straight, and its shape becomes close to a semicircular loop. Thus, the inductance (or the self-inductance) of the wire in the waist-worn configuration will be larger than hand-worn configuration.

The simulation results shown in Figure 5.15 have a reasonable agreement with the measurements, however, there are differences between the two at larger frequencies. This deviation could be attributed to the parasitic elements (capacitance and inductance) between the tip of the inner conductor and the shield of the short coaxial cable (or tip of the metal piece on hand and the metal rod).



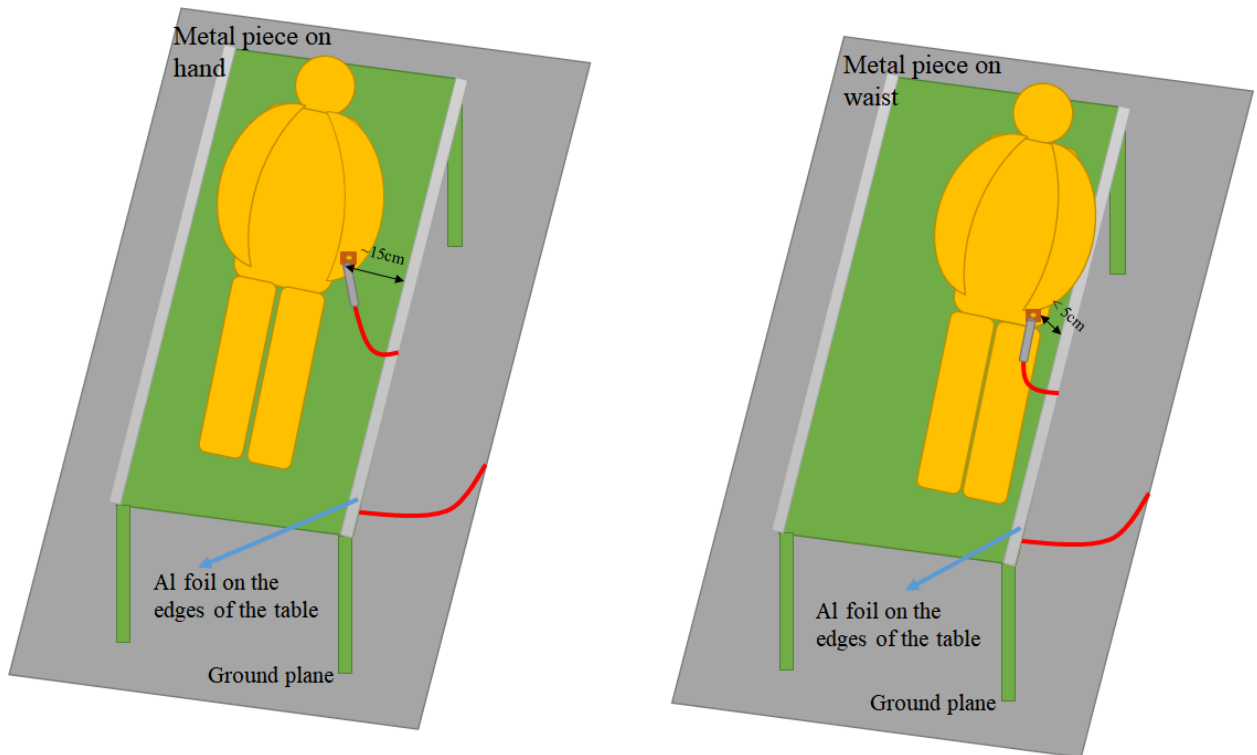


*Figure 5.16. The position of the subject with respect to the edge of the hospital bed during impedance measurement while lying down on the bed (left: The metal piece on hand, Right: The metal piece on waist).*

### 5.3.5. The Validity of The Assumption of Body Capacitance

To evaluate the deviation from capacitive behavior at low frequency, a dashed line is displayed in Figure 5.15 that represents  $-20$  dB/dec (i.e., a capacitance in a log-log plot). Although using capacitance for simulating human body is an intuitive choice based on literature and standards, some researchers have shown that the impedance of the body does not follow a capacitance model, even at a low frequency of 1MHz [22], [46][74]. Figure 5.17 shows the impedance of the human body measured by Zhou et al. [22] and Kagawa et al.'s studies [46], and compares the results with a capacitive behavior. Both measurements were performed for the HMM scenario. The starting frequency of the measurement for

Zhou et al. [22] and Kagawa et al.'s study [46] was 1MHz and 200 kHz respectively. It can be seen from the Figure 5.17 that both results deviate from 20 dB/Dec lines, while Kagawa et al.'s results, which starts at a lower frequency, display less deviation. Note that the results of these articles cannot be directly compared with the measurements of the present study since the impedance configurations used in this study are different from the HMM scenario.

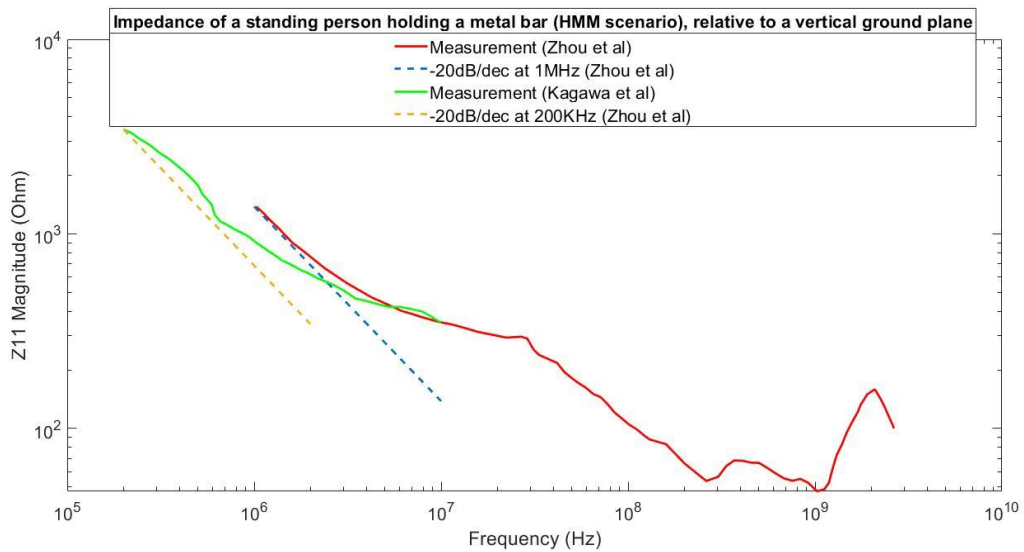
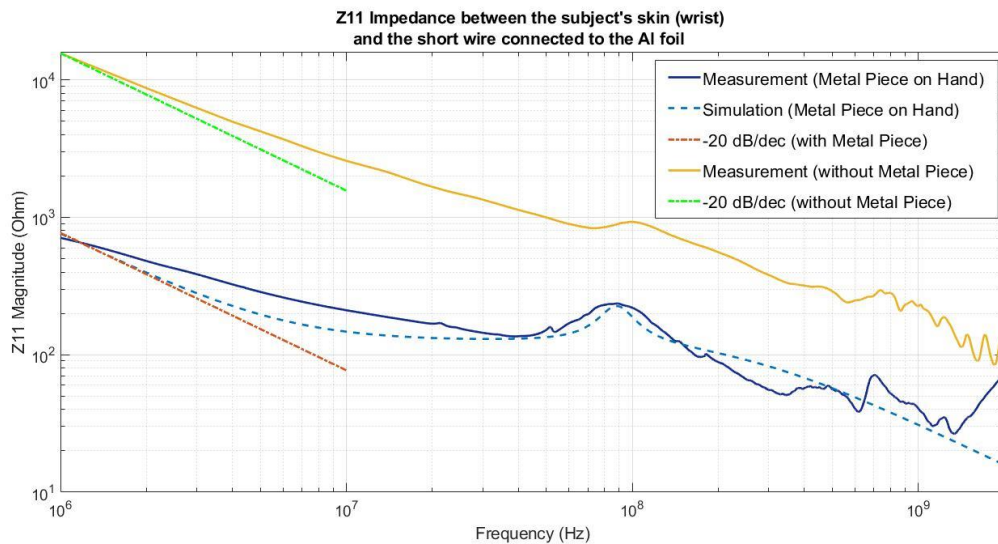


Figure 5.17. Comparison of the impedance of the human body measured in the literature and a capacitance with -20 dB/Dec relationship.

To further explore this behavior of the human body impedance and ensure that the impedance of the metal piece itself does not influence the results, an additional measurement was performed after removing the metal piece. Figure 5.18 shows the impedance measurement with and without wearing the metal piece. The impedance magnitude for the skin is more than 1 order of magnitude larger than the impedance for the metal piece, which is expected due to the resistance of the human skin. The -20 dB/dec line has the same deviation in both conditions, i.e., with and without wearing the metal piece.

A possible explanation for the deviation from -20dB/Dec might be that the frequency range is not low enough to observe a capacitive behavior. In other words, the human body impedance above 100 kHz may not be simulated by a capacitance and resistance. However, as the goal of the study is to obtain a useful equivalent circuit for the purpose of simulating the current, and not a physical representation of each component in the circuit, no further investigations have been performed on the observed deviation from a 20 dB/dec impedance.



*Figure 5.18. The impedance measured between the subject's skin and the short wire connected to the Al foil (comparison with the measurement for which the metal piece is mounted on the subject's body).*

#### *5.4. Equivalent Circuit Model for ESD Current Prediction*

The equivalent circuit for ESD current estimation can be obtained using the circuit obtained for impedance measurements shown in Figure 5.14, however, instead of the VNA

port, the Rompe-Weizel's spark resistance need to be used. The spark can be modeled with a time-varying resistance according to the Rompe-Weizel's law [24]:

$$R_{spark}(t) = \frac{l}{\sqrt{2K_R \int_0^t i(t')^2 dt'}} \quad (5.6)$$

where  $K_R$  is a gas constant related to the gas pressure ( $10^{-4} \frac{m^2}{V^2s}$  was used), and  $l$  is the spark length. Taka and Fujiwara [75] modified the Rompe-Weizel's model and showed that the associated voltage across the spark gap can be simulated by:

$$v_s(t) = \frac{V_C}{\sqrt{1 + \exp\left(\left(\frac{\alpha}{p_{air}}\right) \times \left(\frac{V_C}{l}\right)^2 \times t\right)}} \quad (5.7)$$

In this formula,  $V_C$  is the applied ESD voltage,  $p_{air}$  is the air pressure in *atm*,  $\alpha$  is the gas constant ( $1.1 \text{ atm.cm}^2/V^2s$ ) related to  $K_R$ , and  $l$  is the length of the spark. The spark had to be replaced by this time-varying voltage in the equivalent circuit, as shown in Figure 5.19.

The time-varying voltage across the air gap, and therefore the current waveform depends on the spark length. Due to the complexity of designing a setup for spark measurement, this study only assumed estimated values for spark length. To explore the effect of varying spark lengths on the waveform, current estimations were performed at 3 spark lengths. At first, the spark length will be assumed equal to 100% value of Pashen's length. This assumption is based on the slow speed of approach and presence of seed electrons (by adding graphite on the tip of the metal piece). The second estimated waveform will be at 50% Paschen's length, which is assumed to represent the worst practical discharge since shorter spark lengths lead to a faster rise time and a more severe discharge. Note that this

discharge condition is only a practical assumption for the most severe discharge rather than the absolute worst-case. The third estimation will be at a spark length between 100% and 50% Paschen's law, which corresponds to a rise time (or peak current derivative) close to that of the measurement. Initial observations showed that despite using pencil marks on the discharge tip (to reduce the statistical time lag) and approaching the metal piece with a slow movement, the rise time of the measured waveform usually corresponds to some value less than 100% of the Paschen's length. A transient simulation was assigned to the circuit and the stop time was 500 ns, and the time step was 20 ps.

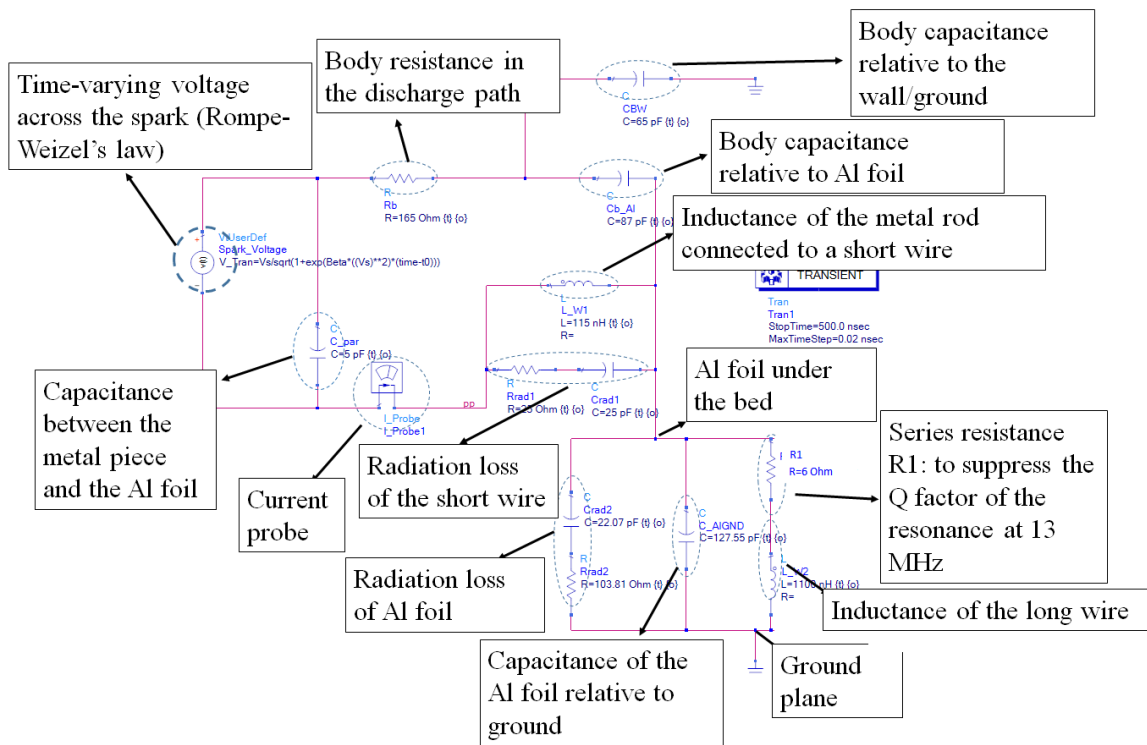


Figure 5.19. The equivalent circuit of the ESD current measurement setup

### 5.5. ESD Current Measurements and Estimation Results

ESD measurements were performed for four voltage levels of 2 kV, 4 kV, 6 kV, and 8 kV at each test configuration (i.e., 3 postures and 2 metal piece locations), resulting in 24 waveforms. Using the same parameters found in impedance measurement experiments, the discharge current was estimated and compared with the measurements. The measurements were compared in terms of their severity indicators including peak current, total transferred charge to the ground, and peak current derivative. At each body voltage, these four parameters are extracted from the waveform and compared among the test configurations. Moreover, the severity parameters were compared with that of the ESD gun calibration waveform. These comparisons will show whether ESD testing in the tabletop configuration is sufficient for wearable medical devices, and which configurations (device locations and postures) result in the most severe discharges.

Figure 5.20 shows an example of ESD waveform for discharge from a hand-worn metal piece, while the subject, who is charged at 6 kV, is lying down on the hospital bed. The current waveform for this test setup shows an initial peak before the largest peak, which is not seen in typical ESD waveforms, such as the calibration current shown in Figure 5.5, or the HMM scenario specified in the IEC 61000-4-2 standard [22], [26], [34], [46]. The initial peak occurs due to the presence of a short wire in the discharge path. In fact, a fraction of the accumulated charge on the subject releases into a local capacitance, and then the rest of the charge on the subject releases into the bed-frame and the large ground plane under the bed. The local capacitance of the wire can be attributed to  $C_{rad1}$ ,

the capacitance associated with the radiation of the wire. An analysis of the wire impedance elements on the waveform is provided in section 5.6.

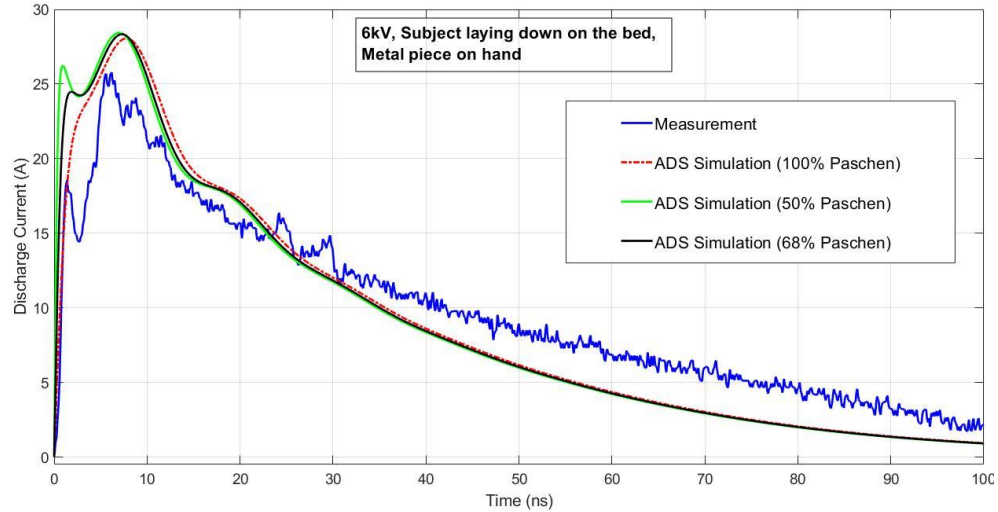


*Figure 5.20. ESD waveform for discharge from the hand while the subject is lying down on the bed (comparison with current estimation)*

Figure 5.20 shows reasonable agreement between the measurement and the estimated waveform using the equivalent circuit. For the test condition in Figure 5.20, the peak current derivative of the measured waveform using the Paschen's length resulted in a 40% error compared to measurement. It was found that by using a spark length equal to 68% of the Paschen's value, the estimated peak current derivative matches the measurement (with 1% error).

The main difference between the three estimated waveforms is in the first initial current rise portion of the waveform (prior to the peak value), and after the peak, the estimated curves are nearly identical. Figure 5.21 shows the initial current rise of the three estimated waveforms as well as the measurement before 5 ns. The dashed red curve has the slowest rise time (or peak current derivative) and corresponds to the 100% Paschen,

and the green curve represents the worst practical case of discharge achieved by 50% Paschen's length, and shows the steepest slope (i.e., largest peak current derivative) among all the waveforms. The maximum slope of the black curve or the peak current derivative is very similar to that of the measured waveform.

The deviations between measurement and the simulation, particularly the initial bump after 1.5 ns, are probably caused by the inaccuracies of the impedance model at higher frequencies (i.e., above 100 MHz). As discussed in section 5.3.3, the limitations of the lumped circuit elements at higher frequency ranges resulted in deviation between the simulation model and the impedance measurements. To overcome these deficiencies, a transmission line model of the human body consisting of discrete elements can be developed, however, it will be much more complicated than the circuit model, and integration with the nonlinear spark resistance model may be challenging.

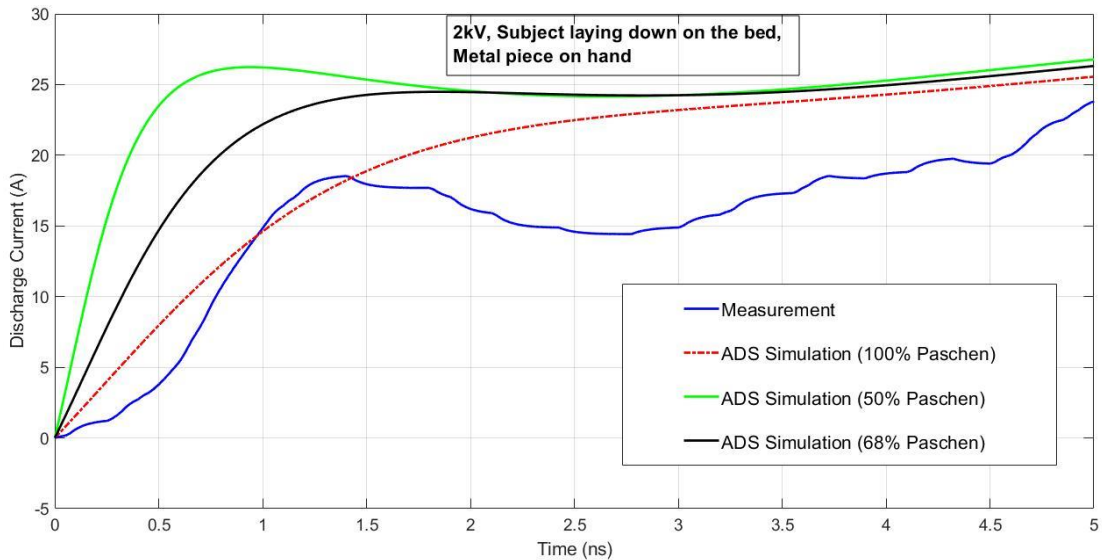


Figure 5.21. Initial peak of the ESD waveform at 6 kV discharge from the subject's hand, while he is lying down on the bed)



The accuracy of the simulation model to predict the waveform parameters including  $I_{max}$ ,  $\left(\frac{dI}{dt}\right)_{max}$ , and  $Q_{ESD}$ , is shown in Table 6. The percent errors associated with the peak current derivative using 100% Paschen's length are rather large (47%) compared to the average for the peak current (12%) and the charge transfer (9%). This large prediction error indicates that 100% Paschen's length is not a valid assumption for the spark length, despite the slow speed of approach and using pencil marking on the tip of the metal piece. An additional factor is the limitations of the lumped model elements for high frequency ranges that lead to inaccuracies in the rising edge of the current waveform (caused by the deviations of the impedance model from the measurements). The relative magnitude of each effect (i.e., deviation of the spark length from 100% Paschen's law or the limitations of the lumped circuit mode) need to be obtained via a sensitivity analysis. In this study, no sensitivity analysis can be performed since spark lengths were not measured and their effects cannot be validated.

The 7<sup>th</sup> column in Table 6 shows the fitted spark lengths relative to the Paschen's length. It is to be noted that the large prediction error for  $\left(\frac{dI}{dt}\right)_{max}$  is in the range of the acceptable error in Zhou et al.'s [22] simulation model.

Table 6. The accuracy of the simulation using the developed equivalent circuit for 6 test configurations at 4 voltage levels

Voltage (V)	Posture	Metal piece location	Percent Errors Using 100% Paschen's length			
			$I_{max}$	$\left(\frac{dI}{dt}\right)_{max}$	$Q_{ESD}$	Fitted L_spark/L_Paschen
2000	Lying down on the bed	Hand	-8%	-18%	5%	91%
4000	Lying down on the bed	Hand	-4%	-43%	-2%	78%
6000	Lying down on the bed	Hand	9%	-52%	-5%	68%
8000	Lying down on the bed	Hand	8%	-20%	11%	88%
2000	Lying down on the bed	Waist	3%	-60%	-7%	100%
4000	Lying down on the bed	Waist	7%	-30%	-4%	85%
6000	Lying down on the bed	Waist	16%	-39%	13%	79%
8000	Lying down on the bed	Waist	18%	-46%	15%	73%
2000	Sitting on the bed	Hand	25%	-41%	-11%	70%
4000	Sitting on the bed	Hand	11%	-10%	-11%	98%

6000	Sitting on the bed	Hand	16%	-65%	8%	72%
8000	Sitting on the bed	Hand	10%	-45%	5%	75%
2000	Sitting on the bed	Waist	11%	50%	-5%	91%
4000	Sitting on the bed	Waist	5%	-32%	-5%	84%
6000	Sitting on the bed	Waist	10%	-30%	-9%	85%
8000	Sitting on the bed	Waist	20%	-30%	-5%	82%
2000	Standing on the floor	Hand	-4%	-43%	-7%	75%
4000	Standing on the floor	Hand	12%	-60%	9%	63%
6000	Standing on the floor	Hand	12%	-69%	9%	54%
8000	Standing on the floor	Hand	14%	-72%	12%	53%
2000	Standing on the floor	Waist	-20%	-10%	17%	98%
4000	Standing on the floor	Waist	6%	-20%	11%	91%
6000	Standing on the floor	Waist	-13%	-16%	-10%	92%

8000	Standing on the floor	Waist	-18%	-34%	-8%	81%
------	--------------------------	-------	------	------	-----	-----

Next sections discuss of the waveform parameters for the test configurations and the ESD gun results. The trends of the parameters for waist-worn and hand-worn configurations in each posture are explained based on the physical elements of the setup.

### 5.6. ESD Gun Discharge Waveform

In general, two phases can be seen in a discharge waveform from an ESD gun: the initial rise until the peak current (within which  $\left(\frac{dI}{dt}\right)_{max}$  occurs), and a falling edge until the current reaches zero. Figure 5.22 illustrates the two phases of the discharge process for an ESD gun and the time at which the peak current derivative occurs. The initial rise time depends on the voltage collapse within the relay (filled with high-pressure sulfur hexafluoride), and the pulse-forming elements in the ESD gun such as the capacitance between the discharge tip and the ground plane, and the lumped resistance shown in Figure 5.22 [35]. The complete details of the elements involved in each phase are discussed in Wang et al.'s study [35].

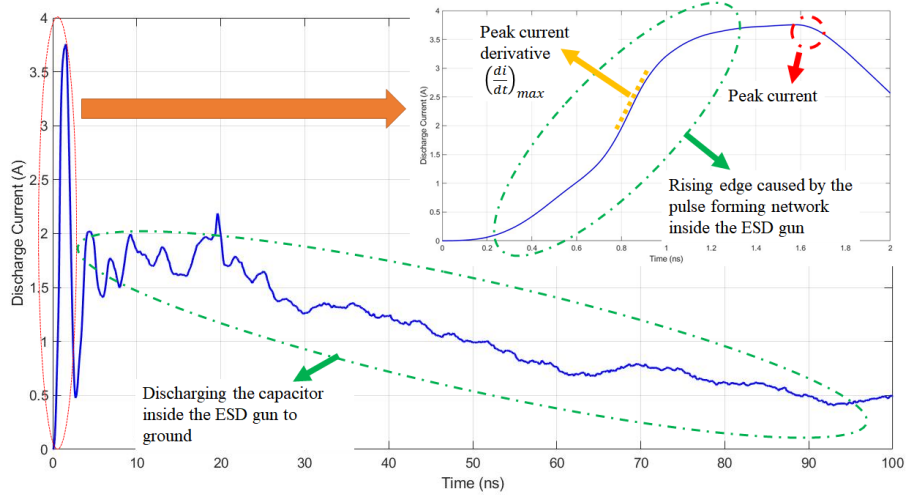


Figure 5.22. Two phases of current waveform from an ESD gun.

Due to the presence of the pulse-forming R-C-R network, specified in [35], the rising edge will behave similarly to an RC circuit discharging with a decay time constant of  $RC$ . Using these assumptions, a first order approximation of  $\left(\frac{di}{dt}\right)_{max}$  in the rising edge of the waveform can be found from the following expression:

$$i(t) \propto \frac{V_s}{R} \cdot \left(1 - e^{-\frac{t}{RC}}\right) \rightarrow \left(\frac{di}{dt}\right)_{max} \propto \frac{V_s}{R} \cdot \frac{1}{RC} \quad (5.8)$$

where  $V_s$  is the charging voltage, and  $R$  and  $C$  are the resistance and capacitance of the pulse forming network of the ESD gun. This expression confirms that  $\left(\frac{di}{dt}\right)_{max}$  for the ESD gun increases linearly with the charging voltages, since the decay constant ( $RC$ ) is the same at all voltage levels.

The falling edge of the waveform represents an RC discharging circuit. Since the capacitor and the resistors of the rising edge ( $C = 20 \text{ pF}$ ,  $R = 36 \text{ Ohm}$ ) are much smaller than the discharge capacitor ( $110 \text{ pF}$ ) and resistor ( $330 \text{ }\Omega$ ) of the falling edge [35],

$\left(\frac{dl}{dt}\right)_{max}$  will always be in the rising edge of the waveform. This is due to the lower decay constant in the rising edge compared to the falling edge, which results in a steeper curve in the rising edge.

These explanations for the behavior of the ESD gun waveform, is only a simplified model compared to the real ESD event, since the inductive effects of the current paths have been ignored in the circuit model. Such inductive effects can only be analyzed with a full-wave model of the gun that considers all the interactions between the electromagnetic fields and the conductive structures.

#### *5.7. Current Waveform of an ESD from a Wearable Device*

The current waveform from a wearable metal piece consists of more complex phenomena than the ESD gun, due to the presence of a spark and the geometry of the subject. Instead of the relay in the ESD gun, the voltage collapse occurs in the gap between the hemispherical tip of the metal piece and the rod. The electrostatic field in the gap collapses from the charged voltage level of the subject (2 kV to 8 kV) to about 25V to 40V within 50 ps to 5 ns, depending on the spark parameters [34]. This electric field collapse results in an electromagnetic wave-front propagating with the speed of light. The associated discharge current expands within the spark length and reaches the person's hand, and further expands on the metallic rod and the short wire connected to the Al foil. This expansion of the current front experiences losses due to radiations of the wire and the subject's hand (assuming they act similar to an antenna). The rising edge of the current during an ESD spark is due to the expansion of the current front after the collapse of the electric field in the gap.

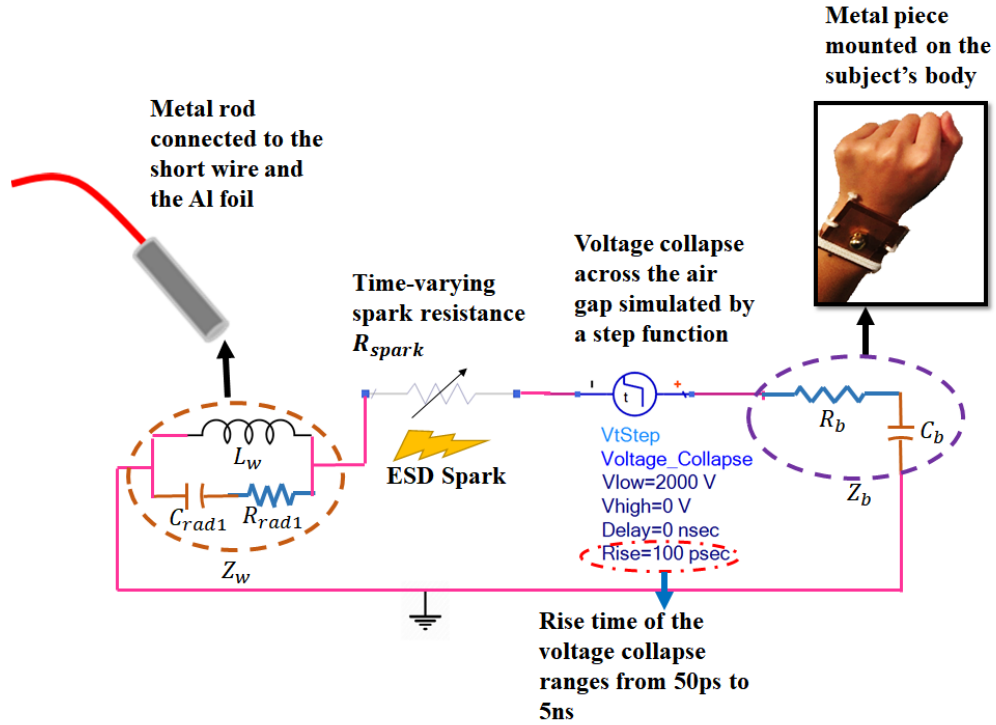


Figure 5.23. Equivalent circuit representation of the spark gap during ESD from a wearable device

The trend of the waveform parameters can be explained in terms of the impedance and the voltage. This section describes the mathematical expressions for  $I_{max}$  and  $\left(\frac{dI}{dt}\right)_{max}$  and  $Q_{ESD}$  as a function of body impedance, spark parameters and body voltage. Figure 5.23 shows a simplified circuit representation of the gap between the metal piece on the subject's body and the metal rod. It assumes that the Al foil acts as a ground. The impedances of the body and the wire in the frequency domain are denoted as  $Z_b(\omega)$  and  $Z_w(\omega)$ . A switch initiates the spark, which is modeled as a time-varying resistor. The voltage across the switch collapses from the initial value of  $V_C$ , which is the charging voltage of the subject. The discharge current can be simulated by the following expression (5.9):

$$I(t) = \mathcal{F}^{-1}\left\{\frac{\mathcal{F}(V_C) - \mathcal{F}(V_{Spark}(t))}{Z_{total}(\omega)}\right\} \quad (5.9)$$

where  $V_{Spark}(t)$  is the time-dependent voltage across the spark gap,  $Z_{total}(\omega)$  is the total impedance of the discharge path that includes impedance of the body  $Z_b(\omega)$  and the wire  $Z_w(\omega)$ ,  $\mathcal{F}$  and  $\mathcal{F}^{-1}$  are the Fourier and inverse Fourier operators, respectively. Considering the spark voltage formula derived by Taka and Fujiwara [75], the current waveform can be expressed by (5.10):

$$I(t) = \mathcal{F}^{-1}\left\{\frac{\left(2\pi\delta(\omega)V_C - \mathcal{F}\left\{\frac{V_C}{\sqrt{1 + \exp\left(\left(\frac{\alpha}{p_{air}}\right) \times \left(\frac{V_C}{l}\right)^2 \times t}\right)}}\right\}\right)}{Z_b(\omega) + Z_w(\omega)}\right\} \quad (5.10)$$

Using the Paschen's formula ( $V_C = 25.4l + 6.64\sqrt{l}$ ), the relationship between the spark length  $l$ , and the applied voltage,  $V_C$ , the discharge current can be derived from equation 5.11:

$$I(t) = \mathcal{F}^{-1}\left\{\frac{2\pi\delta(\omega)V_C - \mathcal{F}(V_C \times K(t,l))}{Z_b(\omega) + Z_w(\omega)}\right\} \quad (5.11)$$

where

$$K(t,l) = \frac{1}{\sqrt{1 + \exp\left(\left(\frac{\alpha}{p_{air}}\right) \times \left(\frac{V_C}{l}\right)^2 \times t\right)}} \quad (5.12)$$

Due to the complexity of the expression 5.11, the exact trend of the current waveform may not be found unless a numerical analysis is performed, given the impedance data for the body and the wires. Here, the overall trend of the waveform (i.e., increasing vs. decreasing) with the voltage, spark length and the impedance data is explained.



As body voltage,  $V_c$  increases, the spark length,  $l$ , becomes longer and the denominator gets smaller (since the ratio  $\frac{V_c}{l}$  decrease with  $V_c$  using the Paschen's law assumption), which results in larger  $K(t, l)$ . The variation of  $K(t, l)$  was numerically analyzed for the time duration  $[0, 50 \text{ ns}]$  with 10 picoseconds intervals, and Paschen's spark length in the range of  $[0.3 \text{ mm}, 3 \text{ mm}]$  corresponding to  $V_c$  in the range of 1.9 kV to 11.2 kV (assuming nominal values of  $\alpha = 10^{-4} \text{ m}^2/\text{V}^2\text{s}$  and  $p_{air} = 1 \text{ atm}$ ). The largest variation of function  $K(t, l)$  with the body voltage  $V_c$  was seen at  $t = 20 \text{ ps}$ , as shown in Figure 5.24. This indicates that the effect of spark voltage is strongest at the initial rising edge of the waveform, corresponding to high frequencies ( $\sim 1 \text{ GHz}$ ).

The term  $\mathcal{F}(V_c \times K(t, l))$  in the numerator of equation 5.11, reflects the effect of the spark voltage on the current waveform. In fact,  $K(t, l)$  is a correction factor smaller than 1 and close to zero. The value of  $K(t, l)$  is close to zero at all times, except the first few picoseconds (about 50 ps). Since  $K(t, l)$  is smaller than 1, the current waveform,  $I(t)$ , always increases with the applied voltage (equation 5.11), for a specific configuration ( $Z_b(\omega) + Z_w(\omega)$ ). The value of  $K(t, l)$  increases with the body voltage  $V_c$  (mainly for the initial rising edge and higher frequencies). This implies that the effect of the spark (i.e., the term  $\mathcal{F}(V_c \times K(t, l))$ ) is more pronounced at higher voltages.

Equation 5.12 shows that for a constant voltage and discharge configuration, decreasing the spark length decreases the value of  $K(t, l)$ , which reduces the spark voltage term  $\mathcal{F}(V_c \times K(t, l))$ . This behavior means that the current waveform increases at lower spark lengths (than the Paschen's value). However, the amount of increase in the current

waveform is time-dependent. The largest increase in the current waveform is in the initial rising edge.

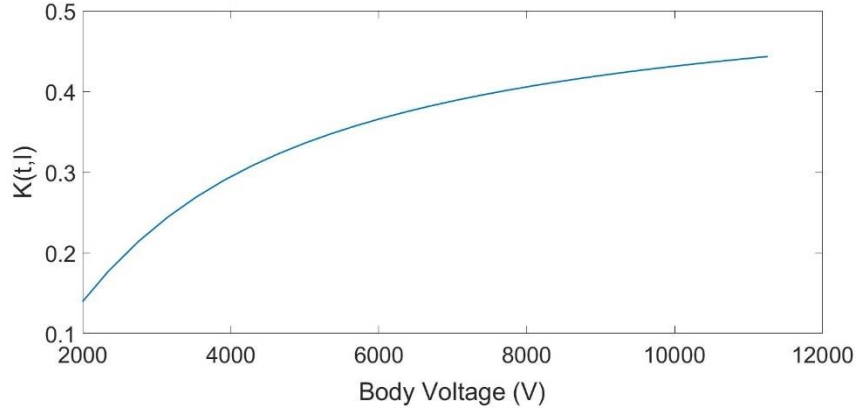


Figure 5.24. The variation of  $K(t, l)$  with the body voltage at  $(t = 20 \text{ ps})$

To obtain the peak current,  $I_{max}$ , the derivative of both sides of equation 5.11 with respect to time need to be found and made equal to zero. However, due to the presence of Fourier and inverse Fourier transforms in the expression, calculation of the time derivative will be complicated. However,  $I_{max}$  is expected to have the general trend of the current waveform with the voltage the impedance. For the same voltage and spark length, reducing the impedance  $Z_b(\omega) + Z_w(\omega)$  results in a larger  $I_{max}$ . Thus, if the discharge configuration (i.e., body posture or device location) changes so that the impedance  $Z_b(\omega)$  is lowered (given the same wire impedance  $Z_w$ ), then  $I_{max}$  will be larger. This condition occurs when the device is worn on the subject's waist, due to the lowered body resistance  $R_b$ , as shown in Table 5. Moreover, if the body capacitance increases in the new configuration, the impedance decreases and results in a larger  $I_{max}$ . This situation also appears in waist-worn compared to hand-worn configurations (due to the variations in the

body position relative to the edge of the bed explained in 5.3.4). The measured and estimated results will be evaluated to confirm this hypothesis.

The current peak for discharges from wearable devices can be compared with that of the ESD gun, using the equation 5.11. To compare the waveforms, the difference between the impedance of the discharge path in both cases need to be investigated. For the ESD gun, the impedance can be explained in terms of a resistance (330 Ohm) and a capacitance (110 pF), whereas for the discharges from a wearable device, the impedance consists of two terms of  $R_b$  and  $C_b$  (ignoring the wire impedance). The body resistance values from Table 5 are much lower (largest body resistance is 50% of the ESD gun resistance) than the resistance of the ESD gun. Moreover, the body capacitance values are larger than that of the ESD gun (except two cases that were 10% and 20% smaller than the ESD gun, the remaining four cases had larger capacitance). Considering equation 5.11, the lower body resistance and the larger capacitance of the discharge scenarios result in a larger peak current than that of the ESD gun.

The mathematical expression for the current waveform (equation 5.11) can be used to predict the behavior of peak current derivative  $\left(\frac{dI}{dt}\right)_{max}$ . The Fourier transform of the current derivative can be written as:

$$\mathcal{F}\left(\frac{dI(t)}{dt}\right) = 2\pi j\omega \mathcal{F}(I(t)) \quad \Rightarrow \quad \frac{dI(t)}{dt} = \mathcal{F}^{-1}\{2\pi j\omega \mathcal{F}(I(t))\} \quad (5.13)$$

Equation 5.13 shows that the trend of current derivative looks similar to the current itself. To obtain  $\left(\frac{dI}{dt}\right)_{max}$ , the derivative of both sides of equation 5.13 need to be found and made equal to zero. However, this calculation will be complicated due to the presence

of the Fourier and inverse Fourier transforms. However,  $\left(\frac{dI}{dt}\right)_{max}$  is expected to increase with  $V_c$ , similar to  $\frac{dI(t)}{dt}$ . Equation 5.13 also shows that the trend of current derivative should be similar to that of the current waveform. Thus, the configurations that result in a larger  $I_{max}$ , are expected to result in a larger  $\left(\frac{dI}{dt}\right)_{max}$ . Therefore, waist-worn configurations are expected to have a larger  $\left(\frac{dI}{dt}\right)_{max}$  than hand-worn configurations (for the same voltage and spark length), due to their lower body resistance  $R_b$ .

Equation 5.13 can be used to compare  $\left(\frac{dI}{dt}\right)_{max}$  between the ESD gun and the discharges from a wearable device. Due to the lower body resistance and larger body capacitance of the test configurations (shown in Table 5) compared to the ESD gun, the peak current derivative of the discharges from a wearable device is expected to be larger than the ESD gun. Note that the effect of spark voltage is more pronounced at higher voltages, therefore, this expectation is valid at lower range of voltages (e.g., 2 kV, 4 kV)

The total charge delivered to ground can also be found using the aforementioned mathematical expressions. Using equation 5.11, charge delivered to ground can be found from equation 5.20:

$$Q_{ESD} = \int_0^{t_{end}} I(t)dt = V_c \times \int_0^{t_{end}} \mathcal{F}^{-1}\left\{\frac{\mathcal{F}(V_c) - \mathcal{F}(V_c \times K(t,l))}{Z_b(\omega) + Z_w(\omega)}\right\} dt \quad (5.14)$$

where  $t_{end}$  is the time at which current reaches zero. The total charge delivered to ground is expected to increase with voltage. Also, considering the equation  $Q_{ESD} = CV_c$ , where  $C$  is the body capacitance, the total charge needs to be linearly changing with voltage. In fact, the charge that is supposed to be delivered to ground is stored in the body capacitance. Due

to the short duration of the initial current rise (less than 5 ps), compared to the total interval of an ESD waveform ( $t_{end} \approx 100 \text{ ns}$ ), the area under the curve (or  $Q_{ESD}$ ) is mainly affected by the second phase (i.e., charge decay). The charge delivered to ground mainly depends on the capacitance, because the discharge process is similar to a discharge of an RC circuit, where  $R$  is the body resistance and  $C$  is the body capacitance. Lowering body resistance will have a negligible impact on  $Q_{ESD}$ , since the time constant of charge decay  $\tau = RC$  is reduced while the peak current increases, and the area under the curve remains relatively unchanged.

In the remaining subsections, the measurement and estimation results for  $I_{max}$ ,  $\left(\frac{dI}{dt}\right)_{max}$  and  $Q_{ESD}$  will be compared with that of the ESD gun and the trends in the data (e.g., variation with the body voltage and waist-worn compared to hand-worn configurations) will be investigated.

#### 5.7.1. Peak Current

Figure 5.25 shows the trend of the peak current of the measurement for the test configurations and the ESD gun waveform as a function of body voltage. Peak current is a severity indicator for ESD waveforms that is related to hard failures (permanent damage to components). In all the test configurations, the peak current for all the test conditions increases with voltage. The peak current values of the IEC 61000-4-2 standard are linearly increasing with voltage, since the ESD gun is discharged in contact mode, and there is no spark that causes nonlinearity and variation in the peak current (except the spark across the relay).

The results for standing posture and metal piece on hand, are close to the peak current from the ESD gun. This discharge scenario is the closest to the wrist-worn brush-by scenario investigated by Zhou et al. [22]. The main difference is that in our experiments, the discharging structure is the short wire and the bed frame, while in Zhou et al. [22], the subject discharged to a large vertical ground plane.

The peak current from the remaining 5 configurations results in a larger peak current than the IEC 61000-4-2 standard. The average peak current for these 5 configurations is 1.6 times larger than the ESD gun results (1.3 times for hand-worn and 1.7 times for waist-worn metal pieces). This result indicates that the IEC 61000-4-2 standard test method may not be a sufficient ESD immunity testing for wearable medical devices.

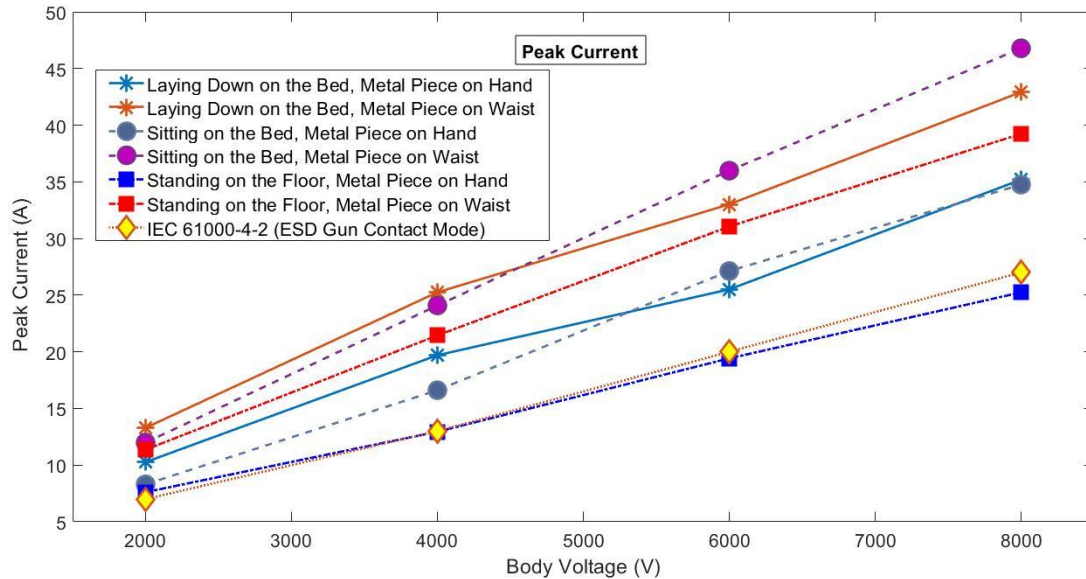


Figure 5.25. Comparison of the measured peak ESD current for six test configurations and the IEC 61000-4-2 standard setup as a function of body voltage

For all the 3 posture levels and all voltage levels, the discharge from waist-worn metal pieces has larger peak currents than hand-worn metal pieces. The ratio of the peak

current from waist-worn to a hand-worn metal piece in three postures and all the voltage levels are computed and displayed in Figure 5.26. The ratio ranges from 1.2 to 1.6 for all postures, however, the largest ratio belongs to the standing posture (1.6), and then sitting (1.4) and lying down postures (1.3).

The variations in the peak currents can be attributed to the differences in the local characteristic impedance in the human body and the current-carrying structures. However, these trends can be explained by the variations in the elements of the equivalent circuit. The larger peak current of waist-worn compared to hand-worn configurations can be explained by their body resistance  $R_b$ , as shown in Table 5. The inverse of the ratio of  $R_b$  for waist- to hand-worn configuration (1.61 for standing, 1.57 for lying down on the bed, and 1.34 for sitting) are within 20% of the ratio of the peak current for the same configurations. In other words, the body resistance in hand configuration is larger than the waist, therefore, the peak current is expected to be larger for waist than hand.

Although the discharge path from waist to the ground is shorter than from hand to ground. this shorter path does not justify the lower resistance for waist-worn configurations. This justification can only be used if the discharge current was DC, while in the ESD event, the discharge current has high-frequency content ( $> 1$  GHz). The resistance value used in this circuit model is obtained by curve fitting and is not equal to the DC resistance of the discharge path. Therefore, this body resistance in the simplified model should be interpreted as a circuit element that can provide a reasonable fit to the measurement.

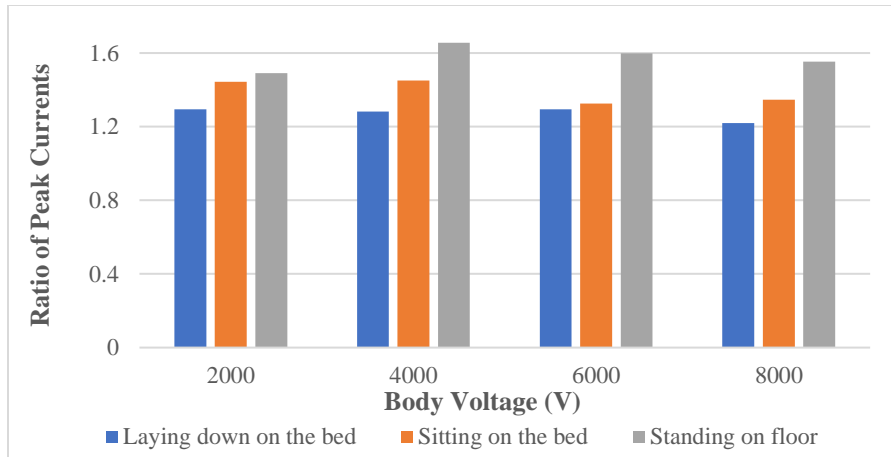


Figure 5.26. Comparison between the ratio of the peak current from waist- to hand-worn discharges at each voltage and body posture

Figure 5.27 shows the effect of body posture on the peak current for hand- and waist-worn configurations. The peak current from standing posture is the least value for both device locations. At 2 kV and 4 kV, the lying down posture results in slightly larger (21% higher) peak currents compared to sitting for both device locations. At 6 kV and 8 kV, the trend is reversed for waist-worn configuration, while the difference between the two is not significant for hand-worn configuration (6% smaller and 1% larger, respectively).

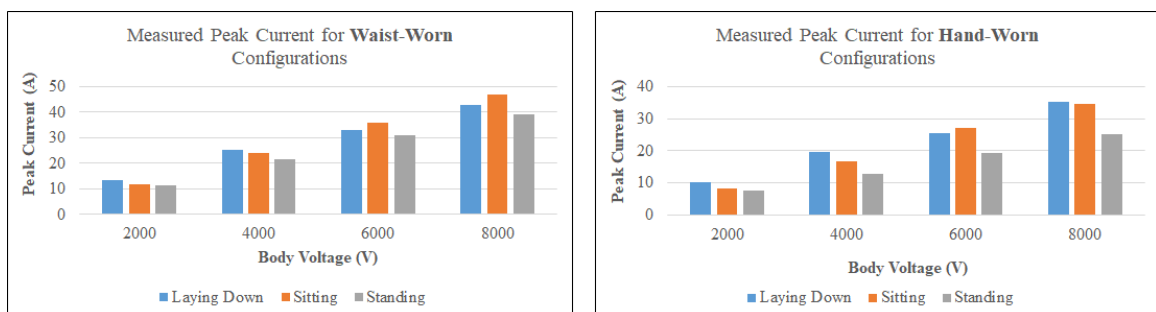


Figure 5.27. Effect of body posture on peak current (Top: Hand-worn metal piece, Bottom: Waist-worn metal piece)



The simulation model was used to investigate the trend of the peak current among test configurations for a constant value of spark length (100% Paschen's length). The prediction error for peak current was rather low (9% on average), and the estimated values follow a similar trend to that of the measurement as shown in Figure 5.28. The estimated peak currents for waist-worn configurations are larger than hand-worn configurations. Moreover, for both device locations and all voltage levels, the peak current from sitting is larger than lying down and standing on the floor. These trends can be interpreted with the body resistance in the three postures. For both hand- and waist-worn configurations, the smallest and largest  $R_b$  belong to sitting and standing postures, therefore, the peak current is expected to be largest in sitting and smallest in standing posture. Note that the variations in the values of  $R_b$  can only be used to explain the trends in the peak current, and the underlying cause is the changes in the local characteristic impedance of the body and the current-carrying structures in each configuration.

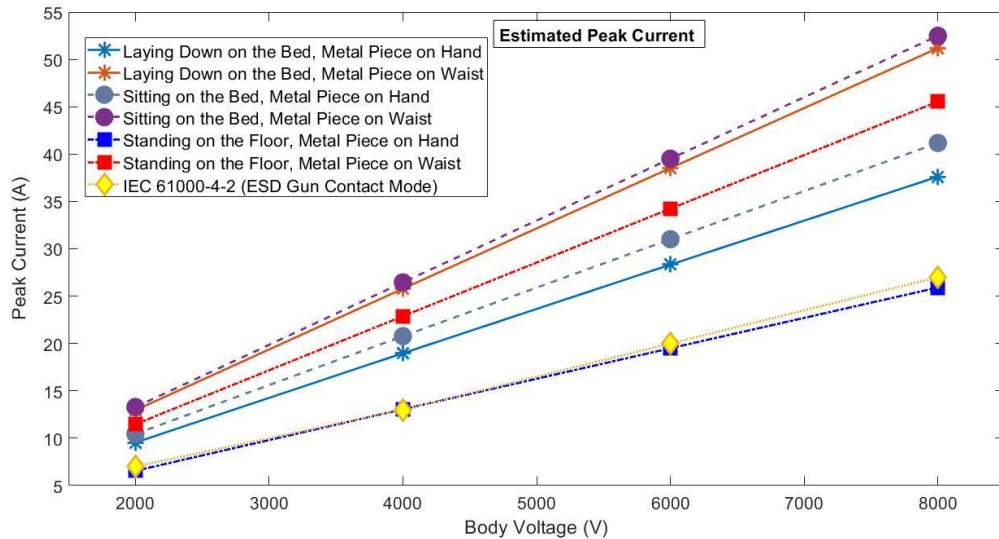


Figure 5.28. Estimated peak current using the developed equivalent circuit compared to the ESD gun results

### 5.7.2. Peak Current Derivative

Peak current derivative is a critical waveform parameter that affects the susceptibility of an equipment to soft failures (i.e., device upsets) during an ESD event [21][22]. Figure 5.29 shows the comparison between the peak current derivative of the test configurations and the IEC 61000-4-2 results. The overall trend of the peak current derivative with body voltage for all test configurations and the ESD gun is increasing. In all voltage levels, the peak current derivative from the metal piece exceeds that of the ESD gun waveform (except at 8 kV, lying down on the bed, metal piece on hand). The largest  $\left(\frac{dI}{dt}\right)_{max}$  occurs when the subject is lying down the bed and the metal piece is worn on his waist. On average, the peak current derivative of the test configurations is 1.6 times larger than the ESD gun results. This larger peak current derivative indicates that the IEC 61000-4-2 standard testing is most likely insufficient to ensure immunity of wearable medical devices against ESD-induced soft failures.

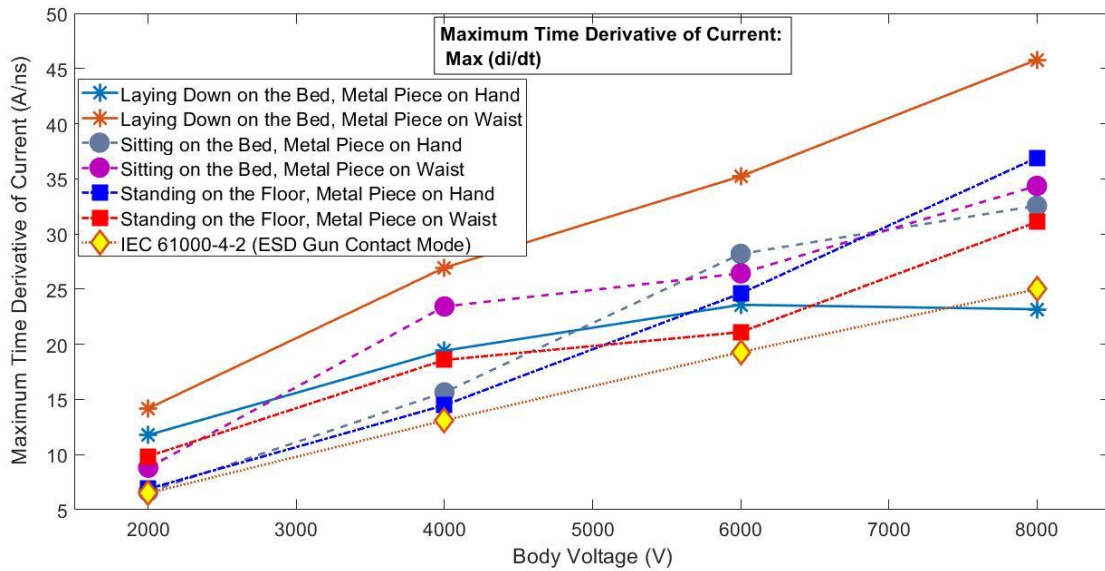


Figure 5.29. Comparison of the peak ESD current derivative for 6 test configurations of a subject wearing a metal piece, and the IEC 61000-4-2 standard setup as a function of body voltage.

The maximum current derivative for the ESD gun varies linearly over the four voltage levels, while for the discharges from a body-worn metal piece, the results deviate from a linear relationship. The variations in the spark length among each test condition can be blamed for the fluctuations in  $\left(\frac{di}{dt}\right)_{max}$  results.

To analyze the hypothesis that waist-worn discharges result in a larger  $\left(\frac{di}{dt}\right)_{max}$ , the results of Figure 5.29 are sorted in Figure 5.30 according to the ratio of waist-worn to hand-worn discharges. Figure 5.30 shows that for all the voltage levels,  $\left(\frac{di}{dt}\right)_{max}$  for the discharges from a waist-worn metal piece are larger than from hand for lying down (1.5 times on average) and sitting on the bed (1.2 times on average), however, standing on the floor shows the opposite trend. Although it is expected that the lower  $R_b$  in waist-worn

configurations result in a larger  $\left(\frac{dI}{dt}\right)_{max}$ , the standing posture shows the opposite trend. The estimated spark length from Table 6 shows that the average spark length when the metal piece is worn on hand is exceptionally much lower than on waist (60% compared to 91%). This could be the reason why  $\left(\frac{dI}{dt}\right)_{max}$  for hand-worn configurations are larger than the waist, only for this posture.

The results of Zhou et al. [22] also shows that the peak current derivatives for the waist-worn brush-by scenarios have relatively larger values than HMM scenarios. However, there is no direct reference to the trend of the data and the underlying reasons.

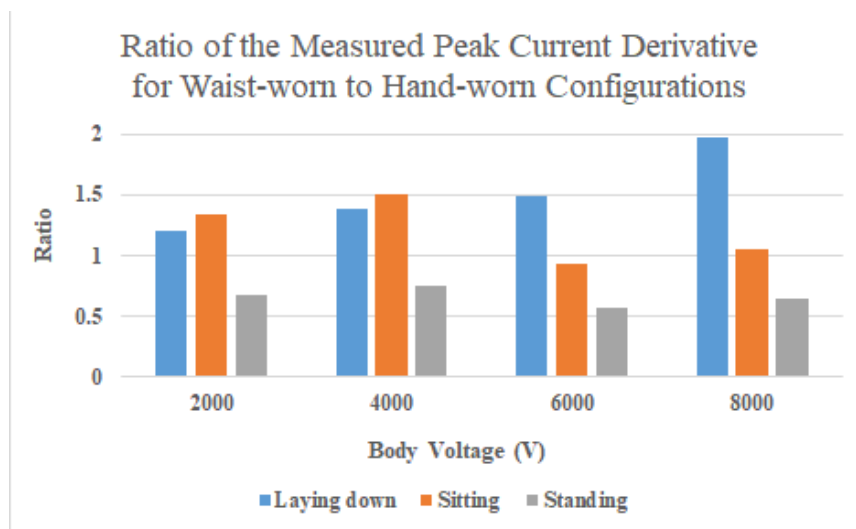


*Figure 5.30. Peak current derivative of waist-worn discharge from measurement compared to hand-worn discharges of the 3 body postures*

The main benefit of using the equivalent circuit is that the spark length can be kept constant and the trend can be investigated without the effect of variation of the spark length (which made it difficult to interpret the measurement results). Moreover, the waveform for

the worst practical case of discharge defined as an ESD with 50% of the Paschen's value can be estimated and compared with the measurement and ESD gun results.

Figure 5.31 and Figure 5.33 show the simulation results for two spark lengths: 100% and 50% of the values calculated based on the Paschen's law, respectively. The result of 100% Paschen's law refers to the minimal risk of ESD since the spark length is at the maximum level, which results in the slowest rise time and  $\left(\frac{dI}{dt}\right)_{max}$ . In all the test conditions a relatively linear increase with voltage level occurs, however, the IEC waveform shows a steeper slope compared to the tests from a wearable metal piece. This steeper slope of the ESD gun results could be due to the spark voltage term  $\mathcal{F}(V_C \times K(t, l))$  in the discharges from wearable devices (in equation 5.11). In fact, the deviation between the results of the ESD gun and the discharges from wearable devices are due to both impedance differences in the discharge path and the effect of spark voltage (which is subtracted from the applied voltage in equation 5.11). at all voltages, the impedance differences between the two remain constants, however, the spark voltage term  $\mathcal{F}(V_C \times K(t, l))$  is expected to increase, which implies that the effect of spark is more pronounced at higher voltages. Therefore, the slope of the peak current derivative is more gradual than that of the ESD gun, mainly due to the presence of the spark length. Although  $\left(\frac{dI}{dt}\right)_{max}$  for discharges from wearable devices are initially (at 2 kV) larger than the ESD gun, due to lower body impedance compared to the ESD gun, the spark discharge term becomes so large at higher voltages (i.e., 8 kV) that the trend of  $\left(\frac{dI}{dt}\right)_{max}$  becomes reversed.

Figure 5.31 also shows that at lower body voltages (2 kV), the peak current derivatives of the ESD waveforms from a wearable metal piece are larger than the ESD

gun, however, at higher voltage levels the opposite trend exists. Therefore, at the minimal risk condition (i.e., 100% Paschen's law), the peak current derivative for ESD from a wearable metal piece is at least at the same level of the ESD gun.

Figure 5.31 shows that at each voltage level, the waist-worn discharges for the three postures result in a larger  $\left(\frac{dI}{dt}\right)_{max}$  compared to hand-worn discharges. This observation is compatible with our previous expectation from waist-worn discharges. Figure 5.32 shows the ratio for each posture, and regardless of the body voltage, the following trend is observed for the ratios of the waist-worn to hand-worn discharges:

$$\left(\frac{dI}{dt}\right)_{max} \Big|_{Sitting} < \left(\frac{dI}{dt}\right)_{max} \Big|_{Laying\ down} < \left(\frac{dI}{dt}\right)_{max} \Big|_{Standing}$$

The larger ratio of  $\left(\frac{dI}{dt}\right)_{max}$  for standing than the other two postures could be because of the largest differences between  $R_b$  and  $C_b$  in the waist to hand configuration occurs in the standing posture.

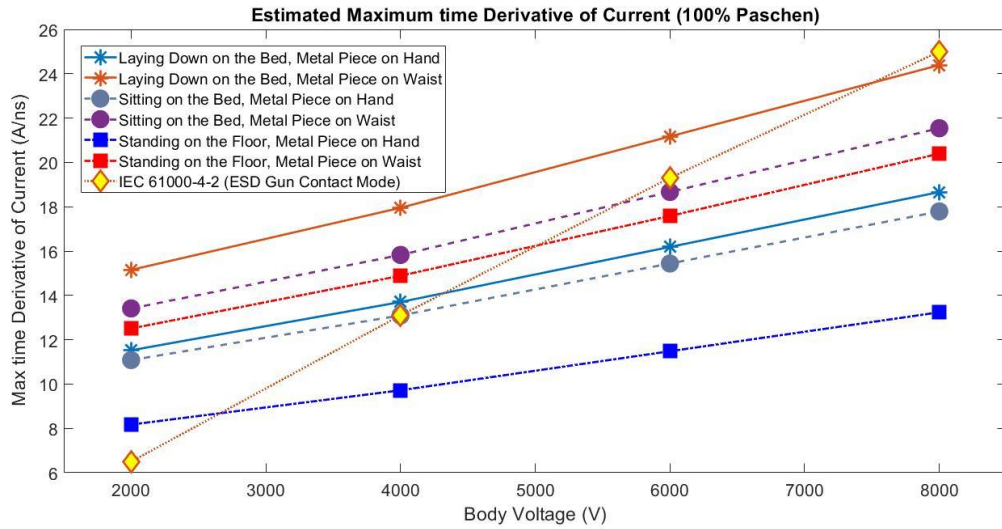
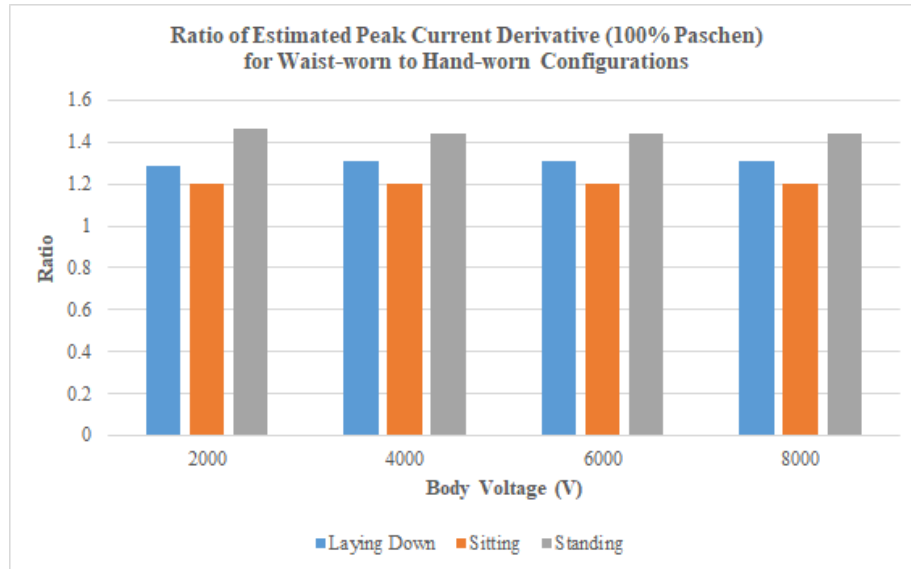


Figure 5.31. Estimated peak current derivative using 100% Paschen's length from the circuit simulation

In this study, the worst practical case is assumed to be at 50% of the value suggested by the Paschen's law. Since it is not feasible to conduct experiments at a pre-determined spark length, the simulation model at 50% Paschen's length was developed and the results are displayed in Figure 5.33. The results show that in this worst practical case, the peak current derivative of discharges from a wearable metal piece exceeds that of the ESD gun at all voltage levels. The peak current derivatives for waist-worn configuration are 5.5 times larger than that of the ESD gun, while this ration for hand-worn configurations is 4.1 times, averaged over the four voltage levels and three postures.



*Figure 5.32. Peak current derivative of waist-worn discharge from simulation compared to hand-worn discharges of the 3 body postures*

Similar to the 100% Paschen's length, the waist-worn configurations exhibit faster rise times and larger  $\left(\frac{dI}{dt}\right)_{max}$  than hand-worn configurations. Considering the risk of soft failures caused by fast rise times, the results of Figure 5.31 and Figure 5.33 show that the IEC 61000-4-2 test setup may not provide sufficient immunity for wearable configurations at the worst practical case of an ESD event.



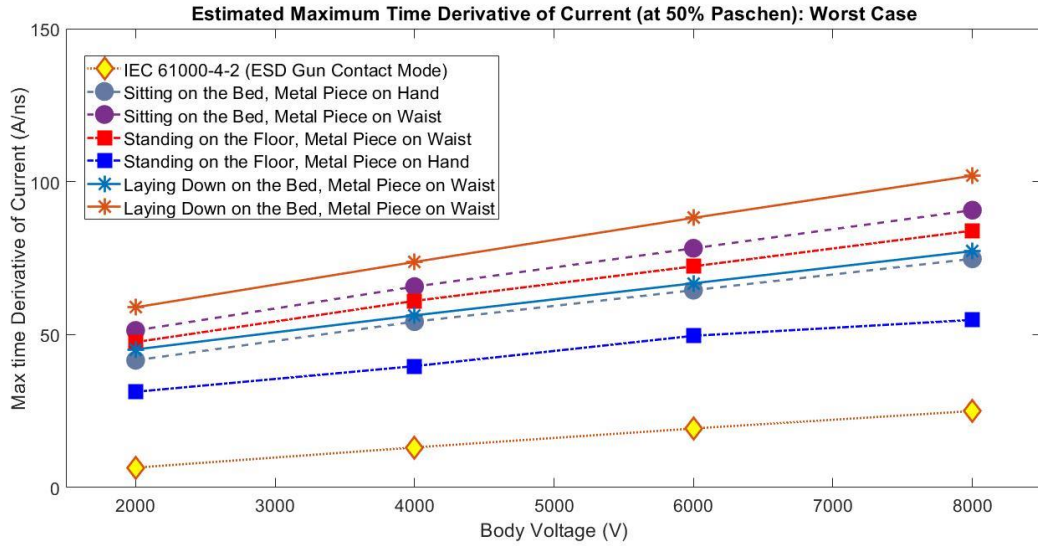


Figure 5.33. Estimated peak current derivative using 50% Paschen's length from the equivalent circuit simulation

### 5.7.3. Charge Transfer

The amount of charge transferred to the ground during an ESD event is an indicator of the risk of permanent damage to components (i.e., hard failure). The area under the current-time curve was calculated for each test condition and the results were compared at each voltage level (Figure 5.34). Since the duration of an ESD pulse is around 300 ns, and the rising edge of an ESD waveform only lasts for the first few nanoseconds, the area under the curve is mostly affected by the charge decay phase of the waveform, not the rising edge. This phase of the waveform is influenced by the capacitance of the body (in case of the wearable discharges) or the internal capacitance of the ESD gun relative to the ground. The area under the curve of an RC discharging circuit can be represented by  $Q = C \cdot V$ , where  $V$  is the voltage across the capacitor. Therefore, a linear relationship between the total charge transfer and the body voltage is expected for all the test configurations.

The results of the charge delivered to the ground during each test configuration are shown in Figure 5.34. For the ESD gun, the charge transfer increases linearly with body voltage. This trend is explained by the discharge capacitor (110 pF) in the ESD gun. Other test configurations also increase with the body voltage; however, the trend for wearable configurations shows some deviations from a linear relationship.

It is expected that the charge transfer from a wearable metal piece, follow the trend of the capacitance of the body relative to the Al foil found during impedance measurements (shown in Table 5). Thus, the charge transfer for the waist-worn metal piece of the standing posture should have the highest charge transfer, while the least should belong to the hand-worn metal piece of the same posture. The results for lying down are also expected to be higher than sitting on the bed due to the higher body capacitance relative to Al foil. Figure 5.34 confirms the expected trend for the standing posture, relative to the other two postures. However, there are deviations in the results which could be attributed to a number of factors such as slight changes in the posture of the subject during the ESD tests compared to the impedance measurements, variations in the postures at different voltage levels, and nonlinear characteristics of the body impedance. It was shown that the assumption of a capacitive behavior may not be a valid assumption, thus the measurement results may not follow the expectations derived from our simplified  $Q = CV$  model assumption.

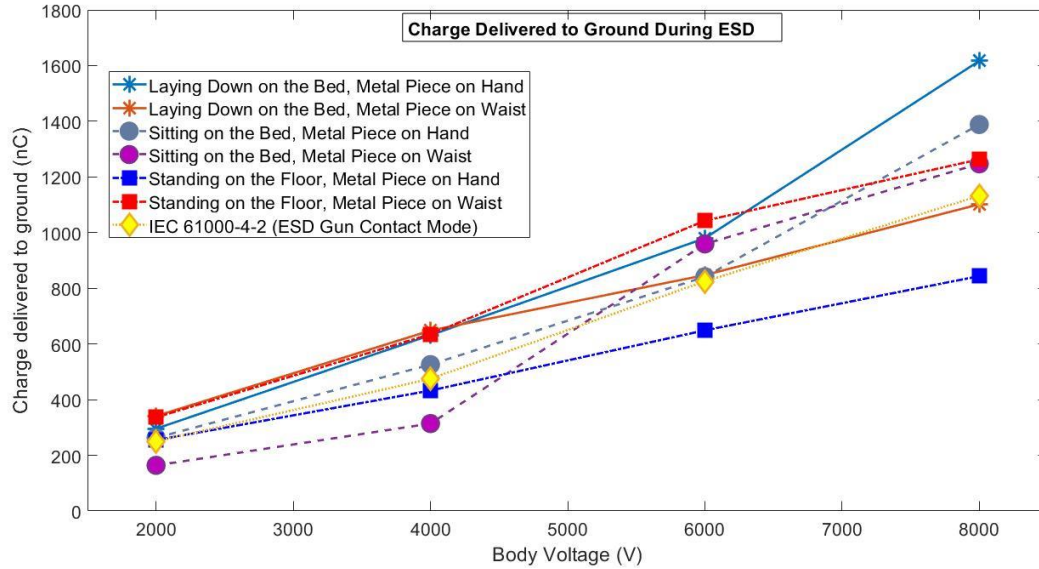


Figure 5.34. The charge delivered to the ground during ESD from a wearable metal piece at various position and postures, compared to an ESD gun

To evaluate our hypothesis that charge transfer must follow the trend of body capacitance relative to the Al foil, the estimated values from the simulation model are compared in Figure 5.35. The linear increase in charge transfer indicates that this parameter is only affected by the capacitance of the body relative to Al foil, which is the same for all voltage levels. The largest and smallest charge transfer belongs to the configurations with the largest and smallest body capacitance, according to Table 5. The largest value was observed for waist-worn standing posture ( $C_b = 250 \text{ pF}$ ), and the smallest value for hand-worn in the same posture ( $C_b = 87 \text{ pF}$ ). The lying down posture shows similar results for both device locations as expected (hand-worn:  $C_b = 173 \text{ pF}$ , and waist-worn:  $C_b = 170 \text{ p}$ ). For the sitting posture, the waist-worn configuration results in a larger charge transfer, which follows the body capacitance (hand-worn:  $C_b = 101 \text{ pF}$ , and waist-worn:

$C_b = 140 \text{ pF}$ ). These results confirm our hypothesis about the trend of charge transfer according to body capacitance.

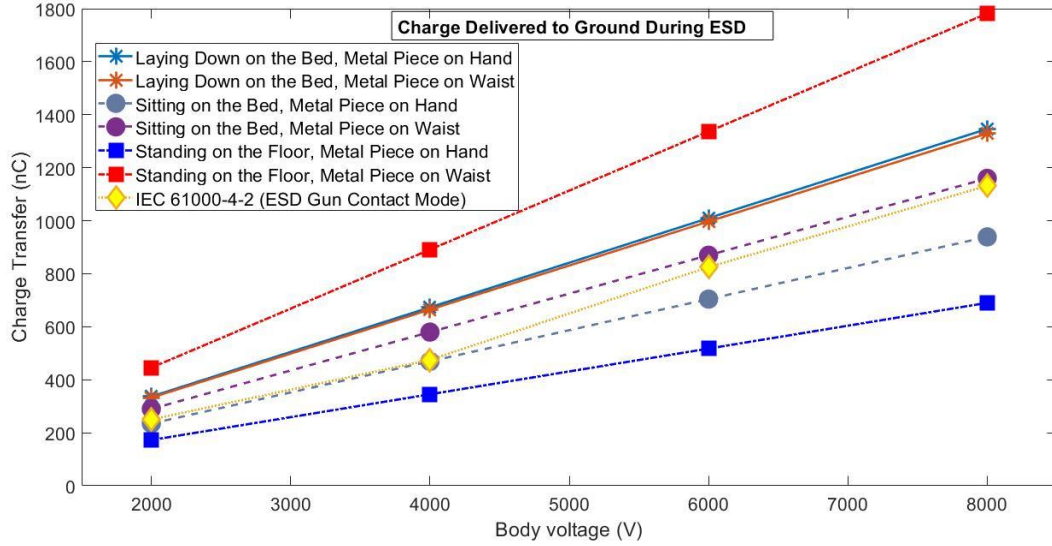


Figure 5.35. Estimated charge transfer to the ground during ESD from a wearable metal piece compared to an ESD gun

### 5.8. Effects of Spark Length

It was mentioned previously that shorter spark length, in general, reduces the spark resistance and increases  $I_{max}$  and  $\left(\frac{dI}{dt}\right)_{max}$ . However, the simulation results in Figure 5.36 shows that for our setup,  $I_{max}$  is almost unaffected by the reduced spark length (<1% change), while  $\left(\frac{dI}{dt}\right)_{max}$  is increasing. When the peak current occurs late in the waveform, the spark length will not influence it. As a result of this shortened spark length, the rise time becomes shorter that increases  $\left(\frac{dI}{dt}\right)_{max}$ . Also, an initial peak emerges in this setup at around 1 to 3 ns, as shown in Figure 5.36, which keeps increasing. This trend in waveform parameters implies that reduced spark length, which could occur due to a number of reasons

(e.g., fast speed of approach, dry environment, or lack of seed electrons on the electrode) could increase the susceptibility to soft failures (due to larger  $\left(\frac{dI}{dt}\right)_{max}$ ). This trend in the initial peak and the peak current is only due to the presence of the series RC elements representing radiation. Any discharge configuration that results in radiation (and can be modeled with RC) shows the behavior in Figure 5.36, which is quite different than the common ESD waveform studied in literature.

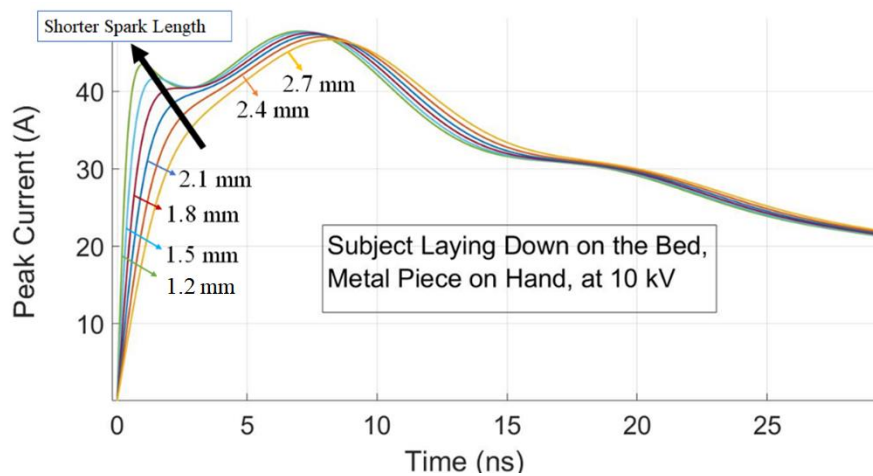


Figure 5.36. Effect of shortening spark length on the waveform

This trend is compared with the results of Zhou et al.'s simulation [22] and Pommerenke's measurement [23]. In Zhou et al.'s study [22], the data for  $I_{max}$  and  $\left(\frac{dI}{dt}\right)_{max}$  at 10 kV and two discharge scenarios of HMM and waist-worn brush-by discharge to a large vertical plane is analyzed via the simulation model are analyzed. Pommerenke [23] measured the current waveform in HMM configuration at four voltage levels of 1.5 kV to 10 kV, for a range of spark lengths. To our knowledge, Pommerenke's results [23] are the only available measurement data in literature on the human discharge at various spark lengths.

The effects of the spark length on the maximum current derivative is shown in Figure 5.37. The increasing trend in Zhou et al.'s simulation [22] is steeper than our results and Pommerenke's measurements [23]. In Zhou et al.'s data [22], waist-worn brush-by is the more severe than HMM. Our simulation results show reasonable agreement with the measurement data until almost 65% Paschen's length (1.4 mm). At 44% Paschen's length, the average  $\left(\frac{dl}{dt}\right)_{max}$  for the six discharge scenarios are 4.8 times larger than that of the Paschen's length, while this ratio in Zhou et al.'s data [22] is 8 to 10 times. This could be due to the presence of the wire and the associated radiation losses.

It is to be noted that the estimated data in Zhou et al.'s article [22] are based on the same gas constant in the Rompe-Weizel's model as in our study ( $K_R = 1 \times 10^{-4} m^2/V^2s$ ). Section 5.9 will investigate the effect of this constant, which is critical parameter in the simulation model and affects the waveform parameters significantly.

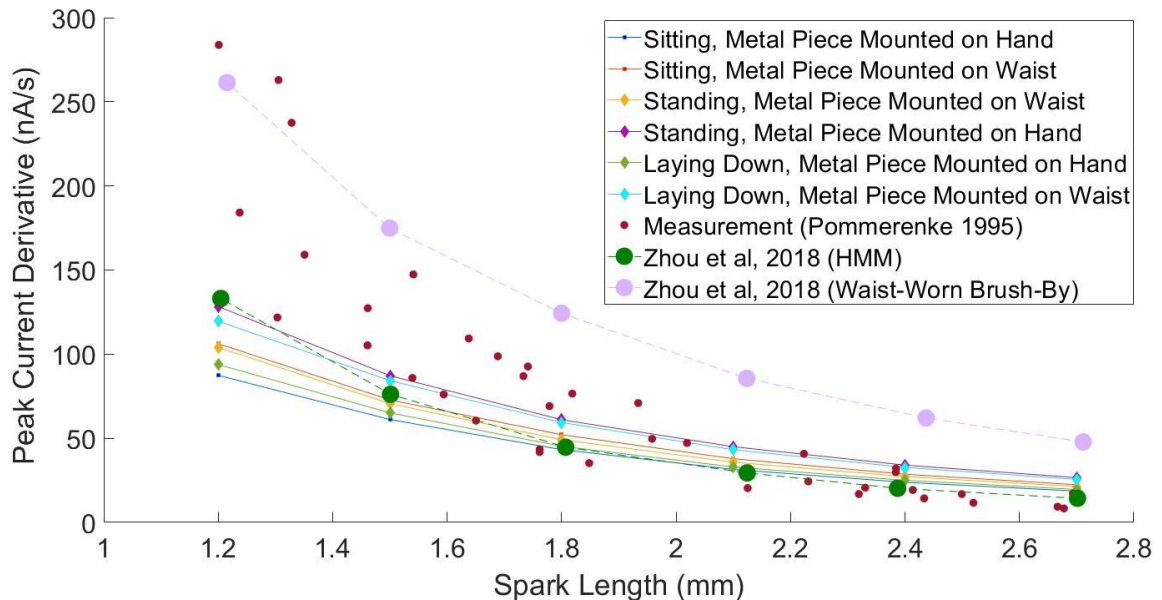


Figure 5.37. Comparison between the estimated peak current at different spark lengths with Zhou et al.'s simulation [22] and Pommerenke's measurements [23]

### 5.9. Effects of the Gas Constant $K_R$ in Rompe-Weizel's Model

The effect of the gas constant in the Rompe-Weizel's model on the waveform parameters has received attention in a number of ESD articles [22], [23], [45], [76]. The most common value for this constant is  $K_R = 1 \times 10^{-4} \text{ m}^2/\text{V}^2\text{s}$ . Since this parameter is in the denominator of the spark resistance formula ( $R_{Spark}(t) = \frac{l}{2K_R \sqrt{\int_0^t i(t)^2 dt}}$ ), changing its value will directly influence the resulting waveform.

Jobava et al. [45] suggested that  $K_R$  should not be used as a constant value for all spark lengths, since measurements at different spark lengths does not result in fast enough rise times, therefore, this parameter needs to be adjusted according to spark length. A list of  $K_R$  ranges for voltage levels of 1.5 kV to 10 kV was suggested for several spark lengths [77]. This range of gas constants were used to investigate its effect on the waveform parameters of the six discharge scenarios in the present work. Only maximum current derivative was influenced by this parameter (since it only affects the spark). Figure 5.38 shows the boxplots of  $\left(\frac{dl}{dt}\right)_{max}$  as a function of  $K_R$ , at two spark lengths of 2.7 mm (Paschen's value) and 2 mm. The two values for gas constant at each spark length is taken from Pommerenke's study [77]. This analysis shows that changing in spark length is directly proportional to  $\left(\frac{dl}{dt}\right)_{max}$ . The mean  $\left(\frac{dl}{dt}\right)_{max}$  at the higher gas constant is twice the lower one for both spark lengths.

This large variation implies that the waveform parameters at each spark length are strongly dependent on the gas constant in the model. In this study, the choice of  $K_R =$

$1 \times 10^{-4} \text{ m}^2/\text{V}^2\text{s}$  in the equivalent circuit resulted in an average 40% error in estimating  $\left(\frac{dl}{dt}\right)_{max}$ . This error could be due to the wrong choice of gas constant, in addition to variation in the spark length during the experiment. Note that the gas constant may increase at smaller spark lengths (as shown in Jobava et al. [45]).

The value of the gas constant is dependent on several parameters such as the electrode material, local electric field, and the geometry of the two objects between which the spark occurs [78]. Therefore, further experimental studies need to be developed to obtain reasonable values for the gas constant at various voltage levels and spark lengths.

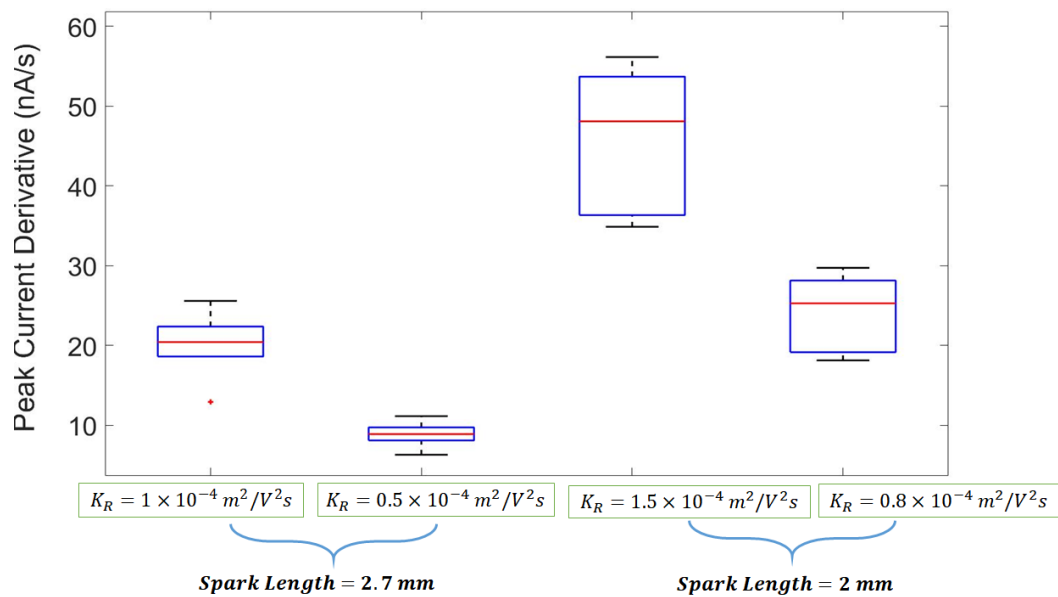


Figure 5.38. Effect of gas constant on the peak current derivative at two spark lengths of 2.7 mm and 2 mm

#### 5.10. Effect of Circuit Elements on the Waveform

This section discusses the effect of 5 circuit parameters of  $L_w$ ,  $R_b$ ,  $C_b$ ,  $C_{rad1}$ ,  $R_{rad1}$  on the waveform. Only one configuration was analyzed for the waveform: lying down on the bed, metal piece on hand, at 2 kV. The parameters extracted from the waveform are  $I_{max}$ ,



$\left(\frac{dI}{dt}\right)_{max}$  as defined in Figure 5.36. The range of values selected for this analysis are within 2 to 4 times larger than the initial values. First, the parameters of the short wire are  $(L_w, C_{rad1}, R_{rad1})$  investigated.

Figure 5.39 shows that increasing the inductance of the short wire to 4 times the initial value results in shifting toward the right and reducing the peak. The rising edge is almost unaffected. Increasing inductance of the wire results in a larger impedance in the circuit and the peak subsequently decreases.

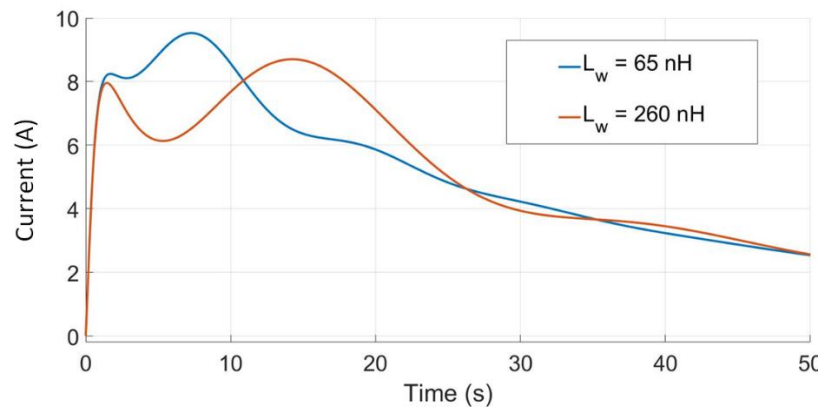


Figure 5.39. Effect of increasing the wire inductance on the waveform

Figure 5.40 shows that increasing the inductance results in a relatively linear reduction in  $I_{max}$ . However, the reduction in these two parameters is not significant: 9% in  $I_{max}$  after inductance is increased to 4 times its initial value.

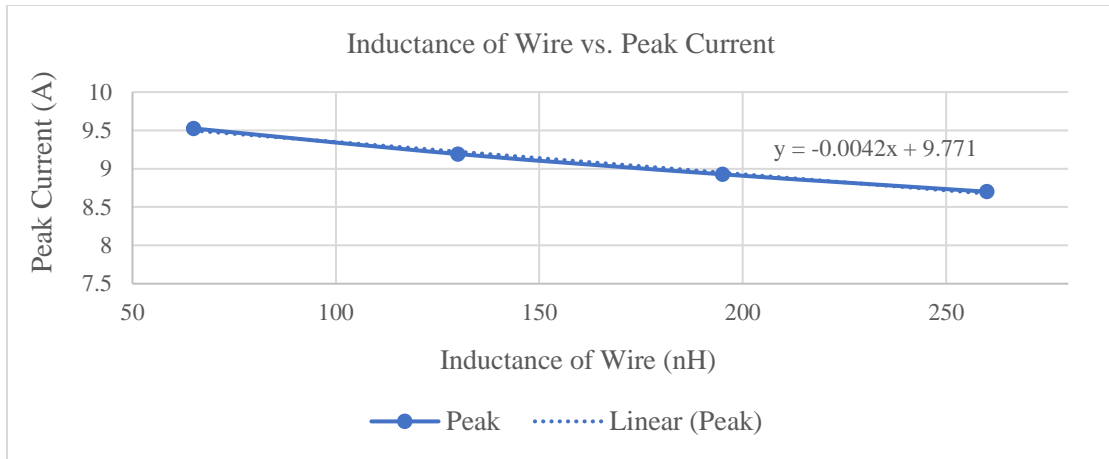


Figure 5.40. Effect of changing wire inductance on the Peak Current

Figure 5.41 shows that increasing the radiation capacitance does not have a noticeable impact on the rising edge, however, it shifts the waveform to left. After 4 times increasing this parameter, the initial peak is eliminated. This trend can be explained by the behavior of the capacitance  $C_{Rad1}$  on the circuit. Increasing this capacitance results in less current in the RC branch (parallel to the inductance), and most of the current flows through the inductor and the effect of radiation is less significant. This pattern results in a waveform closer to the typical HMM shape.

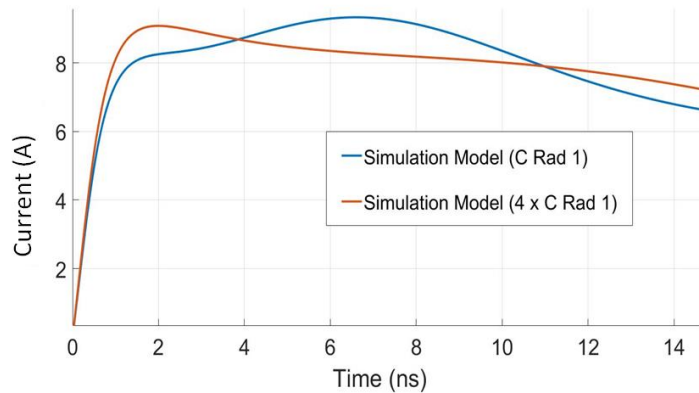


Figure 5.41. Effect of radiation capacitance on the waveform

Figure 5.42 shows that after increasing the radiation capacitance to 4 times its initial value, a 6% decrease in  $I_{max}$  can be observed. The effect on  $\left(\frac{dI}{dt}\right)_{max}$  is negligible (about 1 %).

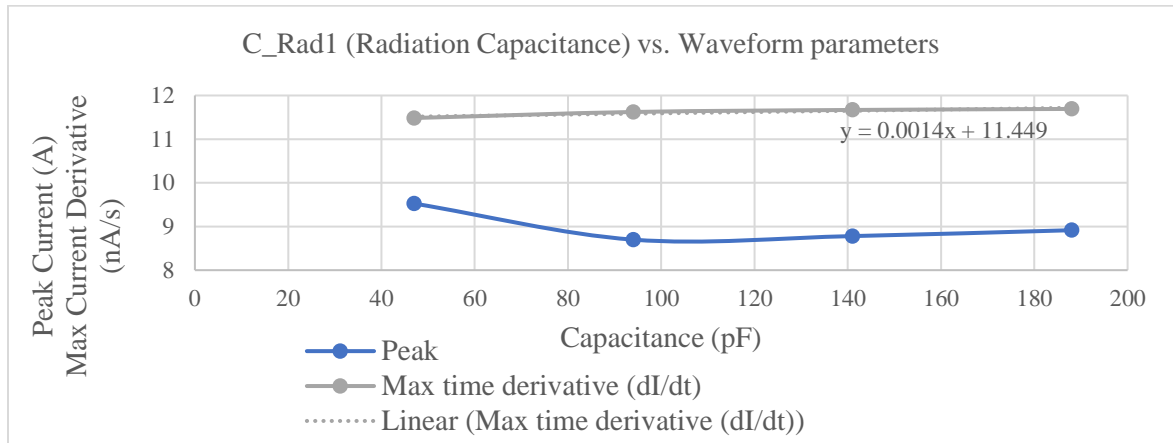


Figure 5.43. Effect of radiation capacitance on the waveform parameters

According to Figure 5.44, as the resistance becomes 4 times larger,  $I_{max}$  and  $\left(\frac{dI}{dt}\right)_{max}$  decrease about 2% and 15% respectively. Increasing the radiation resistance results in a larger impedance in the circuit and a slight reduction in  $I_{max}$ . Since spark length is constant, changes in the rising edge need to be related to changes in the peak current, the reduction in the peak current probably results in a slower rise time.

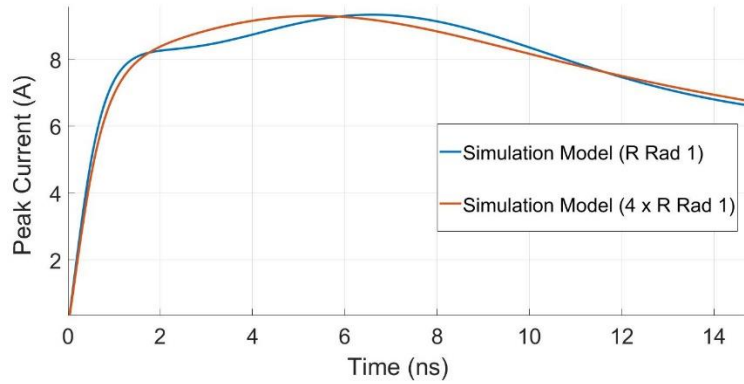


Figure 5.44. Effect of radiation resistance on the waveform

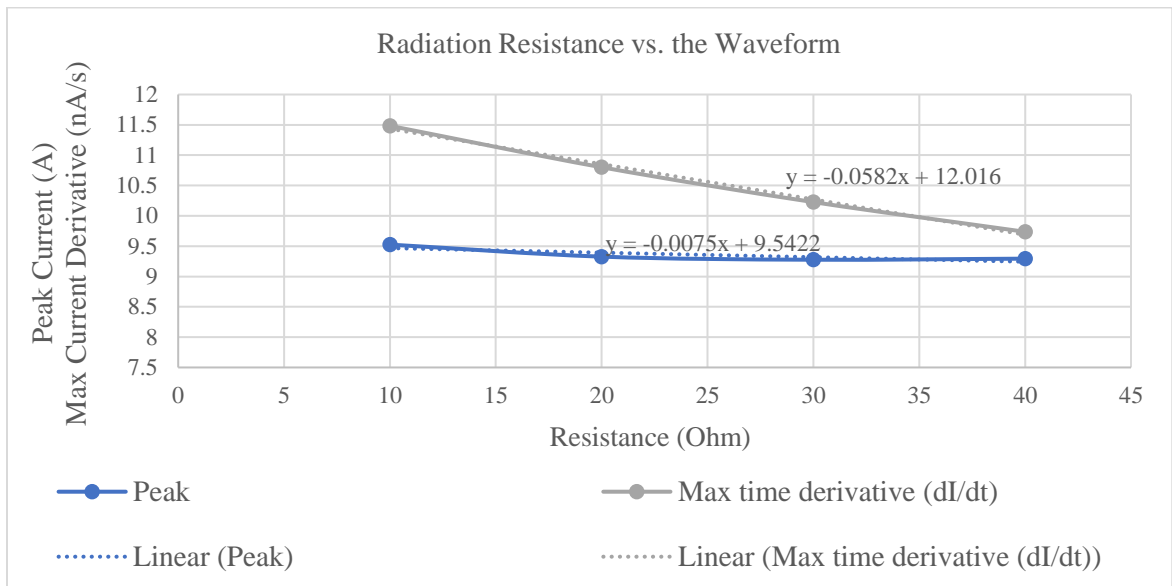


Figure 5.45. Effect of changing radiation resistance on the waveform parameters

After analyzing the elements of the wire, the impedance parameters of the body are investigated. Figure 5.46 shows that increasing the body capacitance has a noticeable effect on the area under the current waveform or the charge transfer. There is also an increase in  $I_{max}$ , most likely due to a larger amount of charge stored by the subject. Figure 5.47 shows a 24% increase in  $I_{max}$  after multiplying the body capacitance to 4. The rising edge is almost unaffected (1% change).

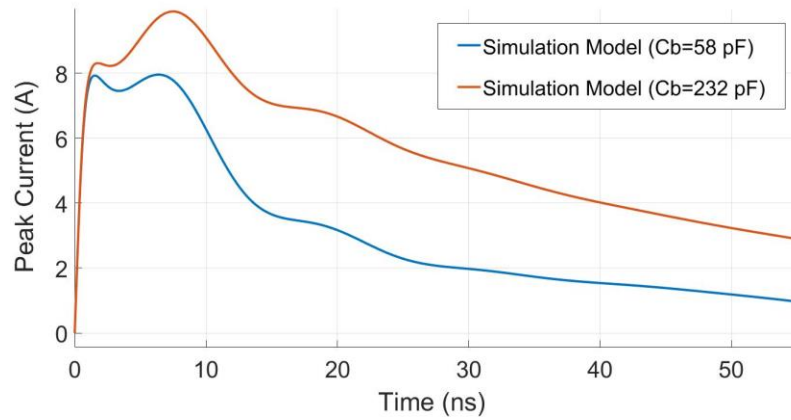


Figure 5.46. Effect of increasing the body capacitance on the waveform

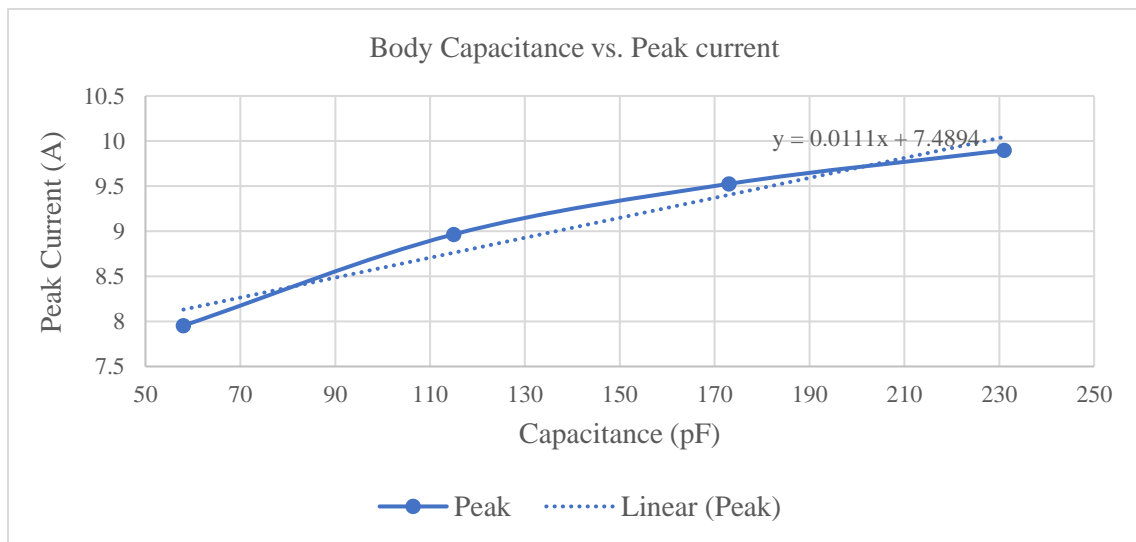


Figure 5.47. Effect of changing body capacitance on the peak current

Figure 5.48 shows that capacitance is linearly related to the total charge transfer, which is according to our expectations (2.4 times increase in charge transfer after capacitance is multiplied by 4). Variations of the spark length, as noted before, does not influence the area under the current waveform.

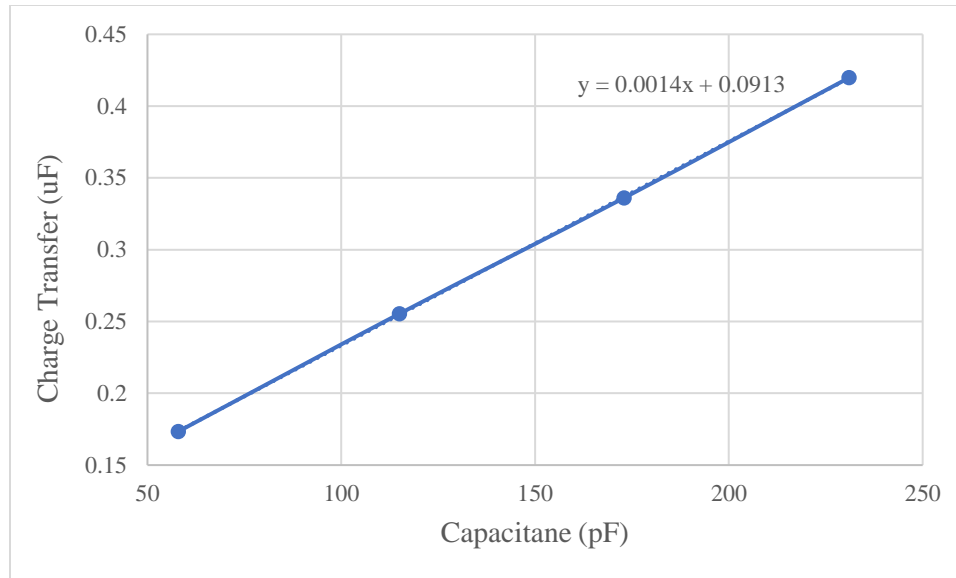


Figure 5.49. Effect of changing body capacitance on transferred charge

Body resistance, as shown in Figure 5.50, has the largest effect on the waveform, compared to the previously discussed parameters. Both  $I_{max}$  and  $\left(\frac{dI}{dt}\right)_{max}$  are significantly affected by the resistance, however,  $Q_{ESD}$  is unaffected. Although the peak is larger at a lower resistance, the area under the curve remains the same since capacitance is unchanged. This trend is compatible with the explanations in section 5.5.2, regarding the effect of resistance on the waveform parameters.

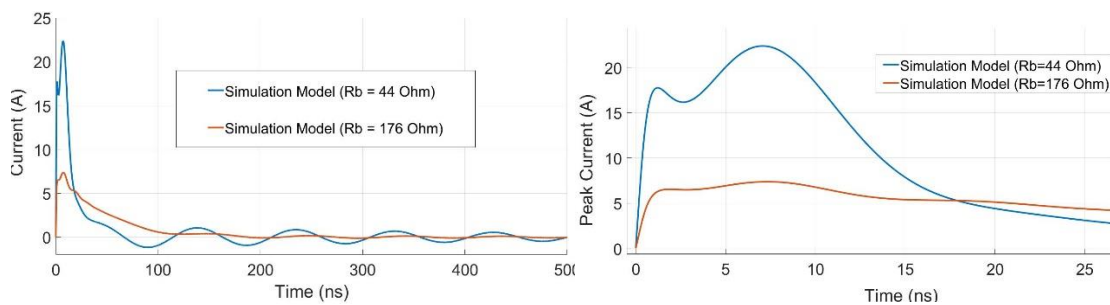


Figure 5.50. Effect of changing body resistance on the waveform (Left: Estimated waveform until 500 ns), Right: Estimated Waveform until 25 ns)

Figure 5.51 shows that  $I_{max}$  and  $\left(\frac{dI}{dt}\right)_{max}$  are 67% and 70% smaller, respectively as the resistance becomes 4 times larger.

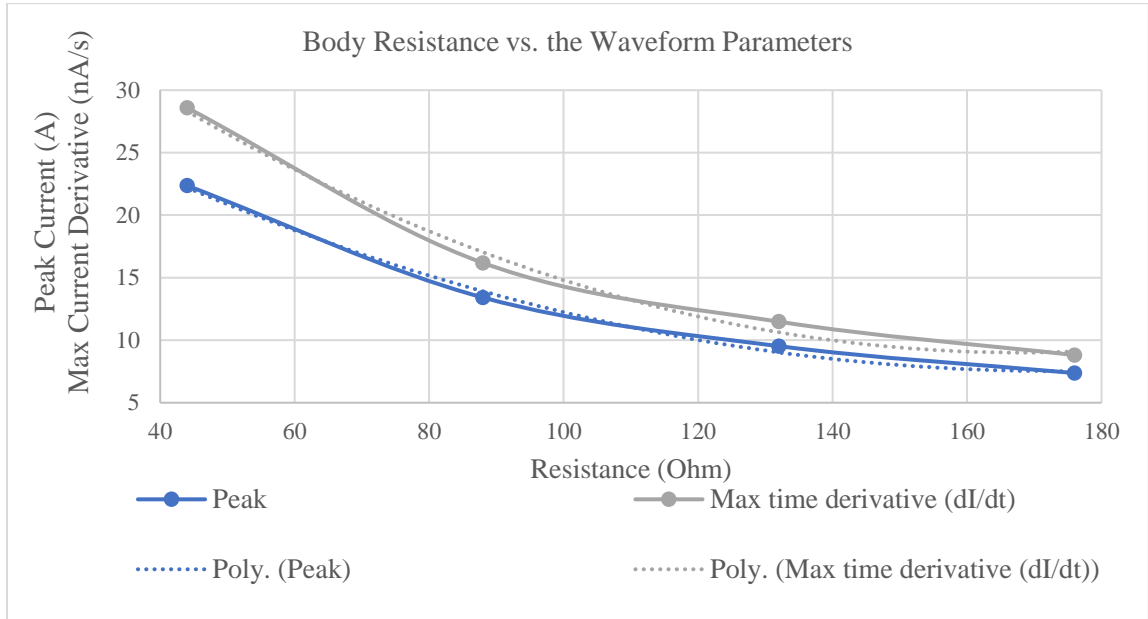


Figure 5.51. Effect of changing body resistance on the waveform parameters

Among the parameters of the model, body resistance and capacitance (relative to the Al foil) showed the largest effect on the waveform, and the rest of the parameters had minimal effect (less than 15% change on  $I_{max}$  and  $\left(\frac{dI}{dt}\right)_{max}$  at 4 times larger than their initial values).

### 5.11. Effect of Removing the Short Wire on the Waveform

Presence of the short wire between the metal piece and the bedframe results in radiation loss. In this section, the simulation model was used to investigate whether this wire reduced the severity of the waveform. It is expected that the waveform without adding the wire will

be more severe (larger  $I_{max}$ ,  $\left(\frac{dI}{dt}\right)_{max}$ ,  $Q_{ESD}$ ). An example of a waveform for ESD from a wearable metal piece is shown in Figure 5.52. In this configuration, the subject is lying down and the metal piece is worn on the subject's waist. Elimination of the short wire resulted in a more severe discharge as expected: 11% increase in  $I_{max}$ , 33% increase in  $\left(\frac{dI}{dt}\right)_{max}$ , and negligible change in  $Q_{ESD}$ . Since the short wire is the first discharging structure in the electromagnetic wave-front of the spark, its effect is mostly on the rising edge and  $\left(\frac{dI}{dt}\right)_{max}$ . Despite the increase in  $\left(\frac{dI}{dt}\right)_{max}$ , the zoomed view of Figure 5.52 shows that the new waveform still has a slower rising edge compared to the worst practical discharge at 50% Paschen's value.

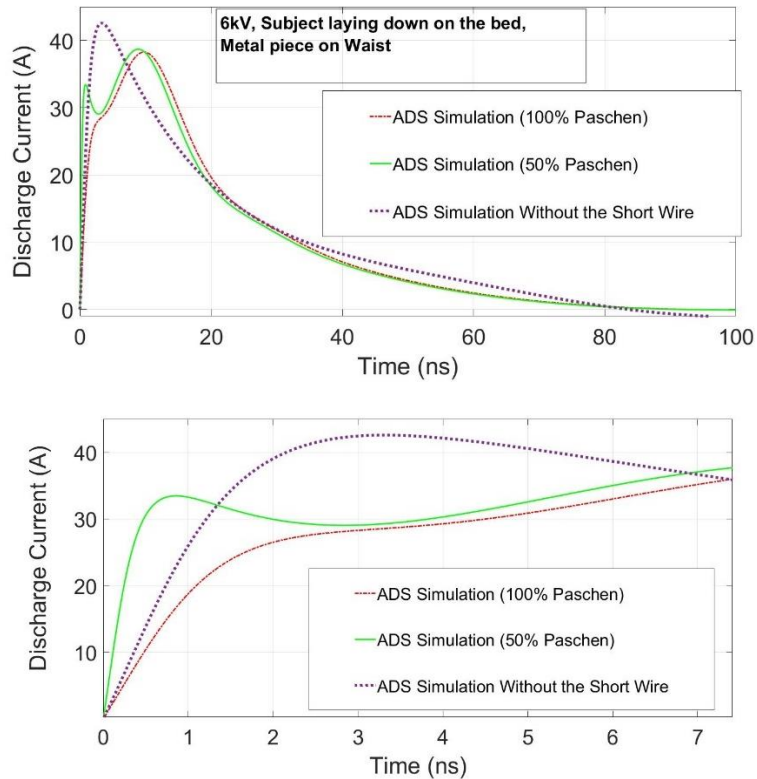


Figure 5.52. Top: Comparison between simulation results with and without adding the short wire, Bottom: Zoomed view of the top figure to show the changes in the rising edge



### 5.12. *Effect of RH and Speed of Approach on the Waveform*

The analysis of the severe charging activities in chapter 4 showed that lowering RH can increase the median of the peak body voltages. It was discussed that lowering RH can increase the statistical time lag due to the lack of seed electrons in dry conditions, and subsequently shorten the spark length. Our analysis of triboelectric voltages during sliding experiments showed a 27% increase as RH reduced from 30% to 20%. Talebzadeh's study also showed that reducing the RH from 45% to 10% results in 2 to 4 times increase in triboelectric voltage levels during routine activities (e.g., walking, sweater removal, sitting and rising from an office chair). The equivalent circuit developed in this chapter can be used to investigate the impact of lowering RH on the severity of the waveform.

An additional parameter that affects the waveform is the speed of approach, as it tends to influence the spark length [47]. In general, when the two electrodes approach faster, the spark length decreases and results in a faster rise time (i.e., more severe discharge) [31]. In the present study, the ESD tests were conducted at a constant RH level (25% RH), and a relatively constant speed of approach (about 3 cm/s). Therefore, the measurement data cannot be used to investigate the effect of RH and speed of approach on the resulting waveform parameters. This section presents an analysis of the waveform at two RH levels: 20% and 80% using literature data on the RH dependence of spark length and speed of approach [31].

Pommerenke [31] performed ESD experiments to investigate the effects of relative humidity and the speed of approach on the spark length during ESD events from a charged vertical rod (75 cm and 6mm). Although the charged object is different from our study, the

overall tendency of the waveform parameters will be investigated. In fact, this section is intended to provide a general approach to investigate the effect of RH on the waveform. However, to generalize this approach to the wearable medical devices discharging to hospital bed, the exact surface conditions of the bed (e.g., painting, coating) need to be known. Such data strongly depends on the surface and the shape of the electrodes.

Figure 5.53 and Figure 5.54 shows the measurements performed by Pommerenke [31] for a low (1.5 kV) and a high voltage level (9.9 kV). There are totally four conditions in these measurements: 1.5 kV and 9.9 kV: dry and humid air. For both voltage levels, as the speed of approach increases, the spark length reduces. The ESD waveform from a wearable metal piece in our setup can be reconstructed from the measured spark lengths at various RH levels and speeds of approach, shown in Figure 5.53 and Figure 5.54.

The developed circuit model showed reasonable accuracy to estimate the waveform parameters of 6 different configurations at 4 voltage levels of 2 kV to 8 kV. Therefore, this model can be extrapolated to predict the waveform at two different voltage levels: 1.5 kV and 9.9 kV. From each fitted curve, four data points are extracted and the associated ESD waveforms at these two voltage levels are reconstructed from the equivalent model.

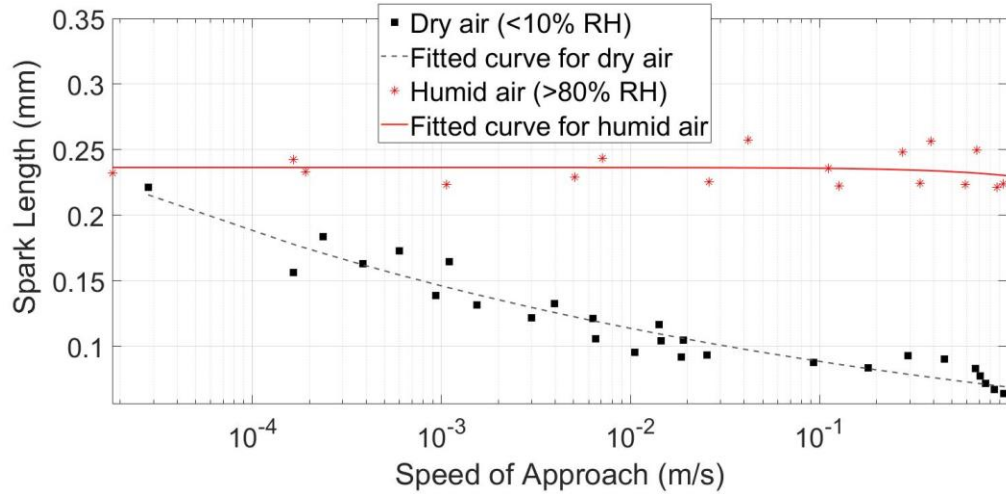


Figure 5.53. Effect of the speed of approach and the spark length at 1.5 kV for dry and humid air, from Pommerenke [31]

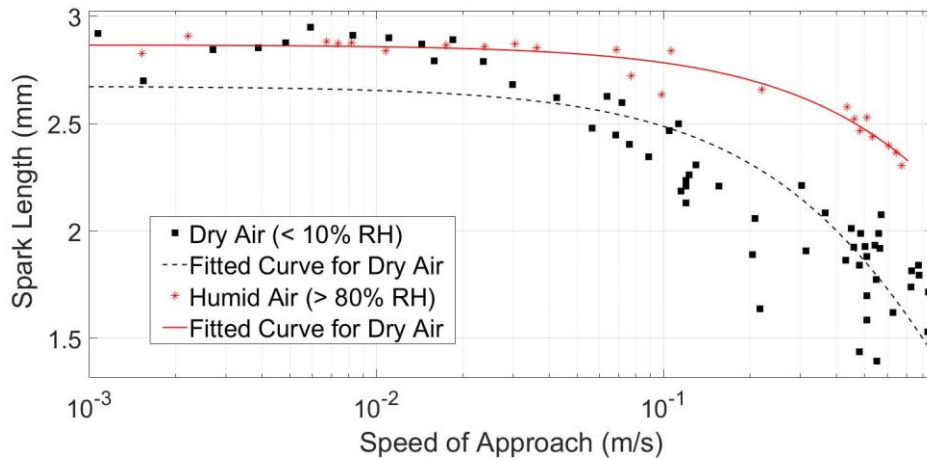


Figure 5.54. Effect of the speed of approach and the spark length at 9.9 kV for dry and humid air, from Pommerenke [31]

Table 7 shows the spark lengths at 4 speeds of approach, extracted from the *fitted curves* of the measurements shown in Figure 5.35 and Figure 5.54. At the lower body voltage (1.5 kV) a polynomial fit was selected, while for the higher voltage (9.9 kV), an exponential curve was used. These values are imported into the circuit model and the

waveform parameters were obtained for one configuration: subject lying down on the bed and metal piece on hand.

The reconstructed waveforms using the spark lengths in Table 7 showed that the  $I_{max}$  and  $Q_{ESD}$  are not affected by varying the spark length, however,  $\left(\frac{dI}{dt}\right)_{max}$  are affected as shown in Figure 5.55 and Figure 5.56. The simulation results show that  $\left(\frac{dI}{dt}\right)_{max}$  of dry air always exceeds that of the humid air, for both voltage levels. At 1.5 kV, the ratio of  $\left(\frac{dI}{dt}\right)_{max}$  for dry to humid conditions vary from 2.6 (slowest approach) to 5.7 (fastest approach). However, at 9.9 kV, this ratio is much lower, starting from 1.15 (slowest approach) to 1.8 (fastest approach). As the speed of approach increases,  $\left(\frac{dI}{dt}\right)_{max}$  for both dry and humid also increases. This is due to the shorter spark length at faster approaches (increased statistical time lag). Moreover, the ratio between dry to humid conditions decreases at the higher voltage. Similar results can be obtained for a different test configuration. Note that these conclusions reflect the overall tendencies, since the RH dependence of the spark length is strongly affected by the shape and geometry of the electrode [79].

Table 7. Spark length versus speed of approach for 1.5 kV and 9.9 kV, extracted from Pommerenke [31]

Speed of Approach (m/s)	1.5 kV		9.9 kV	
	Spark Length (mm)		Spark Length (mm)	
	Dry (10% RH)	Humid (80% RH)	Dry (10% RH)	Humid (80% RH)
0.001	0.146	0.236	2.67	2.86
0.01	0.114	0.236	2.65	2.86
0.1	0.089	0.236	2.49	2.78
0.5	0.074	0.234	1.86	2.47

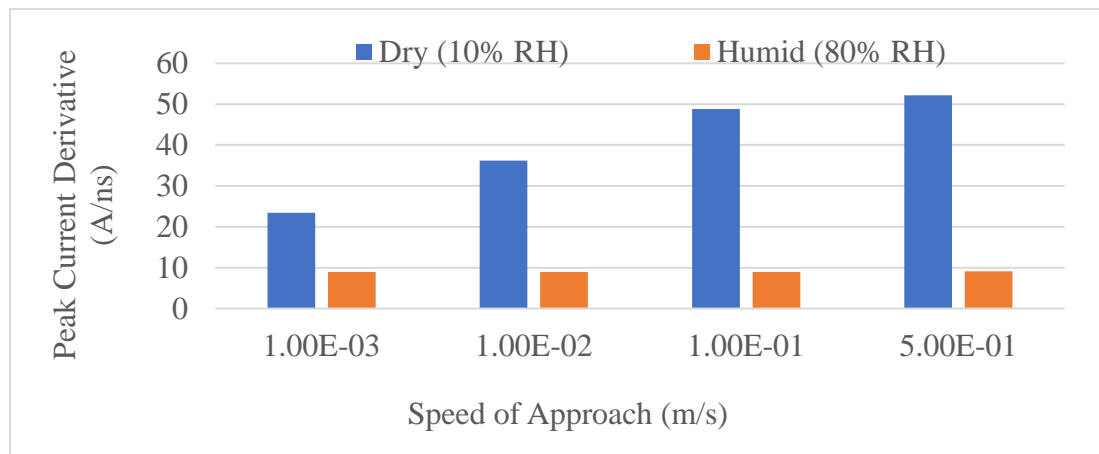
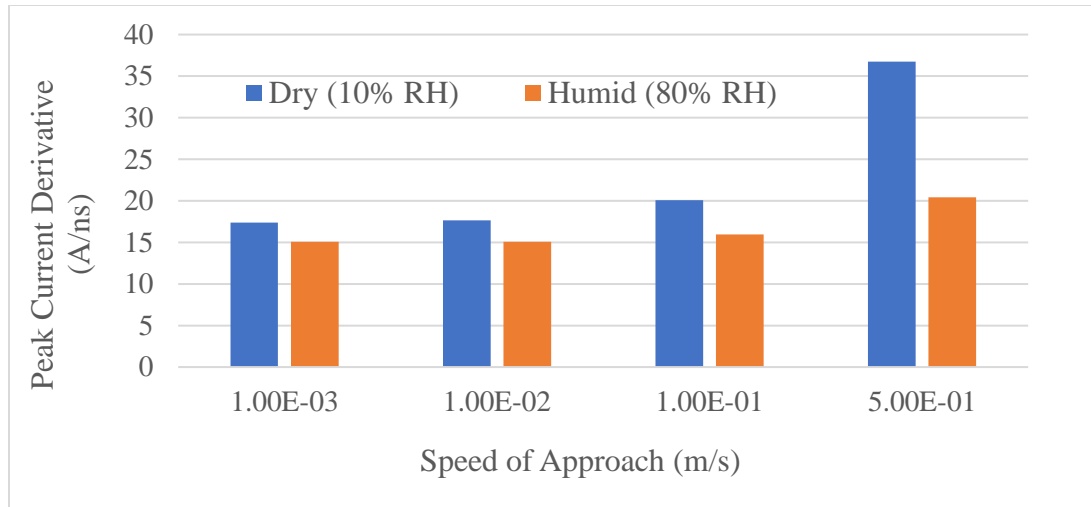


Figure 5.55. Comparison of the 1.5 kV discharge in dry and humid air at various speeds of approach (subject lying down on the bed, metal piece on hand)



*Figure 5.56. Comparison of the 9.9 kV discharge in dry and humid air at various speeds of approach (subject lying down on the bed, metal piece on hand)*

### 5.13. Conclusions

The discharge waveforms from a wearable device are investigated using the test configurations resulting in severe charging conditions in a healthcare facility. An equivalent circuit model is developed to predict the waveform for each test configuration with reasonable accuracy. The ESD measurements were characterized by their peak current, charge transfer to the ground and peak current derivative. The test configurations consisted of two device locations and three body postures at 4 voltage levels of 2 kV, 4 kV, 6 kV, and 8 kV.

Comparison with the IEC 61000-4-2 standard test method showed that 20 tests out of 24 discharge configurations resulted in higher peak currents (up to 1.9 times). For all body postures, the waist-worn scenarios resulted in larger peak current (up to 1.6 times) and peak current derivative (up to 2 times) than hand-worn scenarios, which was expected based on their lower body resistance. The charge transfer during the discharges followed the trend

of body capacitance relative to the Al foil and resulted in the same range of the ESD gun. The charge transfer for three configurations of hand-worn standing posture and both configurations for sitting posture, was 12% less than ESD gun (on average). However, the waist-worn standing posture and both configurations for lying down posture resulted in 24% larger charge transfer than the ESD gun (on average).

Using impedance measurement, an RLC representation of the human body wearing a metal piece (in lieu of a wearable device) at 3 postures, and the associated discharging structures were obtained. The Rompe-Weizel's nonlinear spark resistance model was integrated into the linear circuit mode to obtain the discharge current. While the prediction error for the peak current and transferred charge to the ground for all 24 conditions were in a reasonable range (below 10%), the peak current derivative showed large errors mainly due to the deviation of the spark length from the assumption of the Paschen's law.

The trends in the measurement and the estimated waveforms for the peak current, and peak current derivative were interpreted based on the ratio of body resistance for both device locations and the three body postures. The peak current and the estimated maximum current derivative for both sitting and lying down postures were almost similar (lying down was 4% larger in average  $I_{max}$  and 6% larger in average  $\left(\frac{dI}{dt}\right)_{max}$ ). However, both postures showed more severe waveforms compared to the standing posture (24% larger  $I_{max}$  and 22% larger  $\left(\frac{dI}{dt}\right)_{max}$  for the average of both postures). This result shows that the standing posture, which is the closest configuration to the HMM and brush-by scenario studied in the literature, was the least severe compared to the other postures.

The worst practical case of discharge using 50% Paschen's length showed that the peak current derivative from wearable discharge scenarios was, on average, 4-5 times larger than the IEC 61000-4-2 waveform. This result also indicates that the standard table-top test configuration may not provide sufficient immunity for wearable medical devices that require a high level of reliability and robustness against ESD malfunctions.

The sensitivity analysis on the waveform parameters indicated that spark length, and the gas constant  $K_R$  in the Rompe-Weizel's model, had the largest effect on  $\left(\frac{dI}{dt}\right)_{max}$ , since at 50% of their nominal value, the  $\left(\frac{dI}{dt}\right)_{max}$  became 4.8 times and 2 times larger (averaged for all six configurations). In contrast to typical ESD waveforms, these two parameters did not affect  $I_{max}$ , due to the presence of the radiation elements and the inductance of the wire. The simulation results found for the first configuration (lying down, metal piece on hand at 2 kV), showed that lowering body resistance to 50% of its initial value results in almost 40% reduction in both  $\left(\frac{dI}{dt}\right)_{max}$  and  $I_{max}$ . The only parameter affecting charge transfer was the body capacitance, (2.4 times larger charge transfer at 4 times higher capacitance). For the same configuration, 4 times increasing the radiation resistance resulted in a 15% reduction in  $\left(\frac{dI}{dt}\right)_{max}$ . The rest of the elements in the setup had minimal effect on the waveform.

The effects of RH and speed of approach on the waveform was investigate using the literature data. It was shown that the maximum current derivative is the only parameter of the waveform affected by the RH and speed of approach. At lower RH levels and faster



speed of approach, the maximum current derivative increased up to 5.7 times, depending on the voltage level and speed of approach.

## 6. Contributions

In this study, the following 5 major contributions were achieved. Contributions 1 to 3 are associated with the first research question, while the last two contributions discuss the 2<sup>nd</sup> research question:

- 1) Determined that the ESD testing voltage level (15 kV) specified in the latest (4<sup>th</sup>) edition of the IEC 60601-1-2 is not sufficient for wearable medical devices.
  - a. Identified three routine activities performed by patients wearing wearable devices in a healthcare facility that could result in reasonably foreseeable maximum charging voltage: sitting on and lying down on a hospital bed, and transferring to a hospital bed using a sliding board.
    - i. It was found that 15 kV is not a sufficient voltage level for ESD testing in the IEC 60601-1-2 standard, since in 10% of sitting experiments, 14% of sweater removal tests, and nearly half of the sliding and lying down experiments, the peak body voltages exceeds this threshold.
  - b. Determined the effects of the associated material combinations on the charging level of a person performing these activities:
    - i. Experiments with cotton blankets and nylon sliding sheets, which are the most common type of fabrics used in hospitals, resulted in the highest peak body voltages.
      1. The median voltage during the experiments involving cotton blankets in sitting and lying down experiments were 1.8 and

1.5 times larger than the median of these experiments including all combinations, respectively.

2. The median voltage during the sliding experiments using a cotton blanket and a nylon sheet was 1.4 times larger than the median of these experiment including all combinations.

ii. The effect of the antistatic coating on patient sliding boards was analyzed at 3 relative humidity levels of 30%, 20%, and 10%:

1. The median of the voltage levels while using boards with the coating reduced by 24% (averaged over 3 RH levels), compared to the regular sliding boards.

2. Using antistatic coating, 33% of the voltages exceed 15 kV (37 out of 113 tests), however, this percentage for regular boards is 55% (78 out of 142 tests).

2) Determined that the ESD test method according to IEC 61000-4-2 is not sufficient for wearable medical devices.

a. The ESD events from a wearable device while performing the identified charging activities were more severe than the standard waveform:

i. ESD measurements were performed in 6 discharge configurations (3 postures of standing on the floor, sitting and lying down on the bed, and two device locations: worn on hand and waist) and at 4 voltage levels (2 kV, 4 kV, 6 kV, 8 kV).

ii. Compared to the standards waveform, the peak currents,  $I_{max}$ , and maximum current derivatives,  $\left(\frac{dI}{dt}\right)_{max}$ , of the 6 discharge

configuration in this study, were 1.5 and 1.6 times higher than that of the standard waveform, respectively (averaged over all 6 configurations and 4 voltage levels).

3) Determined the effects of device location and body posture on the waveform parameters

a. Measured  $I_{max}$  from waist-worn devices were found to be larger than hand-worn devices

i. The mean value of the  $I_{max}$  for waist-worn devices during lying down, sitting and standing postures were 1.3, 1.4 and 1.6 times larger than hand-worn ones, averaged over the four voltage levels.

b. Measured  $\left(\frac{dI}{dt}\right)_{max}$  from waist-worn devices were found to be larger than hand worn devices in sitting and lying down postures:

i. For waist-worn configuration during lying down and sitting on the bed,  $\left(\frac{dI}{dt}\right)_{max}$  was on average 1.5 and 1.2 times larger than hand-worn configurations, respectively.

4) Developed a waveform prediction model based on physical elements of the setup

a. The electrical impedance of the setup elements and the human body in 6 discharge configurations were measured in the range of 1 MHz to 2 GHz.

- b. A prediction model was developed using a linear RLC model of the human body and the discharging structures, and a nonlinear spark resistance model based on Rompe-Weizel's law.
  - c. Simulation results for  $I_{max}$  and charge transfer  $Q_{ESD}$  showed less than 15% error compared to measurements.
  - d. Determined the effect of spark length on the waveform parameters:
    - i.  $\left(\frac{dI}{dt}\right)_{max}$  varied between 10 to 21 times with changes in spark length (for voltage level ranging between 2 kV to 8 kV), the effect on  $I_{max}$  and  $Q_{ESD}$  was negligible (<1% change).
- 5) Explained the trend in the waveform parameters for the 6 discharge configurations in terms of the physical parameters of the human impedance
- a. The ratio of the estimated and measured  $I_{max}$  and  $\left(\frac{dI}{dt}\right)_{max}$  for waist-worn to hand-worn discharges were correlated with the ratio of the human resistance for the two device locations, obtained from impedance measurements.
  - b. The trend of the estimated and measured  $Q_{ESD}$  for various postures was correlated with the body capacitance relative to the discharging structure.
- 6) Determined that the spark length and gas constant (in Rompe-Weizel's model) does not affect the peak current in the six configurations:
- a. 50% reduction from their nominal value resulted in 4.8 and 2 times larger  $\left(\frac{dI}{dt}\right)_{max}$

## Appendix: Survey on Electrostatic Risks in Hospitals

1) How do you feel about electrostatic shocks in your work (in general)?

- a) *Insignificant*   b) *slightly annoying*   c) *annoying*   d) *very annoying*   e) *unbearable*

2) How often do you experience static shock?

- a) *Infrequently*   b) *few times a month*   c) *few times a week*,  
b) *few times a day*   e) *Several times a day*

3) What items have you touched when you felt static shock?

- a) *Medical equipment*   b) *patient bed*   c) *display*   d) *door handle*   e) *wheelchair*   f) *bed sheet*   g) *patient chairs*  
*Others, please specify: ...*

4) What you were doing with the device when you experienced static shock?

- a) *picking the device up*   b) *handing the device to another person*   c) *dropping car keys onto the device*   d) *sitting up on a chair*   e) *driving a wheelchair on carpet floor*   f) *wearing or removing garment*   g) *touching plastic surfaces (e.g. on the device's enclosure)*  
*Others, please specify: ...*

- 5) What part of the device did you touch when you experienced static shock?
- a) Buttons      b) Display screen      c) ports (e.g. charging port, USB)
- Others, please specify:....
- 6) How did you notice the static shock?
- a) *A visible spark*    b) *A loud zapping sound*    c) *A slight jolting sensation*
- 7) Was the device's normal operation affected as a result of this static shock?
- a) No
- b) *Yes: temporary disruption, but returned to normal by itself*
- c) *Yes: temporary disruption, required a restart to return to normal*
- d) *Yes: permanent disruption, never returned to normal*
- 8) Was the device's display affected as a result of this static shock?
- a) *No*
- b) *Yes: temporary display flickering*
- c) *Yes: permanent display flickering*
- d) *Yes: temporary decrease in brightness*
- 9) Are you aware of any precautions/guidelines that should be followed by hospital staff to prevent electrostatic risks in the hospital?
- a) *No*                      b) *Yes (but they are just recommendations)*    c) *Yes (and we take it seriously)*

## Bibliography

- [1] P. Lamkin, “Wearable Tech Market To Be Worth \$34 Billion By 2020,” *Forbes*, 2016. [Online]. Available: <https://www.forbes.com/sites/paullamkin/2016/02/17/wearable-tech-market-to-be-worth-34-billion-by-2020/#2215564d3cb5>. [Accessed: 24-Nov-2017].
- [2] M. D. McGinnis, “An ESD-Control Program for Children with Cochlear Implants,” *J. Educ. Audiol.*, vol. 10, pp. 57–64, 2002.
- [3] M. Andresen, M. Juhler, and O. C. Thomsen, “Electrostatic discharges and their effect on the validity of registered values in intracranial pressure monitors.,” *J. Neurosurg.*, vol. 119, no. 5, pp. 1119–24, Nov. 2013.
- [4] M. O’Riordan, “FDA Issues Formal Rebuke to HeartWare,” *Medscape*, 2014. [Online]. Available: <http://www.medscape.com/viewarticle/828007>. [Accessed: 15-Dec-2016].
- [5] S. Lawrence, “Heartware Issues Recall Again for Implantable Heart Pumps Due to Risk of Death,” *FierceBiotech*, 2015. [Online]. Available: <http://www.fiercemedicaldevices.com/story/heartware-issues-recall-again-implantable-heart-pumps-due-risk-death/2015-02-23>. [Accessed: 10-May-2016].
- [6] M. Kohani and M. Pecht, “Malfunctions of Medical Devices Due to Electrostatic Occurrences,” *IEEE Access*, vol. 6, pp. 5805–5811, 2017.
- [7] C. Duvvury and H. Gossner, *System Level ESD Co-Design*. John Wiley & Sons, 2017.



- [8] Electrostatic Discharge Association (ESDA), “ESD TR20.20-2016: Handbook for the Development of an Electrostatic Discharge Control Program for the Protection of Electronic Parts, Assemblies and Equipment,” 2016.
- [9] O. Semenov, H. Sarbishaei, and M. Sachdev, “Introduction,” Dordrecht: Springer Netherlands, 2008, pp. 1–2.
- [10] K. Kim and A. A. Iliadis, “Operational Upsets and Critical New Bit Errors in CMOS Digital Inverters Due to High Power Pulsed Electromagnetic Interference,” *Solid. State. Electron.*, vol. 54, no. 1, pp. 18–21, Jan. 2010.
- [11] M. Moradian, A. Patnaik, Y. Han, F. Wan, D. Pommerenke, and D. Swensen, “Determination of the effect of humidity on the probability of ESD failure or upset in data centers,” *ASHRAE Trans.*, vol. 120, no. 2, 2014.
- [12] P. Clayton, “System configuration and design,” 2nd ed., vol. 184, John Wiley & Sons, 2006, pp. 835–836.
- [13] Y. Yu and X. Wang, “Chemical modification of polymer surfaces for advanced triboelectric nanogenerator development,” *Extrem. Mech. Lett.*, vol. 9, pp. 514–530, Dec. 2016.
- [14] J. Chen *et al.*, “Micro-cable structured textile for simultaneously harvesting solar and mechanical energy,” *Nat. Energy*, vol. 1, no. 10, p. 16138, Sep. 2016.
- [15] Y. H. Kwon, S.-H. Shin, J.-Y. Jung, and J. Nah, “Scalable and enhanced triboelectric output power generation by surface functionalized nanoimprint patterns,” *Nanotechnology*, vol. 27, no. 20, p. 205401, May 2016.

- [16] X. Zheng, R. Zhang, and H. Huang, "Theoretical modeling of relative humidity on contact electrification of sand particles," *Sci. Rep.*, vol. 4, Mar. 2014.
- [17] J. Paasi, S. Nurmi, R. Vuorinen, S. Strengell, and P. Maijala, "Performance of ESD protective materials at low relative humidity," *J. Electrostat.*, vol. 51–52, pp. 429–434, May 2001.
- [18] A. Ille *et al.*, "Reliability aspects of gate oxide under ESD pulse stress," *Microelectron. Reliab.*, vol. 49, no. 12, pp. 1407–1416, Dec. 2009.
- [19] R. Chundru, D. Pommerenke, K. Wang, T. Van Doren, F. P. Centola, and J. S. Huang, "Characterization of human metal ESD reference discharge event and correlation of generator parameters to failure levels- Part I: reference event," *IEEE Trans. Electromagn. Compat.*, vol. 46, no. 4, pp. 498–504, Nov. 2004.
- [20] Jayong Koo *et al.*, "Correlation Between EUT Failure Levels and ESD Generator Parameters," *IEEE Trans. Electromagn. Compat.*, vol. 50, no. 4, pp. 794–801, Nov. 2008.
- [21] K. Wang, D. Pommerenke, R. Chundru, T. Van Doren, F. P. Centola, and J. S. Huang, "Characterization of human metal ESD reference discharge event and correlation of generator parameters to failure levels-part II: correlation of generator parameters to failure levels," *IEEE Trans. Electromagn. Compat.*, vol. 46, no. 4, pp. 505–511, Nov. 2004.
- [22] J. Zhou *et al.*, "Characterization of ESD Risk for Wearable Devices," *IEEE Trans. Electromagn. Compat.*, pp. 1–9, 2018.

- [23] D. Pommerenke, “ESD: transient fields, arc simulation and rise time limit,” *J. Electrostat.*, vol. 36, no. 1, pp. 31–54, Nov. 1995.
- [24] R. Rompe and W. Weizel, “Über das Toeplersche Funkengesetz,” *Zeitschrift für Phys.*, vol. 122, no. 9–12, pp. 636–639, Sep. 1944.
- [25] F. Wan, V. Pilla, J. Li, D. Pommerenke, H. Shumiya, and K. Araki, “Time Lag of Secondary ESD in Millimeter-Size Spark Gaps,” *IEEE Trans. Electromagn. Compat.*, vol. 56, no. 1, pp. 28–34, Feb. 2014.
- [26] D. Pommerenke and M. Aidam, “ESD: waveform calculation, field and current of human and simulator ESD,” *J. Electrostat.*, vol. 38, no. 1–2, pp. 33–51, Oct. 1996.
- [27] M. L. Einsla *et al.*, “Toward Improved Conductivity of Sulfonated Aromatic Proton Exchange Membranes at Low Relative Humidity,” *Chem. Mater.*, vol. 20, no. 17, pp. 5636–5642, Sep. 2008.
- [28] NASA Technical Standards NASA-STD 8739.6A, *Implementation Requirements For NASA Workmanship Standards*. 2016.
- [29] J. Paasi, S. Nurmi, R. Vuorinen, S. Strengell, and P. Majjala, “Performance of ESD protective materials at low relative humidity,” *J. Electrostat.*, vol. 51–52, pp. 429–434, May 2001.
- [30] D. Pommerenke, “ESD: transient fields, arc simulation and rise time limit,” *J. Electrostat.*, vol. 36, no. 1, pp. 31–54, Nov. 1995.
- [31] D. Pommerenke, “On the influence of the speed of approach, humidity and arc length on ESD breakdown,” 1993, pp. 103–111.

- [32] U.S. Food and Drug Administration, “Classify Your Medical Device,” *Center for Devices and Radiological Health*, 2014. [Online]. Available: <https://www.fda.gov/medicaldevices/deviceregulationandguidance/overview/classifyyourdevice/>. [Accessed: 07-Apr-2017].
- [33] U.S. Food and Drug Administration, “Regulatory Controls,” *Center for Devices and Radiological Health*, 2018. [Online]. Available: <https://www.fda.gov/medicaldevices/deviceregulationandguidance/overview/generalandspecialcontrols/default.htm>. [Accessed: 26-Jul-2018].
- [34] IEC 61000-4-2, “Electromagnetic compatibility (EMC)- Part 4-2: Testing and measurement techniques - Electrostatic discharge immunity test.” International Electrotechnical Commission, Geneva.
- [35] Kai Wang, D. Pommerenke, R. Chundru, T. Van Doren, J. L. Drewniak, and A. Shashindranath, “Numerical modeling of electrostatic discharge generators,” *IEEE Trans. Electromagn. Compat.*, vol. 45, no. 2, pp. 258–271, May 2003.
- [36] “Static Electricity and People,” *Compliance Mag.*, 2014.
- [37] T. Ficker, “Charging by walking,” *J. Phys. D. Appl. Phys.*, vol. 39, no. 2, pp. 410–417, Jan. 2006.
- [38] D. Pirici, J. Rivenc, T. Lebey, D. Malec, A. Agneray, and M. Cheaib, “A Physical Model to Explain Electrostatic Charging in an Automotive Environment; Correlation with Experiments,” *J. Electrostat.*, vol. 62, no. 2, pp. 167–183, 2004.
- [39] A. Talebzadeh, M. Moradian, Y. Han, D. E. Swenson, and D. Pommerenke,

- “Electrostatic Charging Caused by Standing Up from A Chair and by Garment Removal,” in *2015 IEEE Symposium on Electromagnetic Compatibility and Signal Integrity*, 2015, pp. 57–62.
- [40] A. Talebzadeh, M. Moradian, Y. Han, D. E. Swenson, and D. Pommerenke, “Effect of Human Activities and Environmental Conditions on Electrostatic Charging,” *IEEE Trans. Electromagn. Compat.*, vol. 58, no. 4, pp. 1266–1273, Aug. 2016.
- [41] P. Holdstock and N. Wilson, “The effect of static charge generated on hospital bedding,” 1996, pp. 356–364.
- [42] T. Viheriakoski, M. Kokkonen, P. Tamminen, E. Karja, J. Hillberg, and J. Smallwood, “Electrostatic threats in hospital environment,” 2014, pp. 1–9.
- [43] H. Salmela and T. Kalliohaka, “Managing static electricity in hospital environments,” in *FiberMed11*, 2011, pp. 1–5.
- [44] D. Pommerenke and M. Aidam, “To what extent do contact-mode and indirect ESD test methods reproduce reality?,” in *Electrical Overstress/Electrostatic Discharge Symposium Proceedings*, 1995, pp. 101–109.
- [45] R. Jobava *et al.*, “Computer simulation of ESD from voluminous objects compared to transient fields of humans,” *IEEE Trans. Electromagn. Compat.*, vol. 42, no. 1, pp. 54–65, 2000.
- [46] Y. Kagawa, Y. Taka, and O. Fujiwara, “Characteristic measurement of spark transients due to finger touch,” *J. Electrostat.*, vol. 68, no. 1, pp. 1–4, Feb. 2010.

- [47] I. Mori, Y. Taka, and O. Fujiwara, "Wideband measurement of discharge current caused by air discharge through hand-held metal piece from charged human body," *Electron. Commun. Japan*, vol. 91, no. 9, pp. 54–61, Sep. 2008.
- [48] Yoshinori Taka and Osamu Fujiwara, "Verification of spark resistance formula for human ESD," in *2008 Asia-Pacific Symposium on Electromagnetic Compatibility and 19th International Zurich Symposium on Electromagnetic Compatibility*, 2008, pp. 152–155.
- [49] T. Ishida, S. Nitta, F. Xiao, Y. Kami, and O. Fujiwara, "An Experimental Study of Electrostatic Discharge Immunity Testing for Wearable Devices," in *IEEE International Symposium on Electromagnetic Compatibility (EMC)*, 2015, pp. 839–842.
- [50] T. Yoshida, "A study on electrical stress induced by electrostatic discharge on wearable devices," in *2015 7th Asia-Pacific Conference on Environmental Electromagnetics (CEEM)*, 2015, pp. 230–233.
- [51] J. Zhou, K. Ghosh, S. Xiang, X. Yan, J. Lee, and D. Pommerenke, "Characterization of ESD Risk for Wearable Devices," *IEEE Trans. Electromagn. Compat.*, 2017.
- [52] W. R. Elliott and G. Gianetti, "Electrostatic discharge interference in the clinical environment. Brief cold snaps or humidification disruptions can cause ESD problems.," *Biomed. Instrum. Technol.*, vol. 29, no. 6, pp. 495–9.
- [53] M. Kohani, A. Bhandare, L. Guan, D. Pommerenke, and M. G. Pecht, "Evaluating Characteristics of Electrostatic Discharge (ESD) Events in Wearable Medical

- Devices: Comparison With the IEC 61000-4-2 Standard,” *IEEE Trans. Electromagn. Compat.*, pp. 1–9, 2017.
- [54] V. Amoruso, M. Helali, and F. Lattarulo, “An improved model of man for ESD applications,” *J. Electrostat.*, vol. 49, no. 3, pp. 225–244, 2000.
- [55] V. Kuznetsov and L. Kechiev, “Charged Board Model ESD Simulation for PCB Mounted MOS Transistors,” *IEEE Trans. Electromagn. Compat.*, vol. 57, no. 5, pp. 947–954, Oct. 2015.
- [56] S. Marathe, G. Maghlakelidze, H. Rezaei, D. Pommerenke, and M. Hertz, “Software-Assisted Detection Methods for Secondary ESD Discharge During IEC 61000-4-2 Testing,” *IEEE Trans. Electromagn. Compat.*, vol. 60, no. 4, pp. 1129–1136, Aug. 2018.
- [57] D. Pommerenke and M. Aidam, “To what extent do contact-mode and indirect ESD test methods reproduce reality?,” in *Electrical Overstress/Electrostatic Discharge Symposium Proceedings*, 1995, pp. 101–109.
- [58] T. Dangelmayr, “Fundamentals of Electrostatics,” in *ESD Program Management: A Realistic Approach*, Springer Science & Business Media, 2012.
- [59] M. Kohani and M. Pecht, “Malfunctions of Medical Devices Due to Electrostatic Occurrences Big Data Analysis of 10 Years of the FDA’s Reports,” *IEEE Access*, vol. 6, pp. 5805–5811, 2018.
- [60] R. W. Welker, R. (Ramamurthy) Nagarajan, and C. E. Newberg, *Contamination and ESD control in high technology manufacturing*. John Wiley & Sons, 2006.

- [61] T. Ficker, "Electrification of human body by walking," *J. Electrostat.*, vol. 64, no. 1, pp. 10–16, 2006.
- [62] B. W. Lee and D. E. Orr, "The Triboelectric Series," *AlphaLab Inc.*, 2018.  
[Online]. Available: <https://www.alphalabinc.com/triboelectric-series/>. [Accessed: 19-Jul-2018].
- [63] A. Torossian, E. Van Gerven, K. Geertsen, B. Horn, M. Van de Velde, and J. Raeder, "Active perioperative patient warming using a self-warming blanket (BARRIER EasyWarm) is superior to passive thermal insulation: a multinational, multicenter, randomized trial," *J. Clin. Anesth.*, vol. 34, pp. 547–554, Nov. 2016.
- [64] M. D. Parks, D. L. Morris, K. Kolcaba, and P. E. McDonald, "An Evaluation of Patient Comfort During Acute Psychiatric Hospitalization," *Perspect. Psychiatr. Care*, vol. 53, no. 1, pp. 29–37, Jan. 2017.
- [65] K. Whale, J. C. Ingram, S. George, F. Spickett-Jones, A. Sack, and A. E. Young, "Exploring the acceptability of using low-friction bedding for patients with burns: Qualitative results from the SILKIE study," *Burns*, vol. 44, no. 5, pp. 1251–1258, Aug. 2018.
- [66] W. Wen *et al.*, "Skill Evaluation and Education Services for Bed-Care Nursing with Sliding Sheet with Regression Analysis," in *Serviceology for Smart Service System*, Tokyo: Springer Japan, 2017, pp. 253–259.
- [67] C. Weiner, L. Kalichman, J. Ribak, and D. Alperovitch-Najenson, "Repositioning a passive patient in bed: Choosing an ergonomically advantageous assistive device," *Appl. Ergon.*, vol. 60, pp. 22–29, Apr. 2017.



- [68] L. M. Bartnik and M. S. Rice, "Comparison of Caregiver Forces Required for Sliding a Patient up in Bed Using an Array of Slide Sheets," *Workplace Health Saf.*, vol. 61, no. 9, pp. 393–400, Sep. 2013.
- [69] Y. Endo, A. Ohsawa, and M. Yamaguma, "Electrostatic hazards of charging of bedclothes and ignition in medical facilities," *Int. J. Occup. Saf. Ergon.*, pp. 1–5, Feb. 2018.
- [70] "ANSI/ESD ESD-STM, 5., 1 – 2007. (2007) ESD Association Standard Test Method for the Protection of Electrostatic Discharge Sensitive Items – Electrostatic Discharge Sensitivity Testing – Human Body Model (HBM) Testing –Component Level. Standard Test Method." .
- [71] S. Yang, J. Zhou, D. Pommerenke, and D. Liu, "A simple frequency response compensation method for current probe measurements of ESD currents," in *2017 IEEE International Symposium on Electromagnetic Compatibility & Signal/Power Integrity (EMCSI)*, 2017, pp. 158–163.
- [72] Y. T. Lo and S. W. Lee, *Antenna handbook*. Van Nostrand Reinhold, 1993.
- [73] F. W. Grover, *Inductance Calculations: Working Formulas and Tables*. Mineola, NY: Courier Publication, 2004.
- [74] V. De Santis, P. A. Beeckman, D. A. Lampasi, and M. Feliziani, "Assessment of Human Body Impedance for Safety Requirements Against Contact Currents for Frequencies up to 110 MHz," *IEEE Trans. Biomed. Eng.*, vol. 58, no. 2, pp. 390–396, Feb. 2011.

- [75] Y. Taka and O. Fujiwara, "Further Validation of Spark-Resistance Formula Applied for Human ESD," in *2009 20th International Zurich Symposium on Electromagnetic Compatibility*, 2009, pp. 393–396.
- [76] G. A. Mesyats and G. S. Kurshonov, "Formation of nanosecond sparks in static breakdown of a gap," *Sov. Phys. J.*, vol. 13, no. 4, pp. 483–489, 1968.
- [77] D. Pommerenke, "Transiente Felder der ESD," Tech. Univ. Berlin, 1995.
- [78] S. Bonisch, W. Kalkner, and D. Pommerenke, "Modeling of short-gap ESD under consideration of different discharge mechanisms," *IEEE Trans. Plasma Sci.*, vol. 31, no. 4, pp. 736–744, Aug. 2003.
- [79] D. Pommerenke, "ESD: transient fields, arc simulation and rise time limit," *J. Electrostat.*, vol. 36, no. 1, pp. 31–54, Nov. 1995.